DEVELOPMENT OF GUIDELINES FOR DESIGNERS AND OPERATORS OF GRINDING MILLS AIMED AT IMPROVING THE SERVICE LIFE OF DRIVETRAIN COMPONENTS

RICHARD DIERING

A research project submitted to the Faculty of Engineering and the Built Environment, of the University of the Witwatersrand, in partial fulfilment of the requirements for the degree of Master of Science in Engineering.

Johannesburg, June 2011

ABSTRACT

Grinding mills are used extensively in the mining, cement and minerals processing industries. Numerous failures of drivetrain components of grinding mills have occurred in recent years. The components are not meeting their required design lives leaving mill owners concerned about the expensive repair costs and lost profits associated with the mill downtime during repairs.

There is a need to research the design methodology of the drivetrain components of grinding mills and the analysis of fatigue failures in mills and similar equipment e.g. kilns in order to develop a comprehensive and improved picture of how to design and operate these mills. As with numerous other engineered items, the critical issue is that a thorough understanding of the type, magnitude, direction, and duration of all loads that the components will experience while in operation is required in order to design them correctly.

A literature survey was performed to research advanced design methods and identify sources of loading data for grinding mills. Many interesting references were identified but no specific examples were found where strain gauge measurements were used to quantify the loads experienced by the drivetrain components of grinding mills.

Strain gauge measurements were conducted on the drivetrains of 30 grinding mills. The measured data was processed and analysed to determine the key operating loads experienced by the grinding mill drivetrain components. These loads were used in a review of the engineering design calculations for these components and the important findings are highlighted. Finally, comprehensive fatigue analysis was conducted using the measured data to understand the major contributors to poor service life of the drivetrain components.

Based on the findings of the investigation, several conclusions and recommendations are made that can serve as useful guidelines for improving the service life of grinding mills for both designers and operators of these machines.

DECLARATION

I declare that this research report is my own, unaided work. It is being submitted for the Degree of Master of Science 50/50 in the University of the Witwatersrand. This work has not been submitted before for any degree or examination in any other University.

_____

____ day of _____ (year) _____

ACKNOWLEDGEMENTS

Many people gave generously of their time throughout the progress of this project, however I would specially like to thank the following people, without whose help this work would not have been possible:

- Sarel Beytell, Nicholas Radebe and Hennie van Zyl from Anglo American Technical Division for the many long hours of mill testing.
- Rod Hamilton from Anglo American Technical Division for his guidance and assistance.
- Investmech for their contribution of mill test data.
- The management and operations personnel at the various sites for making the mills available for testing.
- The vendors of the various mills who have contributed their knowledge.
- Carole, my wife, for all her love and support.

TABLE OF CONTENTS

LIST OF FIGURES

LIST OF TABLES

LIST OF SYMBOLS

Modulus of elasticity	E
Shear modulus of elasticity	G
Moment of inertia	I
Polar moment of inertia	J
Bending moment	M_b
Torque, temperature	T
Section modulus	Z
Polar section modulus	Z_p
Poisson's ratio	ν
Shear stress	τ
Bending stress	σ_b
Shaft diameter	d
Measured voltage	V_s
Indicated voltage	V_i
Measured strain	ε_s
Indicated strain	ε_i
Ultimate tensile strength	S_{ut}
Endurance limit (rotating beam)	S'_e
Endurance limit	S_e
Surface factor	k_a
Size factor	k_b
Reliability factor	k_c
Temperature factor	k_d
Stress concentration factor	K_t
Keyway bottom radius	r

1. INTRODUCTION

Grinding mills are used extensively in the mining, cement and minerals processing industries. One of the popular drive designs for grinding mills in the mining industry in South Africa comprises a wound rotor induction motor, controlled by liquid rheostats, driving a pinion and mill mounted girth or ring gear through a reduction gearbox. These mill drives occur in either single or dual configurations with installed power ranging from 1 to 14 MW. An example of a mill with a single drive is illustrated in Figure 1.

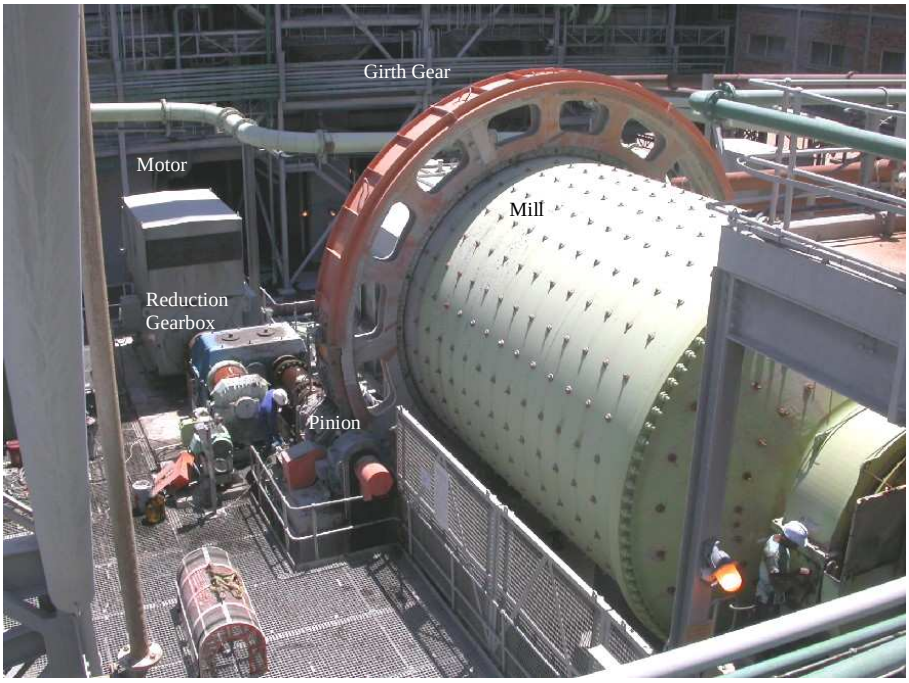

Figure 1 Single Drive Mill

Hamilton[1] notes that over the past 40 years the most common mode of mill failure has been cracking of the mill shell due to high cycle fatigue. Recently, however, numerous failures of grinding mill drivetrains have occurred. These drivetrain component failures have occurred at various mine sites on mills supplied by different vendors.

The components that fail are:

- Pinion shafts
- Reduction gearboxes
- Girth gears
- Mill pinion gears

The results of detailed investigations have indicated that fatigue failures have occurred in the majority of cases. The pinion shaft failures usually occur as a result of a fatigue fracture, which originates from the corner of the keyway in the pinion shaft. Failures in the gearbox include cracked casings, gear damage and

shaft fatigue failures. The girth gears fail by means of contact stress fatigue damage to the flanks of the gear teeth and some cases of fatigue cracking in the roots of the gear teeth have also occurred.

These components are not meeting their required design lives. Mill owners are concerned about the expensive repair costs and lost profits associated with the mill downtime during repairs.

There is a need to research the design methodology of the drivetrain components and the analysis of fatigue failures in mills and similar equipment e.g. kilns. A comprehensive and improved picture of how to design and operate these mills is required.

2. OVERVIEW OF MILL DRIVETRAIN DESIGN STANDARDS

2.1. Machine and Drivetrain Component Design

The main components of a mill drivetrain are the couplings, shafts, bearings, main reducer gearbox and the mill pinion and girth gears. The relevant design methodologies for each of the components are listed in Table 1.

A common component of all of the above mentioned design methodologies is the use of a factor of safety or reserve factor. This factor is the result of comparing the maximum calculated stress to the material failure property. The choice of the factor of safety depends on the component itself and on the expected accuracy of the associated analysis.

Table 1 Design Methodologies for Mill Drivetrain Components

No.	Component	Design Methodology
1	Pinion and girth gears	American Gear Manufacturers Association Standards AGMA 321.05, AGMA 6004-F88 and most recently AGMA 6014-A06 (Metric edition = AGMA 6114-A06)
2	Main reducer gearbox	American Gear Manufacturers Association Standards AGMA 420.04, AGMA 2001-B88 and most recently AGMA 2001-C95 (Metric edition = AGMA 2101-C95)
3	Shafts	Standard strength and stiffness design based on combined torsion and bending. Various methods available. Finite element analysis (FEA) also used in some cases.
4	Couplings	Selected from a supplier catalogue which normally include duty calculation guidelines. Suppliers use techniques such as FEA.
5	Bearings	Bearing forces are deduced by the resolution of forces within the system. A suitable operating life is normally specified between 50 000 and 100 000 hours. The SKF L10h life calculation or similar is then used to size the bearing.

2.1.1. Pinion and Girth Gears

The pinion and girth gears are designed according to AGMA standards, the latest version being AGMA 6114-A06[2]. The standard provides a method to determine the power rating of gear sets for cylindrical grinding mills. Calculations determine the allowable rating for pitting resistance and bending strength of helical involute gear teeth.

When considering system dynamics it is understood that the dynamic response of a system results in additional gear tooth loads due to the relative accelerations of the connected masses of the driving and driven

equipment. Overloads are part of the service factor which is intended to account for the operating characteristics of the driving and driven equipment. Resonant vibrations may cause overloads many times higher than the nominal load. This must be checked for separately by means of a proper torsional vibration analysis as these resonant loads are not accounted for in the AGMA standard.

The standard also accounts for momentary overloads. When the gear is subjected to infrequent (less than 100 cycles during the design life) momentary high overloads approaching yield, the maximum allowable stress is determined by the allowable yield properties rather than the bending fatigue strength of the material.

Despite these and other allowances the standard provides a method by which different gear designs can be rated and compared. It is not intended to assure the performance of assembled gear drive systems. To properly assess the suitability of the gears in terms of the intended application, a review of service factors is required. The service factor is calculated by dividing the calculated allowable power rating for pitting resistance and bending strength by the motor input power. The standard provides values for minimum service factors which have been developed from the experience of manufacturers and users of grinding mills with electric motor prime movers. As an example, for SAG mills, the minimum durability factor based on pitting resistance is 1.75 and the minimum strength factor based on bending is 2.5. The minimum values serve as a guide but user and the gear manufacturer need to agree upon the service factors for the intended application. This should be defined by contractual agreement.

The type of prime mover of a gear system can have a significant impact on the service factor selected and the overall performance of the gear set. The required starting loads, the method of connection between the prime mover, the gear set and the driven equipment should all be reviewed. Motors with high starting torque capacity and an application that has frequent start/stop cycles may require that the gear set be designed to address these peak loads.

Service factors are based on the experience of the application. Unbalanced loads, starting requirements, changes in alignment during operation, and long term reliability all play a role in determining the service factor. It is critical to ensure that during the design process, an understanding of the type, magnitude, direction, and duration of all loads that the gear set will experience are considered. In dual drive applications, the inching or maintenance drive is required to produce the same output torque as in main drive operation. Since the load is transmitted through one side of the gear train, analysis is required to ensure that all components are not stressed beyond design limits.

2.1.2. Main Reducer Gearbox

The main reducer gears are also designed according to AGMA standards, the latest version being AGMA 2101-C95[3]. The standard presents general formulae for rating the pitting resistance and bending strength of spur and helical involute gear teeth operating on parallel axes. The formulae evaluate gear tooth capacity as influenced by the major factors which affect gear tooth pitting and gear tooth fracture at the fillet radius.

There are two major differences between the pitting resistance and bending strength ratings. Pitting is a function of the Hertzian contact stresses between two surfaces and is proportional to the square root of the applied tooth load. Bending strength is measured in terms of the bending stress modelling the tooth as a cantilever plate and is directly proportional to the applied tooth load.

The pitting of gear teeth is a surface fatigue phenomenon and the aim of the pitting resistance formula is to determine a load rating at which progressive pitting in the teeth does not occur. The ratings for pitting resistance are based on the formulae developed by Hertz for contact pressure between two curved surfaces, modified for the effect of load sharing between adjacent teeth.

The bending of gear teeth is also a fatigue phenomenon related to the resistance to cracking at the root tooth fillet in external gears and at the critical section in internal gears. The intent of the strength rating formula is to determine the load which can be transmitted for the design life of the gear drive without causing root fillet cracking.

The formulae account for system dynamics and momentary overloads. The overload factor makes allowance for all externally applied loads in excess of the nominal tangential load. For an overload factor of unity, the rating method includes the capacity to sustain a limited number of up to 200% momentary overload cycles (typically less than 4 starts in 8 hours, with a peak not exceeding one second duration). Higher more frequent overloads are considered separately. In determining the overload factor, consideration should be given to the fact that many prime movers and driven equipment, individually or in combination, develop momentary peak torques appreciably greater than those determined by the nominal ratings of either the prime mover or the driven equipment. Possible sources of overload which should be considered are: system vibrations, acceleration torques, overspeeds, variations in system operation, split path load sharing among multiple prime movers, and changes in process load conditions.

The standard makes a number of allowances for different conditions in an attempt to make the gear rating as accurate as possible, however, it ultimately only provides a method by which different gear designs can be theoretically rated and compared. It is not intended to assure the performance of assembled gear drive systems. Thus, as was the case for the girth and pinion gears, to ensure a design that is fit for purpose, appropriate service factors need to be used. These service factors need

to be contractually agreed by the user and the gear manufacturer for the intended application.

2.1.3. Other Drivetrain Components

The same considerations as for the gears need to be taken into consideration when determining minimum safety factors for other drivetrain components such as couplings and shafts. The intention must always be to ensure that the required service life is attained with a cost effective design. It is also important to choose safety factors that are match those of the other drivetrain components.

2.2. Grinding Mill Operation

AGMA 6114-A06 Annex A provides guidelines on installation and alignment of girth and pinion gears. This is particularly relevant to this project as the alignment of the drivetrain has an influence on the bending moment in the shafts. Guidelines are given for both static and dynamic alignment adjustments.

As far as dynamic adjustments are concerned, most pinions have to be realigned after start-up to correct for dynamic effects such as pinion deflection (torsional and bending), deflection of the gear body under radial and thrust load, deflection of the mill, thermal deformations, and other dynamic factors having an effect on the alignment.

Grinding mills have an additional need for realignment after start-up based on the difference between the operating temperatures measured at both ends of the pinion face. The pinion temperature can be measured in operation using an infrared thermometer. Experience has shown that, on unidirectional equipment, a temperature differential (Delta-T) of $8^{o}C$ or less between both ends of the pinion teeth is satisfactory for long term operation. Higher temperature differentials require realignment.

The physical adjustments typically require more than one pinion move prior to reaching satisfactory alignment. It is critical to gear and pinion integrity that the site allows the necessary equipment down time to conduct these adjustments.

Note that when the initial static alignment is conducted accurately, subsequent adjustments at the pinion are generally small enough for the drivetrain couplings to stay within their angular and offset alignment limits. Nevertheless, these should always be taken into consideration when making corrections to mesh alignment. Realignment of the entire drivetrain could be required in some cases.

Finally, pinion alignment will change with time due to several factors such as bearing wear, tooth wear, significant changes in loading, and foundation movements. It is imperative that pinion alignment be maintained with time

and it should be monitored on a regular basis as part of a regular maintenance program.

AGMA 6114-A06 Annex B provides information on common types of motor drives used on grinding mills. For the purposes of this project the wound rotor motors controlled by liquid rheostats are the most applicable. Wound rotor motors controlled by liquid rheostats provide smooth acceleration while keeping the accelerating torque of the two motors, in the case of dual drive mills, balanced. After obtaining rated speed the liquid rheostats are bypassed by rotor circuit contactors. Advantages include excellent load sharing during starting and constant speed operation as well as soft torque transmission to the gears. A disadvantage of the system, however, is that special liquid rheostat designs are required to prevent large torque transients during liquid rheostat bypass switching operations.

In the summary of Annex B it is stated that various methods can be employed to address the different drive characteristics discussed. Requiring higher service factors or increased individual component ratings are two typical methods used to compensate for drive characteristics. In all cases proper pinion to gear alignment is important.

3. LITERATURE SURVEY

The information in the preceding section detailed how service factors are used as a common component in the design standards for the various drivetrain components. It was shown that the value used depends on the knowledge and experience of the application in question as well as the expected accuracy of the associated design analysis.

The critical issue is that a thorough understanding of the type, magnitude, direction, and duration of all loads that drivetrain components will experience while in operation is required in order to design drivetrain components correctly. The objective of this literature survey was to research advanced design methods and loading data that complement the work described above to arrive at a comprehensive and accurate approach to designing drivetrains for grinding mills.

In summary, it was found that the literature covers aspects such as the failure analysis of drivetrain components using fundamental mechanical and metallurgical techniques and also covers fatigue life assessments and the contribution of various factors on the fatigue life of parts e.g. torsional vibrations. In addition, a number of papers cover computational modelling and simulation of parts in operation to determine the component's operational fatigue life, however, they do not specifically address grinding mills. A few papers detailed the use of strain gauge measurements to investigate failures of drivetrain components but these were mostly focussed on identifying resonant frequencies in the drivetrain. No specific examples were found where strain gauge measurements were used to quantify the loads experienced by the drivetrain components of grinding mills.

The detail of the applicable material is discussed in the following sections.

3.1. Experimental Studies of Drivetrain Components

The research in this section was focussed on machine drivetrain component design and associated stress analysis.

Saxer[4] discusses the investigations made to identify the primary causes for severe gear tooth damage contributing to the unreliable performance of the girth gear drives. Despite the simple design of the girth gear/pinion drive, satisfactory operating reliability had not been achieved. Among the many studies of operating behaviour of driving systems necessary during recent years in the cement industry, a combined measurement–calculation procedure has proven very satisfactory and extremely effective. The details of this particular study however were focussed on the modal analysis of the mill foundations and not on the drivetrain components. The work concluded by determining that two essential factors influenced the operating behaviour of the girth gear drives, namely the dynamic behaviour of the drivetrain and the load distribution along the tooth flanks. These operating parameters can be analysed by means of field measurements with the application of strain gauges and the measured figures can be used for setting up suitable calculation models. This enables operating conditions to be simulated and the individual components of the drive system to be mutually matched in an optimum way. Saxer proposes that a combined use of field measurements and calculations is an optimum way of designing drivetrain components, although as mentioned in

this particular case the work was focussed on the modal analysis of the mill foundations.

Fenton[5] discusses failures on rotary kilns in the cement industry caused by vibration and resonance problems. Observed problems included pitting, spalling and cracking on the surface of the gear teeth of the girth gear and pinion as well as on the gears in the reduction gearbox. The experimental studies involved constructing mechanical and electrical control system models to evaluate torsional natural frequency modes and their resonant frequencies. Coincidence of excitations with natural frequencies were checked. Various parameters including pinion shaft torque and gear tooth bending stress were measured in a field testing programme and analyzed to complement the analysis.

Becker[6] examines various on-line condition monitoring systems supplied by the OEMs of grinding mills and reduction gearboxes. These systems include instrumentation to measure various parameters, in-situ processing capability as well as triggering diagnostic alarms for certain operating conditions and sending reports to global drive specialists via internet technology. While these systems provide valuable condition monitoring information and are capable of diagnosing a wide range of possible drivetrain faults, the systems typically make use of accelerometers and vibration measurements and don't specifically measure the loads in the drivetrain system. The information is not used to verify or validate design inputs.

3.2. Failure and Fatigue Analysis

The research in this section was focussed on failure investigations of drivetrain components on similar equipment as well as fatigue analysis techniques.

The failures of shafts of coal pulverizer mills attached to the boiler of an electricity generating thermal plant were analyzed by Parida[7]. The shafts which had a recommended operating life of 100 000 hours were failing after typically only 8000 hours due to fatigue. The objective of the investigation was to determine whether the shafts were failing due to operational reasons due to manufacturing problems. The fabrication of the shafts involved hot forging, homogenisation and proof machining, followed by austenitisation, oil quenching and tempering to obtain the desired hardness. All of the failures occurred in the vicinity of the keyway near the load-bearing end. The failures were unmistakeably due to fatigue, evident from the beach marks on the failure surfaces. The failure analysis was metallurgical in nature and consisted of chemical analysis to determine the composition of the material, microstructural examination of the failed surfaces and hardness profiling. The conclusion of the analysis was that the failures were due to fatigue crack extension under reversed torsional loading and that the initiation and growth of the cracks was due to the brittle microstructures and low material toughness resulting from improper heat treatment. It was recommended that the material specification of components like coal pulverizer mill shafts should not only consist of a minimum strength criterion like hardness, but should also specify a toughness parameter. A quality assurance provision should state that all forgings submitted for heat treatment should make allowance for coupons to be extracted from which impact specimens may be fabricated and tested to verify the material properties.

The multiaxial fatigue failures of welded shaft-flange connections of stirrers under random non-proportional torsion and bending were analyzed by Sonsino[8]. Several multiaxial random fatigue failures of welded coupling flanges of stirrers occurred in a fertilizer plant after a relatively short service life of approximately six months. An investigation was required to determine the reasons for the failures as well as to develop an improved design. Strain measurements carried out at the shaft showed that the stirrers experienced fluctuating torsional loads due to the upward and downward driving from the gearbox and bending loads due to the viscous fluid stirred by impellors at the bottom of the shafts. The analysis of this variable-amplitude loading resulted in two particular cumulative frequency distributions for torsion and bending which then had to be combined to a single equivalent loading spectrum and extrapolated to the estimated period of usage. When using this spectrum for the combined multiaxial loading of the shafts and an appropriate damage accumulation hypothesis, the failures of the welds could be explained and a redesign and optimization of the shaft-flange connections achieved. Of particular interest was that strain measurements were required to quantify the loading on the stirrer shafts and only with this information could a proper analysis be done. It was noted that design of smaller scale stirrers had not experienced any operational problems and that the smaller stirrers had been designed by means of simple calculations and the extensive experience of the manufacturer. Only once the design had been scaled up did the failures start occurring. Some comparisons can be made to the experience with grinding mills. Interestingly the combined loading of bending and torque had to be used to explain the failures. Hamilton's[1] experience with grinding mills concurs – originally the alignment and hence the bending stress in the drivetrain shafts was considered to be negligible and only the torque was measured and analyzed. Later it was realized that a combined loading of bending and torque needed to be measured.

Vogwell[9] describes an investigation which was carried out on a failed wheel/drive shaft component used on an unmanned, remotely operated vehicle for manoeuvring military targets, to determine the cause of the failures and the likelihood of them reoccurring. A study of the broken shaft highlights how vulnerable such a component can be to fatigue failure, even when operating under steady conditions. The analysis considers the effects of both transmission torque and weight (thus bending) upon stress levels and assesses their individual affect on the breakage. The fatigue failure was confirmed by the presence of beach marks radiating outwards from the corner of the keyway are clearly visible. The wheel shaft failure is a classic fatigue problem – high magnitude bending stresses (which alternate between tension and compression) occur together with shear stresses at a sudden change of section location (causing a stress raiser) and premature failure results. The position of the failure, interestingly, is not exactly where the maximum nominal bending occurs (which is at the step change of diameters) but nearby at the end of the keyway region – where stress concentration is greater. At the fillet radius at the step change in diameters, though, the shaft is nearly as vulnerable. Calculations show that bending stress magnitude is much greater than the shear stress caused by torsion due to accelerating and braking, and this combined with the much lower frequency of occurrence of fluctuation of shear stresses effectively eliminates torsion effects as a significant contribution to fatigue damage. This finding has important implications upon possible improvement made to the design. The work concludes

by recommending modifications to the design including shortening the length of the keyway groove, increasing the diameter of the inner portion of the shaft hub and increasing the shoulder fillet radius. Recognition of the vulnerability to fatigue of a rotating component subjected to bending and torsion loading should lead automatically to taking preventative measures at the detail design stage. It is essential to avoid having high stress concentrations at locations of greatest nominal stress if at all possible. Even taking relatively simple measures, such as those described, will greatly improve component reliability without affecting manufacturing costs and prolong the life of components.

JianPing[10] presents a failure investigation of a gear shaft connected to an extruder and details the methods used to identify the causes of the failure on this machine used in a packaging company. Confirmation of the fatigue failure was determined by visually inspecting the fracture surface – beach marks emanating from the vicinity of the key slot were evident. This is typical of a fracture caused by a low stress, high cycle fatigue. The failure investigation comprised of a torsion moment measurement on the operating shaft for two different types of packaging material as well as using a finite element model (FEM) to analyze the stress and strength of the gear shaft. The results from the measurement were used as input loads for the FEM and an equivalent Von Mises stress for the gear shaft was calculated. This equivalent stress was then used in the fatigue analysis. The analysis showed that the fatigue stress amplitude was very close to the fatigue limit of the material but did not exceed it. It was subsequently found that the extruder had often run at higher production rates and that had been a key contributor to the shaft fracture.

In the above examples, the fatigue analysis was primarily conducted by calculating an equivalent fatigue stress and then calculating the expected life of the component, usually by using a simple linear damage rule to predict the life expectancy. Specific details to differentiate between constant and variable amplitude loading and cycle counting methods were considered where applicable. In general, though, this simplified approach seems to have provided satisfactory results and indicates that a similar approach could be used in the case of drivetrain components for grinding mills.

Sutherland[11] in his work on fatigue analysis of wind turbines, reviews the developments made in the fatigue design of wind turbines and describes the “best practices” for the fatigue analysis of wind turbine components. The Palmgren-Miner linear damage rule is used to formulate the fatigue analysis of wind turbines. He notes that this damage rule is currently used throughout the industry, and is a good starting point to begin fatigue analysis.

A final review of cumulative fatigue damage and life prediction theories was conducted to establish whether a more appropriate technique should be applied in the case of drivetrain components for grinding mills.

Fatemi[12] discusses cumulative fatigue damage analysis and the key role it has played in the life prediction of components and structures subjected to field load histories and provides an excellent overview of available techniques. Since the introduction of the damage accumulation concept by Palmgren about 80 years ago and the “linear damage rule” by Miner about 6o years ago, the treatment of cumulative fatigue damage has received increasingly more attention. As a result, many damage models have been developed. Even though early theories on cumulative fatigue damage have been reviewed by several researchers, no

comprehensive report has appeared recently to review the considerable efforts made since the late 1970s. This article provides a comprehensive review of cumulative fatigue damage theories for metals and their alloys, emphasizing the approaches developed between the early 1970s to the early 1990s. These theories are grouped into six categories: linear damage rules; nonlinear damage curve and two-stage linearization approaches; life curve modification methods; approaches based on crack growth concepts; continuum damage mechanics models; and energy-based theories. More than 50 fatigue damage models have been developed since the Palmgren damage accumulation concept and the Miner linear damage rule were introduced, yet unfortunately none of them enjoys universal acceptance. Due to the complexity of the problem, none of the existing predictive models can encompass all of the relevant factors. Consequently, the Palmgren-Miner linear damage rule is still dominantly used in design, in spite of its major shortcomings.

Čačko[13] has developed a computer algorithm for the continuous counting of hysteresis loops of simulated operational processes. This renders possible the continual monitoring of both time history and fatigue damage accumulation. This particular work is highlighted as this technique could be used in conjunction with an on-line monitoring system as discussed earlier to estimate the residual fatigue life of engineering components and structures.

For the purposes of this thesis, however, the Palmgren-Miner linear damage rule will be used as the basis for all fatigue analysis.

3.3. Grinding Mill Case Studies

Failure analysis of ball mill gears by Meimaris[14] details an investigation undertaken to determine the cause of the failure of the pinion and girth gears of two 9MW ball mills which exhibited severe scoring within five months of commissioning. Lubrication failure, torsional vibrations, alignment and gear stiffness were all considered. It was found that the differential stiffness across the face of the girth gears due to casting and structural features, together with sudden power draw changes were the proximal causes of failure.

The torsional vibration investigation involved measuring torque in the pinions in order to assess torsional vibration that may have caused the damage. Strain gauges were attached to both pinion shafts on both ball mill gears and the torsion in the shafts was recorded. The maximum steady-state torque measured was within the design torque of the gears. A frequency spectrum of the torque signals showed that the principal frequencies were the pinion running speed, the third harmonic of this speed and the tooth mesh frequency. The magnitudes of these frequency components were typical of most twin pinion ball mills. Torsional measurements were undertaken several times during the 12 months after the damage was observed. Results proved to be very consistent between tests. In one case, the dynamic torques were measured for a period of three weeks to determine if deviations in the torque were occurring that may not have been picked up in the short term measurements. Results from these tests showed that the torque in the pinions was steady over the three weeks of measurement. The only variations in torque fluctuation amplitudes were those related to changes in the power drawn by the mill. The results from the long-term tests were generally identical to those obtained from the short-term tests over the previous twelve months. This showed that the mill drives were very stable. Only one set of torsional tests showed any

evidence of unsteady torsional behaviour. This set of data was from a test performed approximately two weeks after the gear damage was first observed. The torsional signal recorded during these tests exhibited spikes at random times. The signal showed an increase in torque once per revolution of the pinion for a short time and then the signal returned to steady-state. This behaviour was not noticed in any of the tests taken after this time. It is possible that these torque spikes may have been evidence that metal was being removed from the gears during operation. The generally unremarkable nature of the results obtained from the torsional measurements indicated that torque fluctuations in the drivetrain could be rejected as a contributory cause of the gear damage.

Fenton[15] investigated harmonic wear due to vibration in autogenous and semi autogenous mills. The wear is related to transient and steady-state vibrations which can lead to failures such as heavy wear on gear and pinions, cracked teeth, pinion bearing failure, gearbox and clutch frame failures. Strain gauges mounted in the pinion teeth and on the pinion shaft were used to evaluate the contact stress and shaft stress. Motor shafts were monitored with shear gauges to see the response of the motor shaft. The data from one mill showed the effect of transient shock loads that occurred during start-up due to the inability of the liquid rheostat to function properly and optimize the starting and ring shorting shocks. In this case, a weak starting shock was followed by large ring shorting shock of 4.5 times the rated power, which cracked the mill foundations and caused misalignment of the gear and pinions. In a second case, high transient shock loading occurred in a SAG mill which was accelerating to full load in approximately one second. The controller for startup was not optimized since the ring shorting shock was low. Repeated starts in this condition caused broken pinion and gear teeth which lead to long repair times. Data was presented which shows the magnitude of the shock load and the improvement made by using strain gauge methods to determine electrolyte density for optimum conditions. Other cases where steady-state vibrations resulting in harmonic wear were also discussed.

Kress[16] provides some insight on the use of service factors in the design of gears. The design starts with power and speed specified by the mill builder. The user then determines the life requirements, the reliability and the downtime risk acceptability. Evaluating these parameters sets the service factor to be used in the AGMA 321.05 pitting resistance rating formula. The service factors range from 1.50 to 2.00 with 1.50 being the AGMA minimum. In addition to pitting resistance, a bending strength service factor must also be calculated. The AGMA minimum is 2.4 with the normal accepted values between 2.40 to 3.00. In large SAG operations many consultants are recommending 1.75 for pitting resistance and 2.50 for bending strength. It was not mentioned on what basis the consultants make this recommendation.

The author has also attended an international conference on milling (SAG Conference 2006) and has co-authored two conference papers concerning mill failures entitled:

- “Grinding mill drivetrain failures in the minerals processing industry” (Wainwright KA and Diering RP, Failures 2006, February 2006) and
- “Lessons learned from recent failures of gear drives on mills in South Africa” (Hamilton RH, Wainwright KA and Diering RP, SAG Conference, September 2006).

In summary, the literature highlights the effectiveness of the approach of using load data from field measurements in conjunction with calculations and/or other techniques such as FEM to accurately design drivetrain components. No literature could be found which specifically addresses quantifying the loads in the drivetrain components of grinding mills by means of field measurements hence highlighting the necessity for the work covered by this thesis.

4. OBJECTIVES

Numerous failures of drivetrain components of grinding mills have occurred within the mining industry in South Africa indicating a need to research and resolve this problem. A literature survey has shown that strain-gauging has been used extensively to determine the bending moment and torsional stresses in drivetrain components. Cumulative fatigue damage models and computational simulation techniques have also been successfully applied to predict the fatigue damage of drivetrain components. No research, however, on the specific application of strain-gauging and fatigue analyses applied to grinding mill drivetrain components can be found in the literature.

The objectives of this research are to:

1. Use strain gauges to measure the bending stress and torsional shear stress in the drivetrain shafts of grinding mills to quantify the loading the drivetrain components are exposed to.
2. Record the number of times grinding mills are stopped and restarted again per month over an extended period to develop a usage profile and understand the operating practices that these machines are exposed to.
3. Process the measured data (from objective 1) and verify that the current design methodology is appropriate and that the failures are not due a poor design.
4. Use the data (from objectives 2 and 3) to estimate the total fatigue life of the drivetrain components when subjected to the measured loading. The analysis will be used to assess the contribution of distinct operating patterns to the overall fatigue damage of the drivetrain components.
5. Use the conclusions (from objectives 3 and 4) to develop guidelines for designers and operators of grinding mills to improve the operational life of these components.

5. EXPERIMENTAL PROCEDURE AND DATA PROCESSING

In order to accurately quantify the loading on the mill drivetrain, the test procedure involved measuring the shaft torque on the high speed shaft as well as the shaft torque and the bending moment on the low speed shaft by means of strain gauges. The measured signals would be transferred from the rotating shafts to stationary recording equipment by means of a telemetry system, the details of which are given below. The measurements were to be carried out on both single and dual drive mills with installed power ranging from 1 MW to 14 MW so as to obtain a representative sample of the installed base of mills. Due to the cost of the loss of revenue for the operators of these mills, the testing time had to be kept to a minimum. For each mill therefore, 3 stop/start cycles of approximately 5 minutes each were recorded.

A total of 22 single drive mills and 8 dual drive mills were tested. The details are included in Appendix A and a summary is given in Table 2.

The majority of the mills tested are owned by Anglo American Platinum and are situated around Rustenburg. A number of mills belonging to AngloGold Ashanti, Goldfields and Lonmin Platinum were also tested. All tests were conducted by Anglo American Technical Division.

Table 2 Summary of Mills Tested

Drive Configuration	Anglo American Platinum	AngloGold Ashanti	Other	**Total**
Single Drive	15	2	5	**22**
Dual Drive	7	0	1	**8**

5.1. Instrumentation

The details of the instrumentation and test equipment used for the measurement exercises are provided in this section.

5.1.1. Sensors

Kyowa 350Ω T-gauges (KFG-5-350-D16-11L1M2S), configured as full bridges were applied to the motor and pinion shafts to measure torsion. The gauge pairs were mounted 180° apart to eliminate transverse shear sensitivity on the torsion bridge. The setup is illustrated Figure 2. The strain gauge details are included in Appendix B.

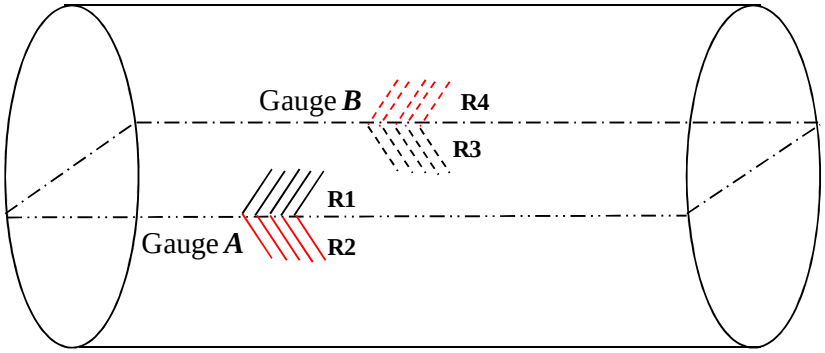

Figure 2 Strain gauge setup for torque measurements

The identical Kyowa 350Ω T-gauges were also used to measure bending. The gauge setup for the bending measurements is illustrated in Figure 3.

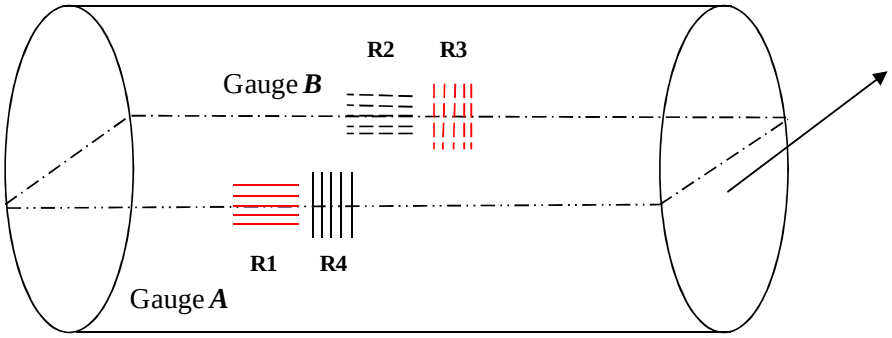

Figure 3 Strain gauge setup for bending measurements

The gauges on the motor shaft were placed between the motor and the high speed coupling (See Figure 4). The gauges on the pinion shaft were placed between the low speed coupling and the drive-end bearing (See Figure 5). A schematic diagram of the pinion shaft is also included in Figure 6. The overall layout of the instrumentation is illustrated in Figure 7.

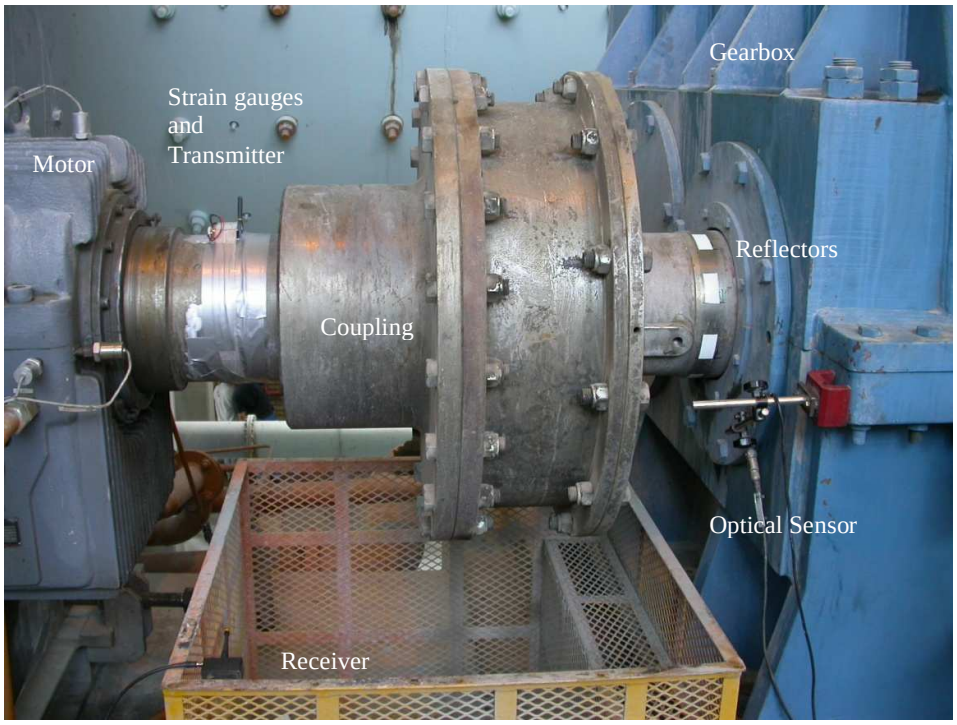

Figure 4 Instrumentation on Motor Shaft

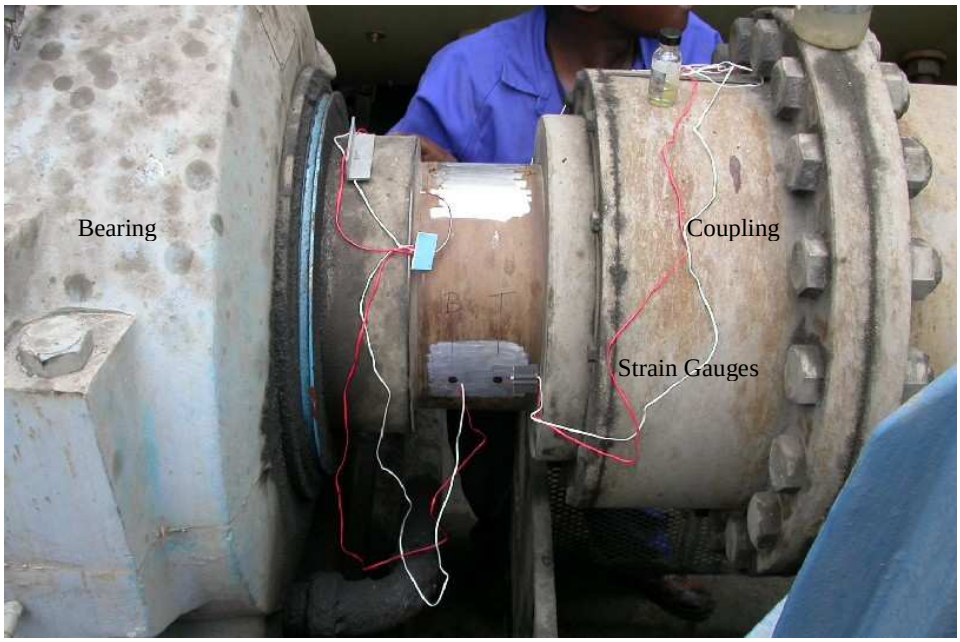

Figure 5 Instrumentation on Pinion Shaft

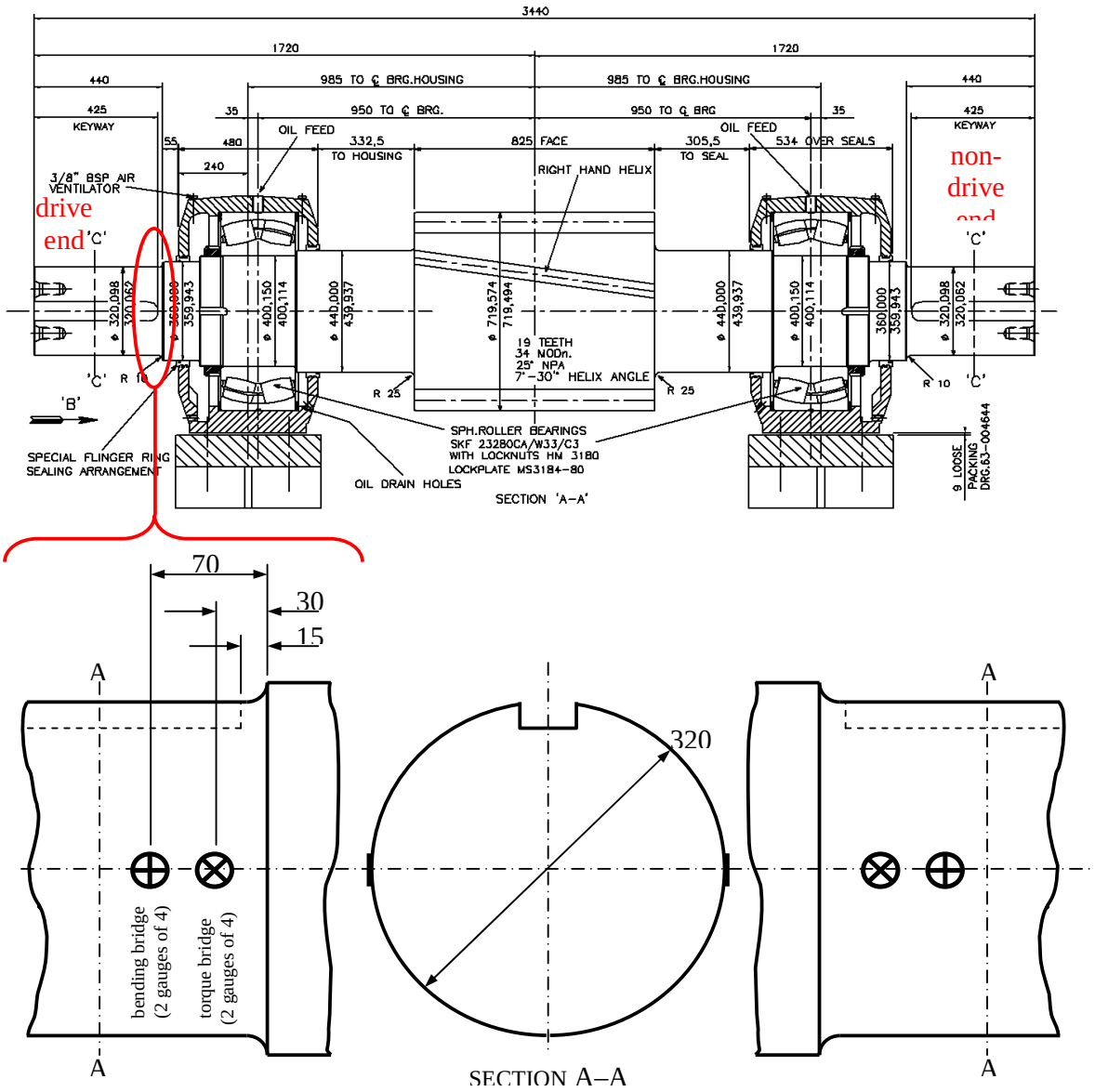

Note: Typical dimensions in mm are indicated on the schematic – actual values vary from mill to mill.

Figure 6 Schematic diagram of pinion shaft

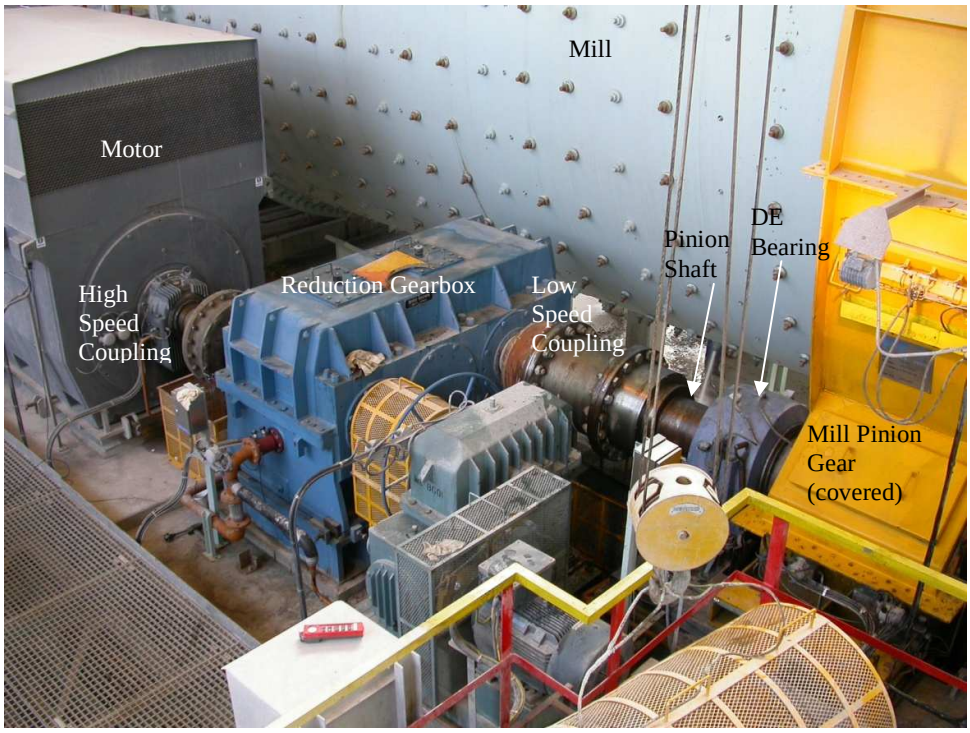

Figure 7 Overall Layout of Mill Drivetrain

Optical sensors (See Figure 4) were used to measure the motor and/or the pinion shaft speed. The sensors would detect reflectors that were stuck to the shaft to produce a pulse trace which was then converted to speed. The accuracy of the measurement depended on the number of reflectors which were used. Often due to time constraints the number of reflectors was limited to 6 which limited the accuracy of the speed data. The instrumentation was therefore changed and a tachometer was used to measure the speed (See Figure 8). For some of the tests, the optical sensors were used to detect the position of the girth gear joints, which was required for the frequency analysis.

Figure 8 Speed Measurement by means of Tachometer

5.1.2. Telemetry

A Binsfeld TorqueTrak 9000 digital telemetry system was used to transfer the measured signals from the rotating shafts to the stationary recording equipment. The system consists of a battery powered transmitter that is fixed to the rotating shaft and transmits the signals directly to the stationary receiver unit. The receiver unit is connected to separate recording equipment. The transmitter and receiver units are illustrated in Figure 9 and the specification sheet is included in Appendix B.

Figure 9 Binsfeld TorqueTrak 9000 Telemetry System

The connections between the strain gauges and the Binsfeld shaft-mounted transmitter are illustrated below. Figure 10 shows the connections for the torque measurements and Figure 11 shows the connections for the bending measurements.

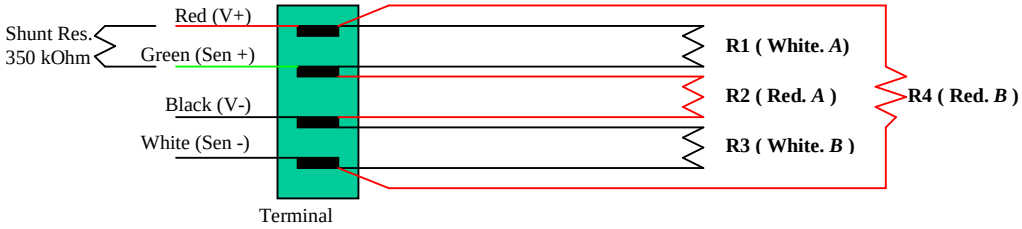

Figure 10 Connection diagram for torque measurements

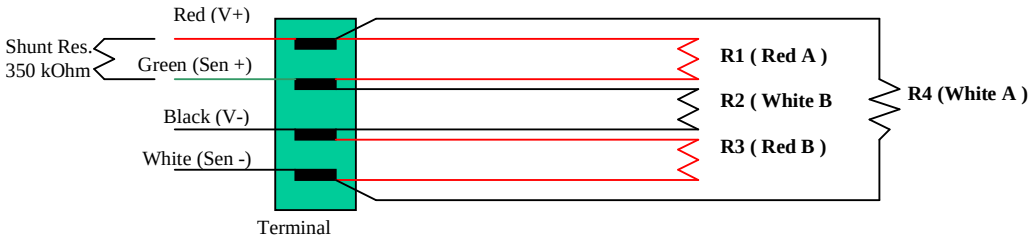

Figure 11 Connection diagram for bending measurements

5.1.3. Recording

The analogue signals from the Binsfeld telemetry receivers and the optical sensors are coupled to a SOMAT e-DAQ lite field computer, which records the test data. The unit is capable of a range of sample rates, however for the majority of the tests the sample rate was set to 1000 Hz per channel. The signals were not filtered or modified in any way during the recording process. The durations of the recordings varied due to operational influences, however, were all short-term and did not exceed 60 minutes. The unit is pictured in Figure 12 and the specification sheet is included in Appendix B.

Figure 12 SOMAT e-DAQ lite Field Computer

5.1.4. Calibration

The signals are calibrated by shunting each of the strain gauge bridges in turn with a 350 kΩ shunt resistor. The calibration is required to measure the full scale voltage of the installed instrumentation and is recorded for each test to be used in the data processing thereby ensuring the accuracy of the measurements. Full details of the conversion from measured voltage to engineering units are discussed in Section 5.2. An example of the Matlab routine used to perform this function is included in Appendix C.

5.2. Data Processing

Test results are processed using Matlab to convert the measured voltage signals into engineering units e.g. kNm and MPa. The formulae used together with sample data of a typical mill are included below. An example of the Matlab routine used to perform this function is included in Appendix C.

5.2.1. Shunt Calibration of Strain Gauge Bridges

The principle of shunt calibration described by Hoffmann[17] involves using a shunt resistor, R_p, to unbalance the bridge circuit (See Figure 13).

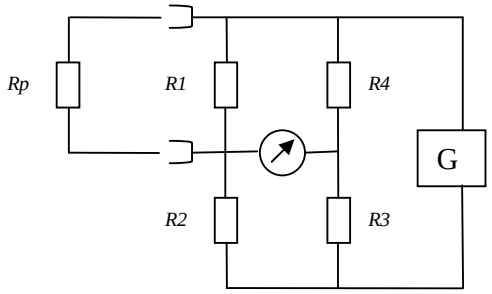

Figure 13 Principle of Shunt Calibration

Gauge factor (k) = 2.11

Gauge resistance (R) = 350.9 Ω

Shunt resistance (Rp) = 350 kΩ

The shunt-induced strain is calculated using the following formula:

$$\varepsilon_s = \frac{1}{k}\left(\frac{R_s}{R+R_s} - 1\right) \qquad = 474.68\ \mu m/m$$

The signals are recorded while the shunt resistor is placed across each of the strain gauge bridges. The shunt-induced voltage is calculated from the recorded trace as shown in Figure 14 below. The shunt-induced voltage is 1.2 volts.

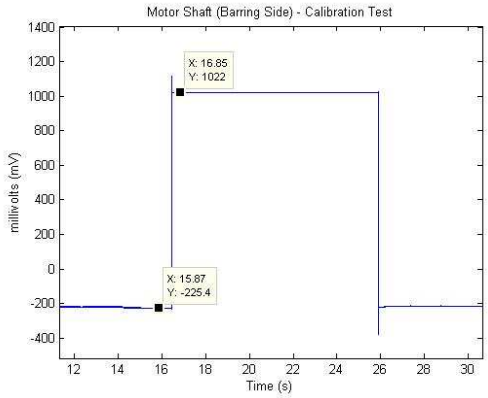

Figure 14 Shunt Induced Voltage

5.2.2. Signal Interference

The raw data from the tests would have to be "cleaned" due to a number of telemetry errors caused by interference from two-way radios and mobile phones used by plant personnel. A typical example of raw test data with the signal errors is illustrated in Figure 15. Several automatic "despiking" routines were investigated to remove the erroneous parts of the signal but it was discovered that the routines could not distinguish between errors and actual transients accurately enough (See Figure 16). The result was that important parts of the signal were being filtered out. The "cleaning" of the raw data was therefore done manually in Matlab where the user could select a corrupt section of the signal and replace it with an artificial signal of equivalent size (data points) and average magnitude by means of interpolation.

The erroneous parts of the signal were also typically very short in duration and hence the replacement method did not adversely change the overall integrity of the data.

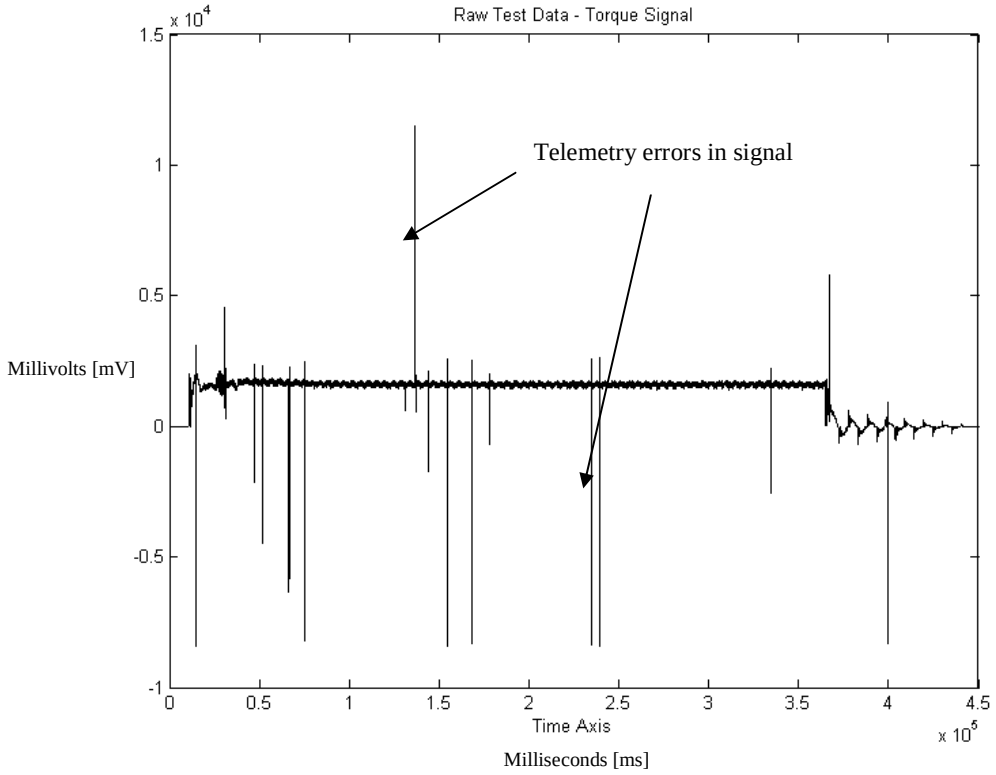

Figure 15 Raw data with telemetry errors

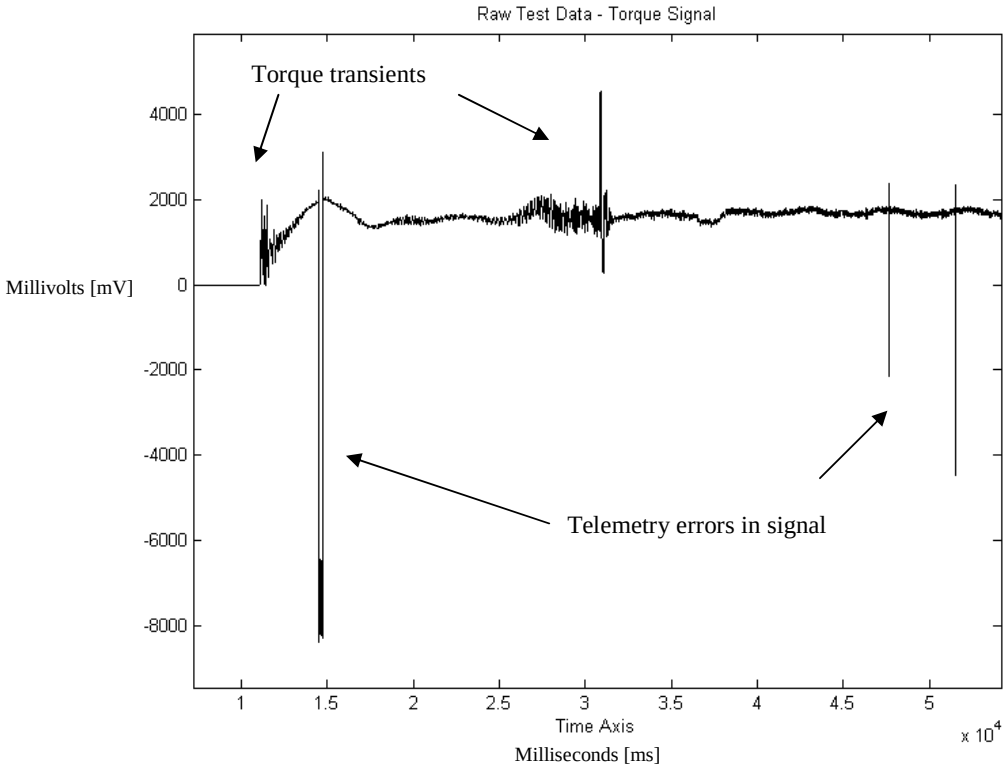

Figure 16 Zoomed view of raw test data with telemetry errors

5.2.3. Torque Measurements

The pertinent input data (example values for a typical mill are included) and formulae used to process the torque data are shown below.

Elastic modulus (E) = 207 x 10^9 Pa

Poisson's ratio (v) = 0.3

Motor shaft diameter (dp) = 0.2 m

Pinion shaft diameter (ds) = 0.31 m

Shear modulus

$$G = \frac{E}{2(1+v)}$$ = 79.6 x 10^9 Pa

Polar section modulus (keyway ignored in calculation)

$$Z_p = \frac{\pi d^3}{16}$$ = 1.57 x 10^{-3} m^3 for the motor shaft

Shear stress to indicated strain ratio

$$\frac{\tau}{\varepsilon_i} = \frac{G}{2}$$

Overall factor for shear stress

$$\frac{\tau}{V_i} = \frac{\tau}{\varepsilon_i} \times \frac{\varepsilon_s}{V_s} \qquad = 15 \text{ MPa/V}$$

Torque to shear ratio

$$\frac{T}{\tau} = Z_p$$

5.2.4. Bending Measurements

The pertinent input data and formulae used to process the torque data are shown below.

Section modulus (keyway ignored in calculation)

$$Z = \frac{\pi d^3}{32} \qquad = 2.92 \text{ x } 10^{-3} \text{ m}^3 \text{ for the motor shaft}$$

Bending stress to indicated strain ratio

$$\frac{\sigma_b}{\varepsilon_i} = \frac{E}{2(1+\nu)}$$

Overall factor for bending stress

$$\frac{\sigma_b}{V_i} = \frac{\sigma_b}{\varepsilon_i} \times \frac{\varepsilon_s}{V_s} \qquad = 30 \text{ MPa/V}$$

Bending moment to bending stress ratio

$$\frac{M_b}{\sigma_b} = Z$$

5.2.5. Speed Measurements

An optical sensor was used to detect reflectors that were mounted to the shaft to produce a pulse trace (See Figure 17) which was then converted to rotational speed (rpm) (See Figure 18). An example of the Matlab routine used to perform this function is included in Appendix C.

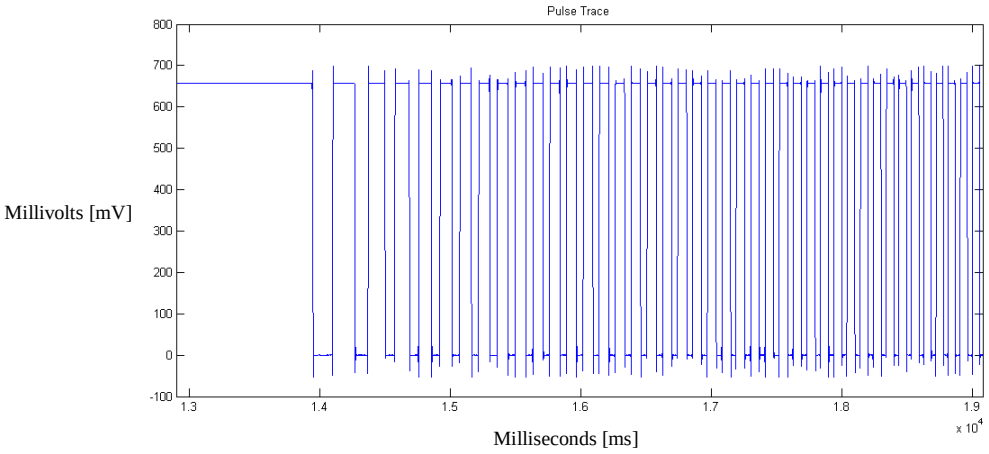

Figure 17 Pulse Trace

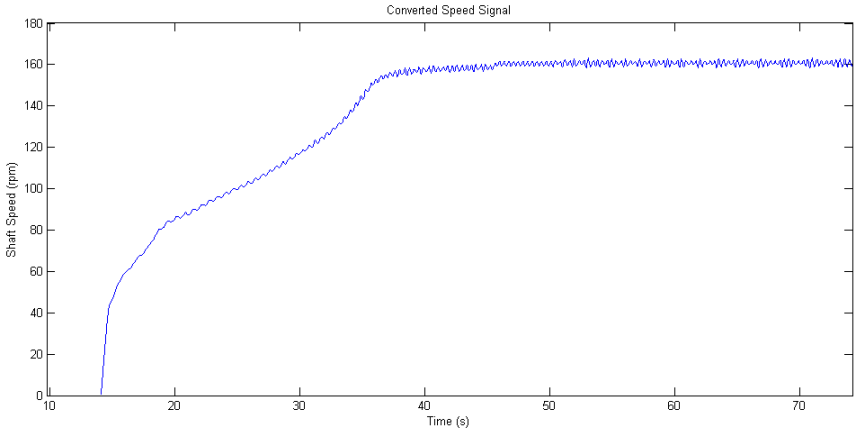

Figure 18 Converted Speed Signal

5.2.6. Processed Data

The test data was processed using a series of Matlab routines that subtract the zero offset of the test signal and multiply by the gain factors for torque and bending discussed above to convert the measured voltage signals into engineering units. An example of the Matlab routine used to perform this function is included in Appendix C.

An example of processed data for a typical mill is shown in Figure 19 shows the motor shaft torque, the pinion shaft torque and bending as well as the pinion shaft speed.

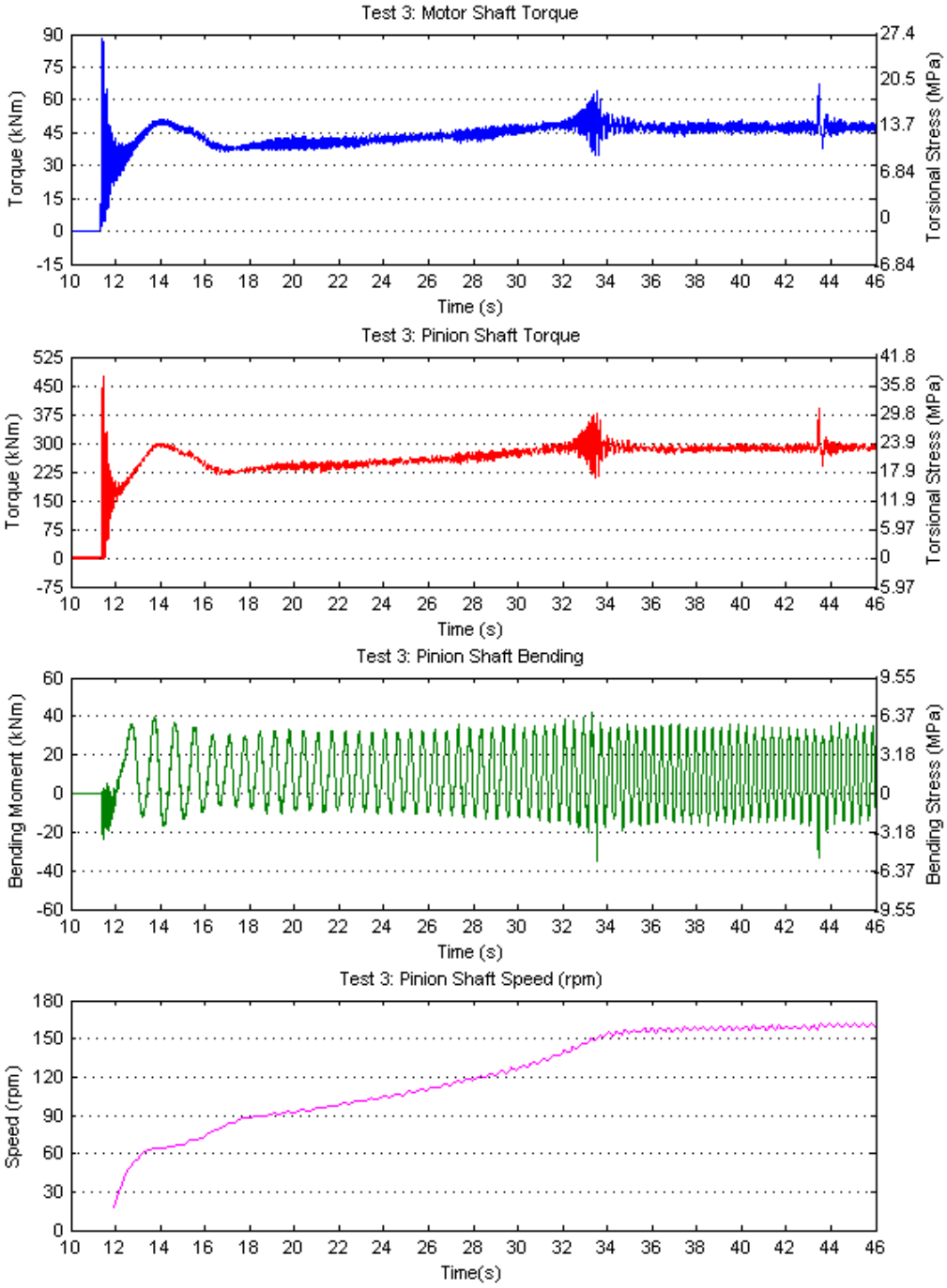

Figure 19 Example of Typical Processed Test Data

6. DATA ANALYSIS AND TEST RESULTS

6.1. Data Analysis

6.1.1. Quantitative Analysis

The test data was analyzed and several distinct characteristics were identified. Matlab routines were used to extract the peak and average values from the test data. An example of the Matlab routine used to perform this function is included in Appendix C. The values were expressed as a percentage of the motor rated torque so as to quantify the magnitude of the loads in relation to the design capacity of the mill drivetrain. The distinct torque characteristics for a single drive mill are illustrated in Figure 20, where:

1 – Maximum switch-on torque – the peak transient torque when the motors are energised

2 – Torque variations as the mill accelerates to full speed influenced by the material behaviour in the mill as well as possible torsional resonance of the mill and drivetrain

3 – Maximum short-circuit torque – the peak transient torque when the motor slip rings are short circuited by the contactor at the liquid resistance starter once the mill has reached full speed

4 – Average operating torque – the average steady-state torque

5 – The range of the steady-state torque oscillations

6 – Switch off

7 – Side to side rocking action of the mill as it comes to a complete stop

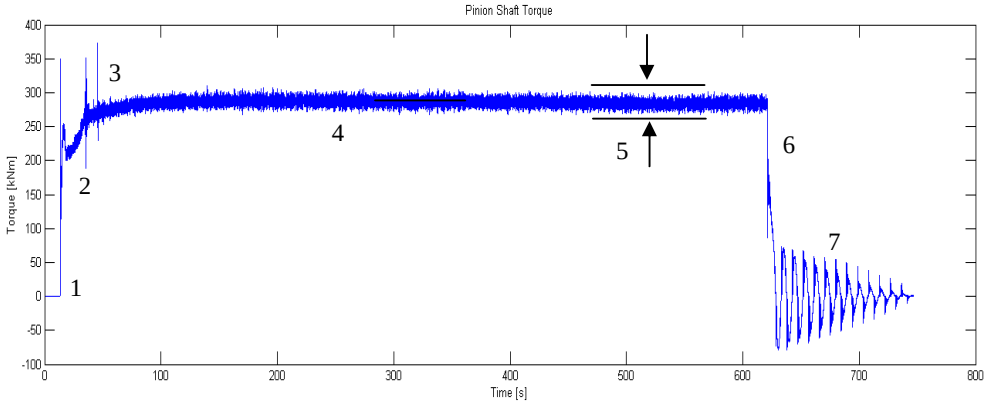

Figure 20 Torque Trace with Identified Characteristics

The torque characteristics for a dual drive mill are very similar except that an additional characteristic is present which occurs when the first rotating, shaft-mounted slip ring is short-circuited and the brush lifting gear operates. The result is a temporary increase in torque on the side with the motor whose slip rings are short-circuited first. The acceleration of the mill plus the two motors causes the motor with the slower operating short-circuit gear to momentarily deliver less torque. This is illustrated in Figure 21 and Figure 22.

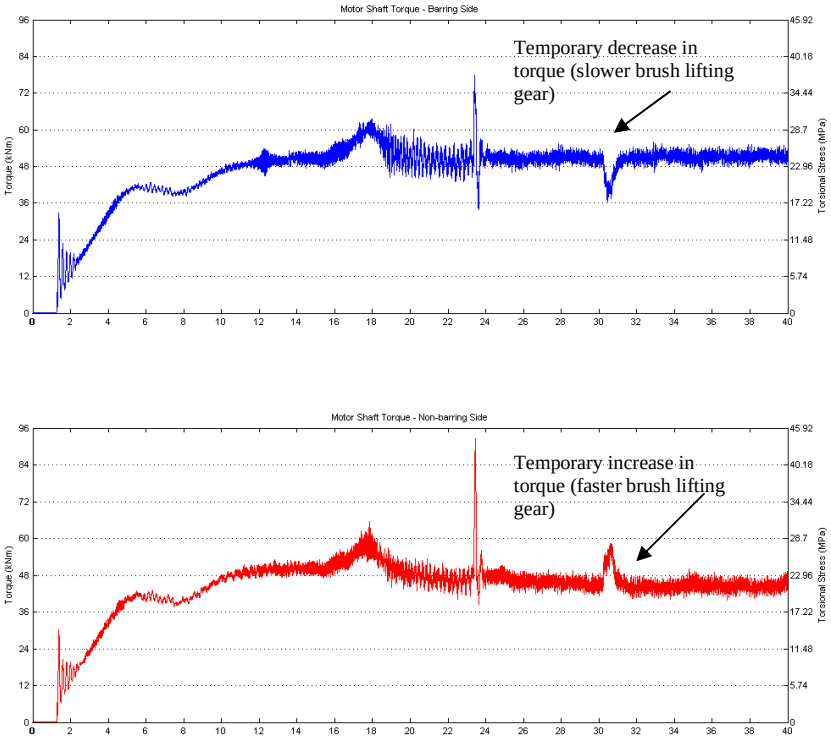

Figure 21 Torque changes due to the operation of brush lifting gear – Example 1

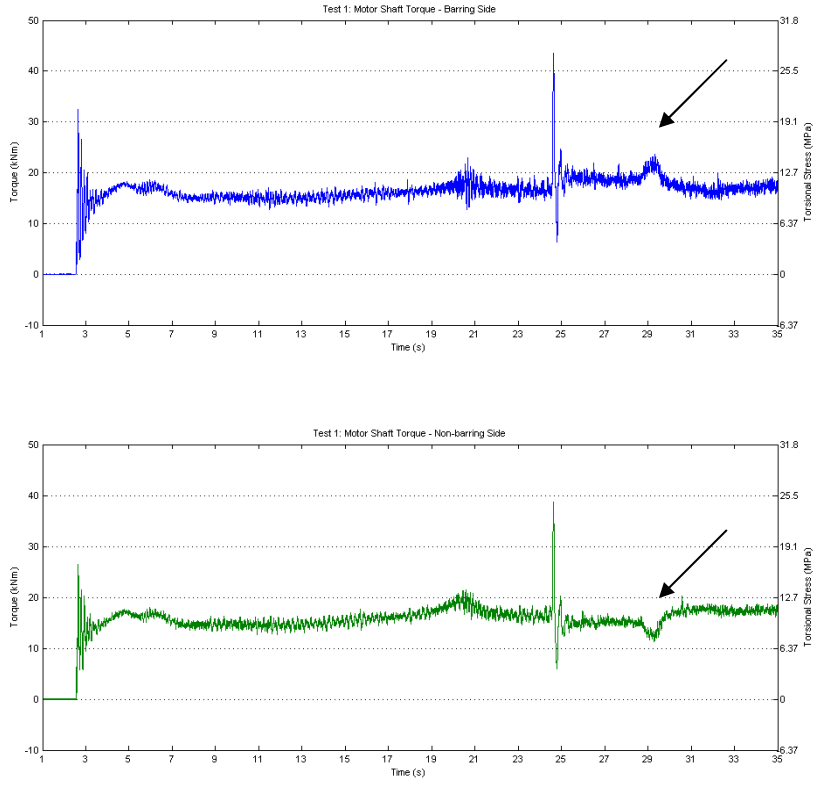

Figure 22 Torque changes due to the operation of brush lifting gear – Example 2

In order to study the torque variations during the acceleration of the mill, the torque was compared to speed as well as the mill angle of rotation. This section of the torque data has two distinct features. The first is the peak torque reached before the material starts to fall in the mill and usually occurs between 45 and 60 degrees of mill rotation depending on the material type. The second distinct feature resembles a vibration or resonance in the drivetrain and usually occurs as the mill reaches approximately 90% of full speed. Examples from two different mills (but with the same drive power and configuration) are included in Figure 23 and Figure 24 below to illustrate how these torque characteristics can vary from one mill to another.

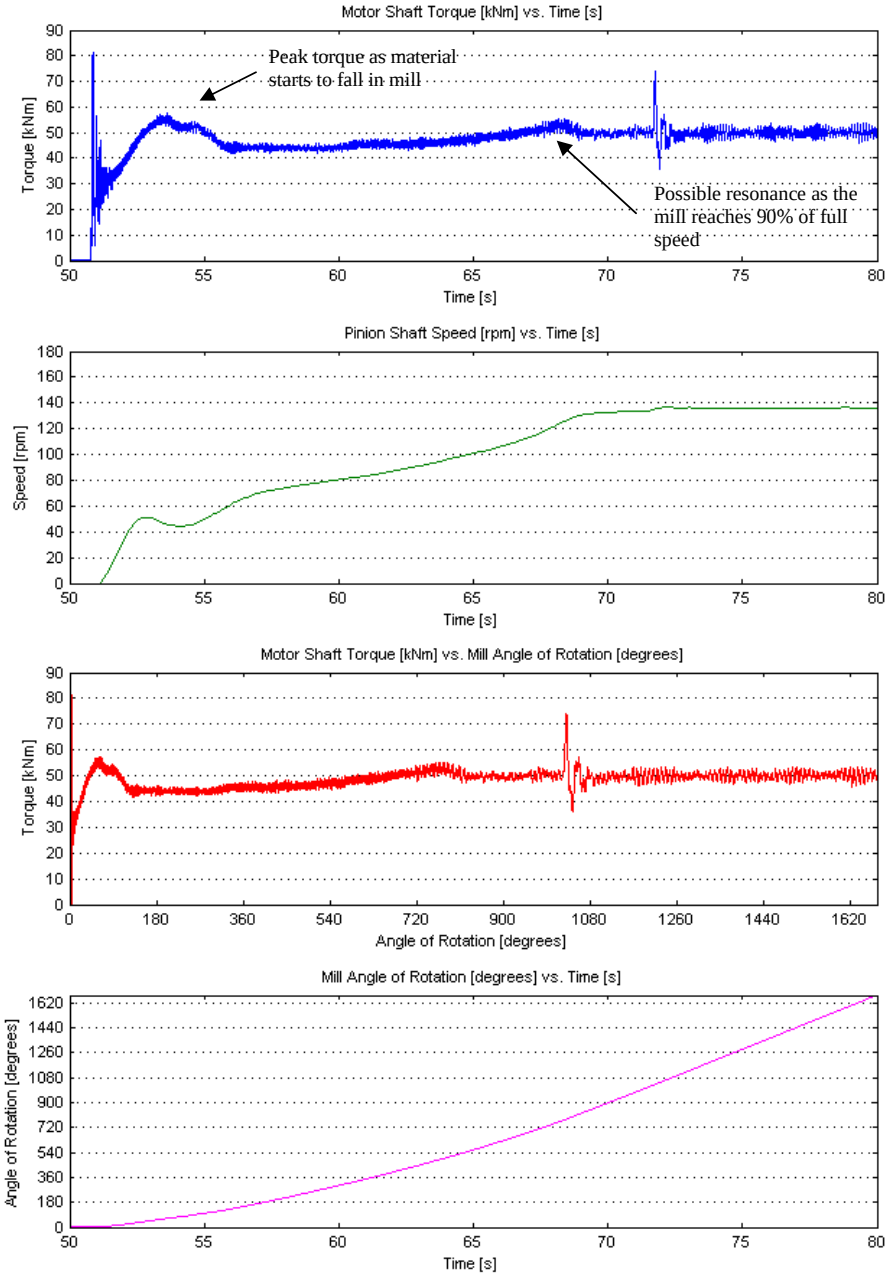

Figure 23 Mill Angle of Rotation – Example 1

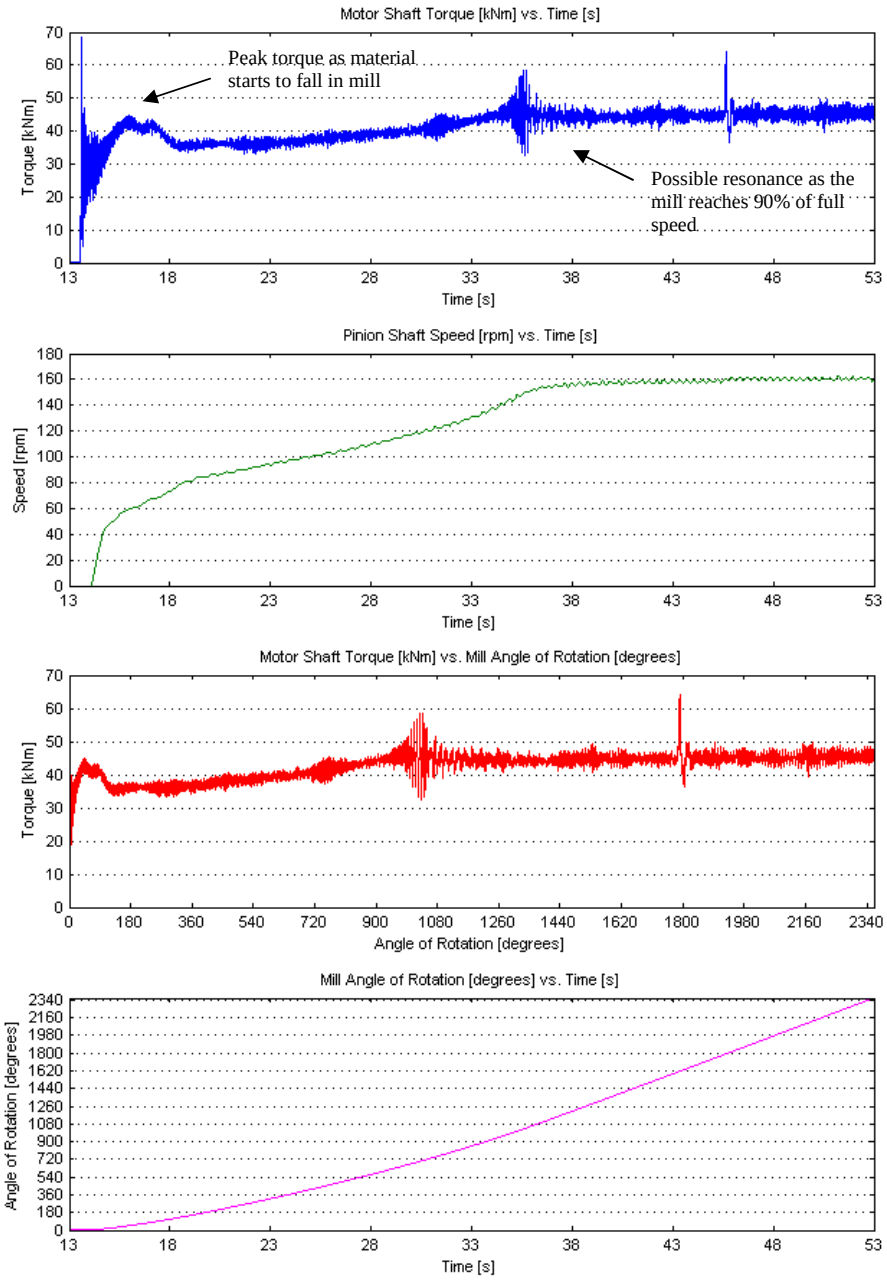

Figure 24 Mill Angle of Rotation – Example 2

The average bending stress range values (peak to peak) measured on the pinion shafts during the steady-state condition were also calculated. The peak transients in the bending signal correspond to the characteristics identified in the torque signal i.e. switch-on, peak material load, torsional resonance and short-circuit. An example is included in Figure 25.

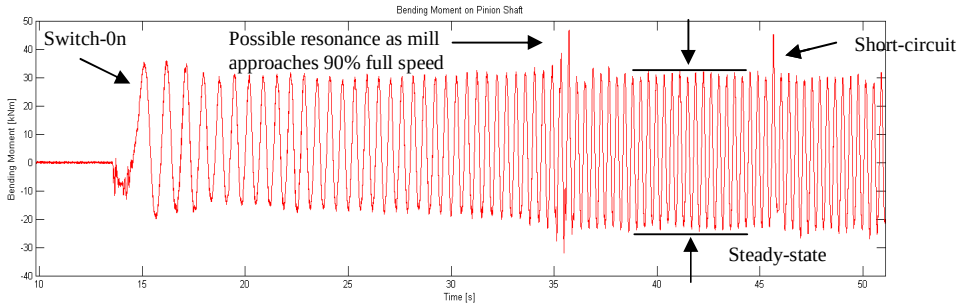

Figure 25 Bending Moment on Pinion Shaft

Apart from normal operation, the mills also undergo a process known as barring. Operators use this technique to break up settled material in the mill after long stoppage periods. To bar the mill, a separate inching drive is used, which turns the mill very slowly and thus gives the material enough time to break up as it reaches its highest point in the mill. This is an important procedure and prevents a locked charge event which results when settled material moves right around to the top of the mill shell (when started normally) and then suddenly collapses resulting in catastrophic damage to the mill. The process is illustrated in Figure 26.

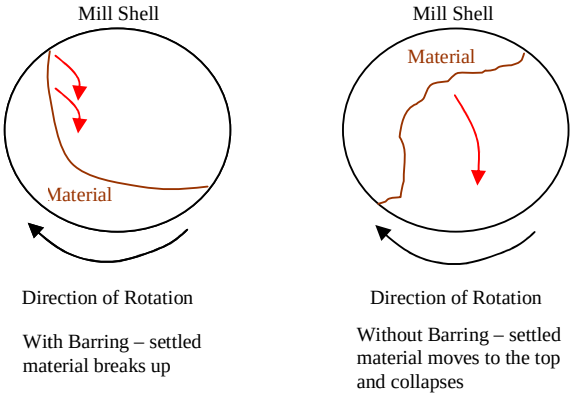

Figure 26 Barring Procedure

The torque and bending on the pinion shaft were measured during the barring process. A typical example is shown in Figure 27. Note that in the case of the dual drive mills that were tested, all of them had a single drive barring arrangement i.e. the inching drive was only fitted on one side hence the terms barring and non-barring side of the dual drive mill.

Several distinct torque characteristics were identified during the barring process. The distinct torque characteristics are illustrated in Figure 27, where:

1 – Maximum switch-on torque – the peak transient torque when the motors are energised

2 – The peak torque reached before the settled material starts to break up

3 – The average operating torque as the material turns over itself

4 – A constant torque as the inching drive is stopped and the inching drive brakes are applied thus holding the mill in a fixed position

5 – A reduction in torque as the operator allows the mill to rotate back towards a position of equilibrium by releasing the brakes. The mill overshoots its position of equilibrium and the brakes are reapplied.

6 – The inching drive turns the mill in the opposite direction until the material starts to break up again

7 – Operators can typically drive the mill from side to side until they are satisfied that the material is sufficiently loose and then return the mill to its equilibrium position ready for a normal start

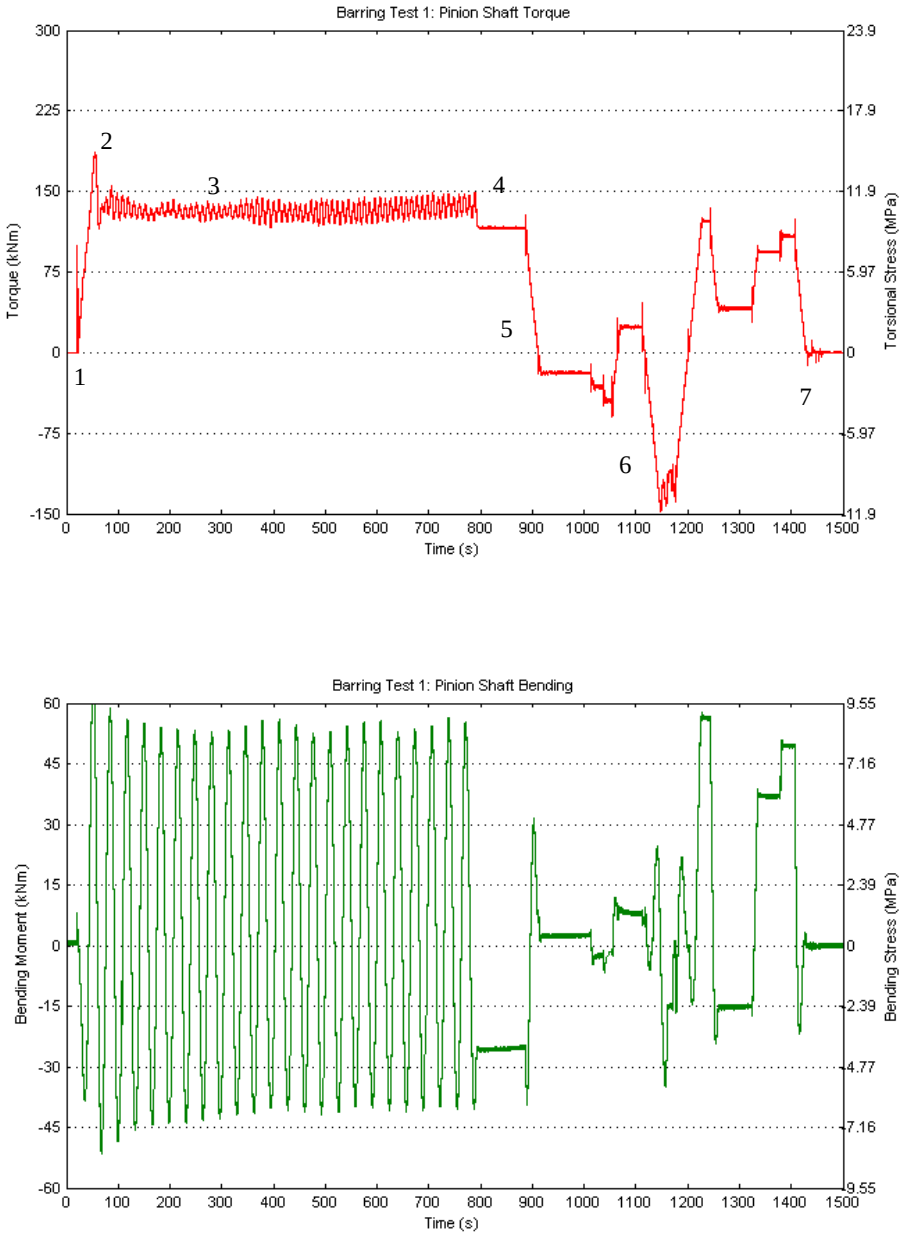

Figure 27 Pinion Shaft Torque and Bending for the Barring Procedure

The bending stress values (range) measured during barring and normal operation were also compared. A typical example of the bending stress measured during barring operations is also included in Figure 27.

Some analysis of the rise times of the peak switch-on torque and the peak short-circuit torque was carried out to understand the nature of the applied load. Two cut-off criteria were used, namely 10% and 90% of the value of the peak transient as well as 20% and 80% of the value of the peak transient. These criteria are the two norms for calculating rise times. It was found that in all cases the rise times were between 10 ms and 40 ms, which classify the torque transients as shock loads.

6.1.2. Frequency Analysis

Power spectral density (PSD) plots of the steady-state torque oscillations were created for each of the test signals in order to identify the dominant frequency components of the torque signal. The dominant frequencies were then compared to the expected frequencies within the drivetrain to check for torsional resonance which increases the magnitude of the torque oscillations and thus the loading on the drivetrain.

The expected frequencies are listed below.

- Mill Speed
- Pinion Shaft Speed
- Mill Shell Liner Passing Frequency. The mill shell liner passing frequency is caused by the mass of the wear liners installed inside the mill shell. The number of wear liners vary between 20 and 35 and are evenly spaced around the circumference of the mill shell.
- Motor Shaft Speed
- Mill Pinion Gear Mesh Frequency
- Main Reducer Gear Mesh Frequency

Comparisons were made between the results for the motor and pinion shafts as well as between the two sides of the mill in the case of dual drive mills.

6.1.3. Mill Stop/Start Frequency

The mill stop/start frequency is the number of times the mill has had to be restarted after it has tripped or been stopped for some reason and provides a useful gauge of the operational usage profile of the grinding mill. Typical reasons for mill stoppages include mechanical, electrical or instrumentation problems or for scheduled maintenance or for process reasons. The mill start/stop frequency is normally calculated

monthly and should range between 3 and 5 stops per month. Suppliers always recommend that the number of starts should be kept to a minimum in order to reduce the number of times the drivetrain components are exposed to the high start-up loads.

Due to the short-term nature of the tests, the mill stop/start frequency for the mills tested could not be determined from the test data. This information though is important, especially from a fatigue analysis point of view, and was hence recorded by the site management at the various test operations by means of the plant control systems.

6.2. Test Results

The test results are presented in this section as follows:

- Torque results for single and dual drive mills for the identified characteristics i.e. peak switch-on torque, peak short-circuiting torque, amplitude of the steady-state torque oscillations, barring operations and switch off.
- Bending results for normal and barring operations
- Frequency analysis
- Mill stop/start frequency

6.2.1. Torque Results for Single Drive Mills

The motors of the grinding mills are controlled by a soft start device which limits the current supplied to the motor and hence controls the torque response during start-up. The torque characteristics as described in Section 6.1.1 were found to vary depending on the soft start device employed. Three different types of soft start devices were encountered across the various mills that were tested. They were fixed grid resistor type starters (Grid), liquid rheostat or liquid resistance starters (LRS) and enhanced liquid resistance starters (E-LRS). The majority of the single drive mills tested had liquid resistance starters installed. The test results in this section are presented in three parts per soft start device.

The switch-on peak torque and the short-circuiting peak torque values have been analyzed and the average and standard deviation values for each of the mill powers are presented in tabular format. The results for the mills with LRS are also presented graphically.

The torque values are expressed as a percentage of the motor rated torque in order to simplify the comparison of results between the different mills as well as to easily indicate by what factor the measured values exceed the nominal rated value. The calculation of the motor rated torque for a typical mill is shown below.

Motor rated power [P]	= 5200 kW
Motor speed [N]	= 995 rpm
Reducer gearbox ratio	= 113/20
Pinion shaft speed	= 176 rpm
$P = T.\omega$	
$\omega = 2.\pi.N$	
Motor rated torque [T]	= 49.91 kNm
Pinion shaft torque	= 281.97 kNm

The measurements were taken at different times and with different operating loads for the different mills. An indication of the mill loading was the average operating torque as a percentage of the motor rated torque. The mill loading ranged between 60% and 100% for the different measurements taken. For the purposes of comparing the measured data all values were factored so that the average operating torque equalled the motor rated torque i.e. 100%.

Table 3 Test Results for Single Drive Mills with Grid Starters

Mill Power [kW]	Switch-on Torque [% Motor Rated Torque]		Short-circuit Torque [% Motor Rated Torque]	
	Average Peak Value	Standard Deviation	Average Peak Value	Standard Deviation
1200	**542.73**	**331.99**	**323.57**	**59.83**

Table 4 Test Results for Single Drive Mills with LRS Starters

Mill Power [kW]	Switch-on Torque [% Motor Rated Torque]		Short-circuit Torque [% Motor Rated Torque]	
	Average Peak Value	Standard Deviation	Average Peak Value	Standard Deviation
6400	220.09	50.50	222.51	37.77
5200	149.62	52.03	180.14	55.49
4000	267.65	39.42	190.14	10.10
3250	257.86	35.63	221.79	11.58
3200	207.69	34.47	170.27	1.64
2800	198.92	20.25	166.96	5.38
2500	289.32	28.20	207.74	3.32
1800	273.83	46.97	214.33	45.35
Average	**233.12**	**38.43**	**196.74**	**21.33**

Table 5 Test Results for Single Drive Mills with E-LRS Starters

Mill Power [kW]	Switch-on Torque [% Motor Rated Torque]		Short-circuit Torque [% Motor Rated Torque]	
	Average Peak Value	Standard Deviation	Average Peak Value	Standard Deviation
5200	**91.80**	**19.82**	**118.85**	**4.46**

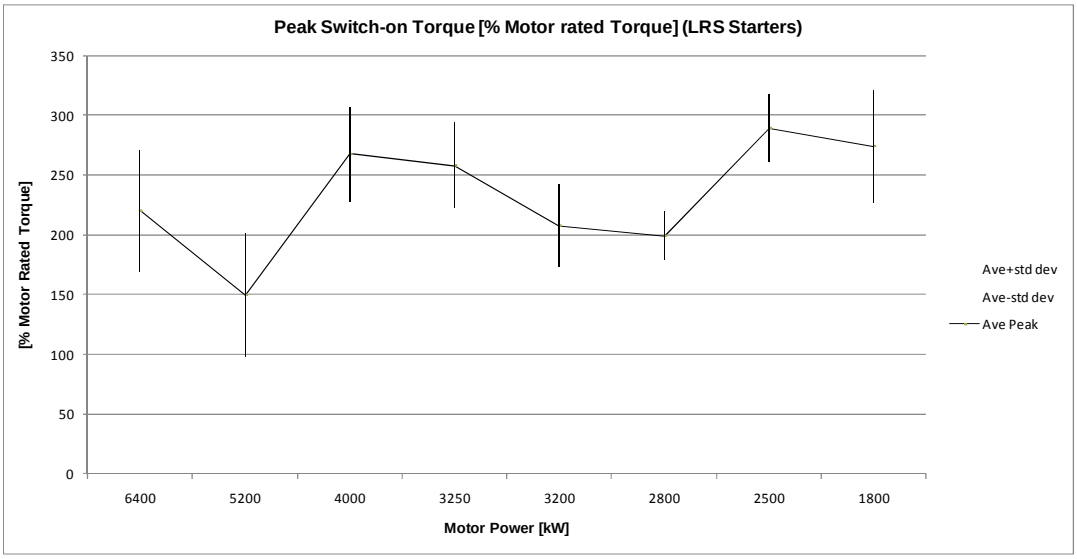

Figure 28 Peak Switch-on Torque for Mills with LRS Starters

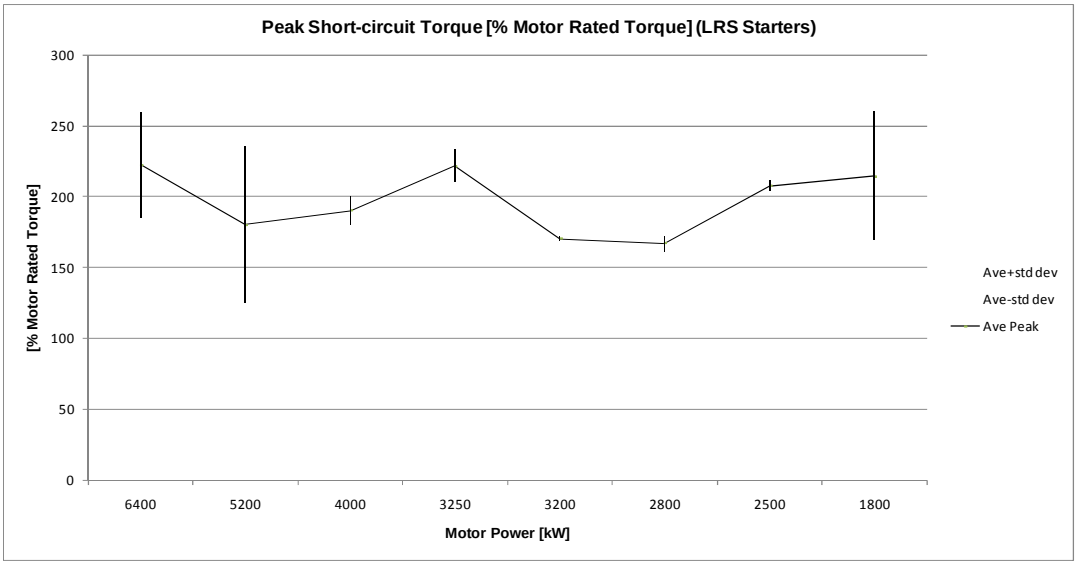

Figure 29 Peak Short-circuit Torque for Mills with LRS Starters

The average results for the three different types of starter for single drive mills are included in Table 6. The results show that the E-LRS starter is the best system from a peak loading point of view with an average peak switch-on torque of 92% of motor rated torque and an average peak short-circuit torque of 119% of motor rated torque. The E-LRS is approximately twice as good as a conventional LRS system which has an average peak switch-on torque of 233% of motor rated torque and an average peak short-circuit torque of 197% of motor rated torque.

The Grid starter system is poor and results in very high peak loads being transferred into the drivetrain system. It has an average peak switch-on torque of 542% of motor rated torque and an average peak short-circuit torque of 324% of motor rated torque. The Grid system is approximately twice as bad as the LRS system.

As was mentioned, the majority of the mills tested had LRS starters installed. The results show that on average the drivetrain of a single drive mill will experience a peak switch-on torque of 2.3 times the motor rated torque and a peak short-circuit torque of 2 times the motor rated torque. Trend analysis of the LRS data presented in Figure 28 and Figure 29 shows a slight decrease in the peak switch-on torque as the motor power, and hence mill size, increases. The peak short-circuit torque remains relatively constant as the motor power increases.

Table 6 Overall Results for Single Drive Mills per Starter Type

Mill Power [kW]	Switch-on Torque [% Motor Rated Torque]		Short-circuit Torque [% Motor Rated Torque]	
	Average Peak Value	Standard Deviation	Average Peak Value	Standard Deviation
LRS	233.12	38.43	196.74	21.33
Grid	542.73	331.99	323.57	59.83
E-LRS	91.80	19.82	118.85	4.46

6.2.2. Torque Results for Dual Drive Mills

The dual drive mills that were tested only had LRS and E-LRS type starters installed.

The test results for dual drive mills with LRS starters are presented in Table 7 and Table 8. These results are also presented graphically in Figure 30 to Figure 33. The test results for dual drive mills with E-LRS starters are presented in Table 9 and Table 10. An overall comparison between the average results for dual drive mills with LRS and E-LRS starters is given in Table 11.

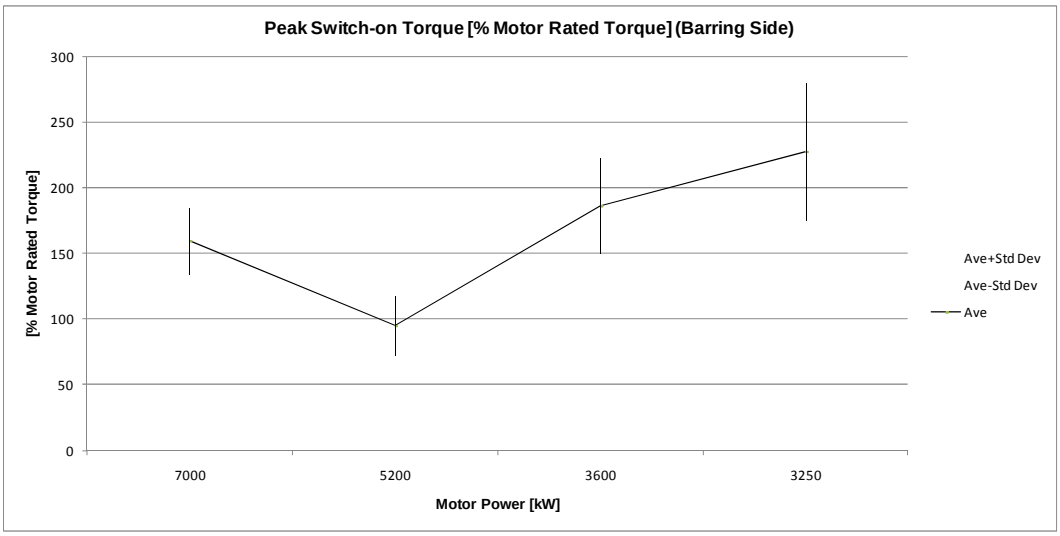

Figure 30 Peak Switch-on Torque for Dual Drive Mills with LRS Starters (BS)

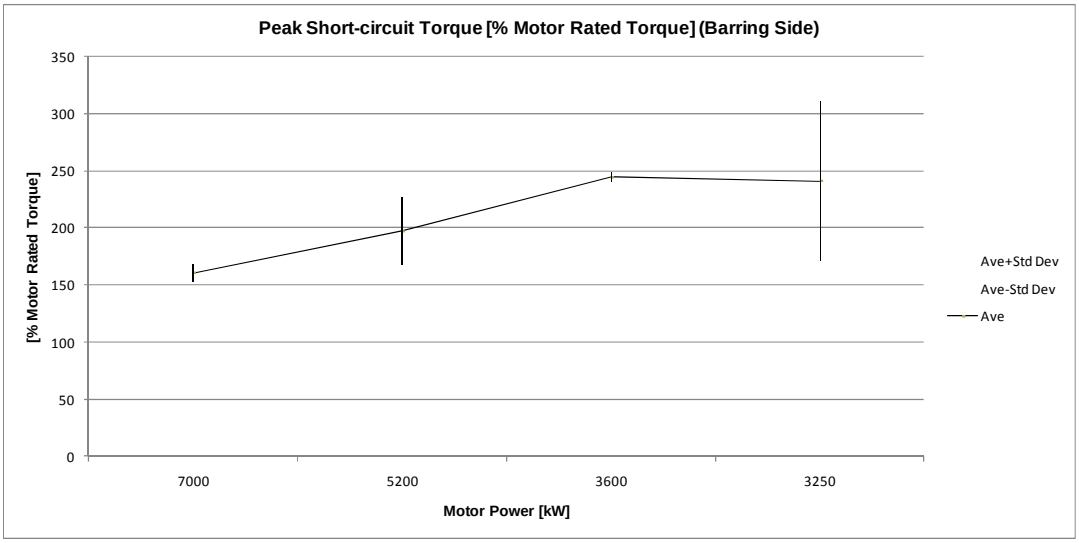

Figure 31 Peak Short-circuit Torque for Dual Drive Mills with LRS Starters (BS)

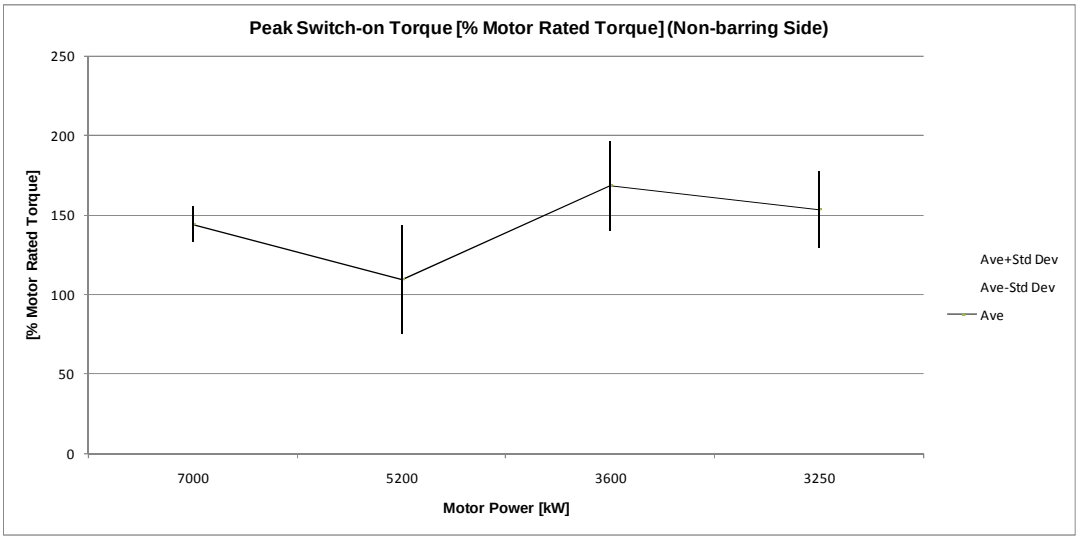

Figure 32 Peak Switch-on Torque for Dual Drive Mills with LRS Starters (NBS)

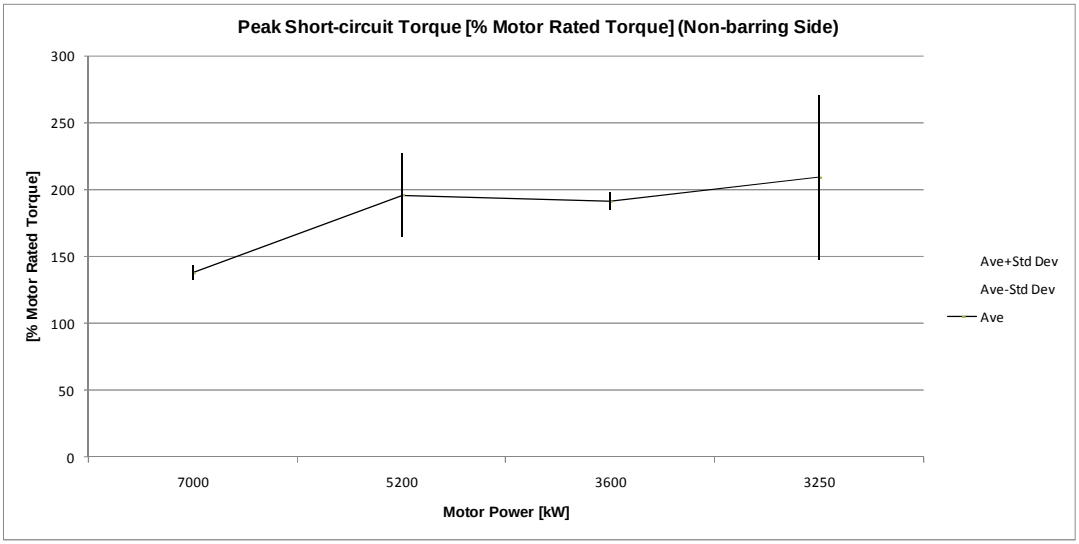

Figure 33 Peak Short-circuit Torque for Dual Drive Mills with LRS Starters (NBS)

Table 7 Test Results for Dual Drive Mills with LRS Starters (Barring Side)

Mill Power [kW]	Switch-on Torque [% Motor Rated Torque]		Short-circuit Torque [% Motor Rated Torque]	
	Average Peak Value	Standard Deviation	Average Peak Value	Standard Deviation
7000	159.43	25.39	160.69	7.25
5200	94.78	22.83	197.04	29.41
3600	186.11	36.20	244.41	3.80
3250	227.36	52.40	240.84	69.65
Average	**166.92**	**34.21**	**210.74**	**27.53**

Table 8 Test Results for Dual Drive Mills with LRS Starters (Non-barring Side)

Mill Power [kW]	Switch-on Torque [% Motor Rated Torque]		Short-circuit Torque [% Motor Rated Torque]	
	Average Peak Value	Standard Deviation	Average Peak Value	Standard Deviation
7000	144.20	11.42	137.83	5.33
5200	109.42	34.21	196.08	31.46
3600	168.60	28.16	191.47	6.45
3250	153.60	23.87	209.12	61.26
Average	**143.95**	**24.42**	**183.62**	**26.13**

The results show that for dual drive mills fitted with LRS starters, the drivetrain components will on average experience a peak switch-on torque of 1.66 times the motor rated torque and a peak short-circuit torque of 2.1 times the motor rated torque.

Table 9 Test Results for Dual Drive Mills with E-LRS Starters (Barring Side)

Mill Power [kW]	Switch-on Torque [% Motor Rated Torque]		Short-circuit Torque [% Motor Rated Torque]	
	Average Peak Value	Standard Deviation	Average Peak Value	Standard Deviation
5200	**55.88**	**20.43**	**142.58**	**10.14**

Table 10 Test Results for Dual Drive Mills with E-LRS Starters (Non-barring Side)

Mill Power [kW]	Switch-on Torque [% Motor Rated Torque]		Short-circuit Torque [% Motor Rated Torque]	
	Average Peak Value	Standard Deviation	Average Peak Value	Standard Deviation
5200	**60.30**	**18.84**	**152.51**	**27.05**

The results again show that the E-LRS starter is the better system from a peak loading point of view and show that the drivetrain components will on average experience a peak switch-on torque of 0.6 times the motor rated torque and a peak short-circuit torque of 1.52 times the motor rated torque.

The results also show that dual drive mills fitted with either LRS or E-LRS starters exhibit a common difference in the torque between the two motors i.e. there is unbalanced load sharing between the two drives. This difference is, however, lower for mills fitted with the E-LRS starters.

Table 11 Overall Results for Dual Drive Mills per Starter Type

Mill Power [kW]	Switch-on Torque [% Motor Rated Torque]		Short-circuit Torque [% Motor Rated Torque]	
	Average Peak Value	Standard Deviation	Average Peak Value	Standard Deviation
LRS – BS	166.92	34.21	210.74	27.53
LRS – NBS	143.95	24.42	183.62	26.13
E-LRS – BS	55.88	20.43	142.58	10.14
E-LRS – NBS	60.30	18.84	152.51	27.05

6.2.3. Torque Results for Barring

The torque results for the barring operations are included in Table 12 and Table 13 for single and dual drive mills respectively.

Table 12 Torque Results for Barring of Single Drive Mills

No.	Mill	Peak Torque [% Motor Rated Torque]	Average Barring Torque [% Motor Rated Torque]
1	Mill A	53	53
2	Mill B	60	42
3	Mill C	185	134
4	Mill D	71	58
5	Mill E	70	64
6	Mill F	76	60
7	Mill G	75	58
	Average	**84.29**	**67.00**

Table 13 Torque Results for Barring of Dual Drive Mills

No.	Mill	Peak Torque [% Motor Rated Torque]	Average Barring Torque [% Motor Rated Torque]
1	Mill A	214	182
2	Mill B	227	185
3	Mill C	214	182
4	Mill D	246	188
5	Mill E	215	182
6	Mill F	314	190
	Average	**238.33**	**184.83**

The torque results for barring operations show a large difference between single and dual drive mills. The average peak torque values for dual drive mills are approximately 2.8 times higher than for single drive mills. The single barring arrangement for the dual drive mills is the primary reason for this difference although other factors such as ore type and standing time before barring also play a role.

The torque results for barring show that the peak value reached before the material starts to break up was 185% of the motor rated torque for single drive mills and 314% of the motor rated torque for dual drive mills.

Generally speaking the longer the period for which the mill is stopped the higher the peak torque value. This is verified by single drive Mill C and dual drive Mill F which both stood for longer than 12 hours. In all cases the torque value then reduces after this peak and remains relatively constant for the remainder of the barring operation.

The important point from a design perspective is that the drivetrain must be designed to cope with the peak loads i.e. 185% for single drive mills and 314% for dual drive mills.

The torque measurements on mills with E-LRS starters differ quite considerably from barring measurements on mills with LRS starters. With mills with LRS starters, the torque climbs linearly after the start until a maximum value is reached when the material starts to tumble and a definite torque peak is typically observed.

The E-LRS deliberately initially connects a very much larger - than typical resistance across the slip rings in order to limit the torque transient at switch on. The resistance in the slip ring circuit is only slowly reduced (to control torque spikes). When the mill is started, the mill is initially at (or close to) a balanced condition and the mill can relatively easily be rotated. Thus, even though the torque developed by the motor is low, the mill turns quickly and the motor accelerates. However, as the motor speeds up, the slip ring voltage (which is inversely proportional to motor speed), falls. Hence the slip ring current - and torque developed by the motor - also falls. As the motor torque falls, the mill coasts to a lower speed, but the mill angle - and mill load torque - continues to increase as the mill continues to rotate under its own momentum. A condition may be reached whereby the mill load torque exceeds the torque developed by the motor and the mill then rocks backwards. The lower the motor torque is at switch on, the more pronounced will be the mill rocking. Mill vendors report that this initial rocking has no detrimental effect on the mill and that the mill rocking is desirable as it contributes to loosening the ore charge, thus assisting to reduce the possibility of damage by solidified charge. A standard start is very rapid and imparts a significant amount of centrifugal force to the ore, increasing the angle at which the ore will eventually tumble. The measured data indicates that the E-LRS, in rocking the mill, has indeed contributed to loosening the ore as the peak torque during the starts are significantly lower.

6.2.4. Torque Results for Steady-state

The range of the steady-state torque oscillations were analyzed and the average, maximum and minimum ranges for single and dual drive mills are shown in Table 14 and Table 15. The range of the steady-state torque oscillations are expressed as a percentage of the motor rated torque in order to normalize the results so that comparisons can be made between the different mills.

The results for single drive mills and the barring side of dual drive mills are very similar and show the non-barring side of dual drive mills to be on average lower than the barring side.

The results show the magnitude of the range of the steady-state torque oscillations to be consistently higher on the motor shaft than on the pinion shaft. Only in two cases were the results between the motor and pinion shafts comparable and they were both single drive mills with 1.8 MW motors.

Table 14 Range of Steady-state Torque Oscillations for Single Drive Mills

	Motor Shaft [% Motor rated Torque]	Pinion Shaft [% Motor rated Torque]
Average	23.61	16.38
Max	45.41	31.95
Min	11.25	7.93
Std Dev	7.77	6.01

Table 15 Range of Steady-state Torque Oscillations for Dual Drive Mills

	Motor Shaft - Barring Side [%]	Motor Shaft - Non-barring Side [%]	Pinion Shaft - Barring Side [%]	Pinion Shaft - Non-barring Side [%]
Average	23.92	20.24	18.36	14.01
Max	40.75	30.07	34.94	21.84
Min	12.27	11.19	10.43	8.96
Std Dev	6.59	5.20	5.19	2.95

The torque oscillations are existent in all mills and are normally caused by a combination of the pinion/girth gear mesh frequency, the mill shell liner passing frequency, the pinion shaft rotational frequency and to a lesser extent by the reducer low speed rotational frequency and the reducer gear mesh frequency.

The net result of the oscillating torques will vary the nominal running torque by about 10% of the full load running torque in a new or well maintained mill. The component of the oscillating torque caused by the gear mesh is a function of the pinion to gear transition errors. As the gears wear and change shape, so the gear mesh component of the oscillating torque increases. Thus one would typically find higher oscillating torques of the order of 15 to 20% in older mills with more worn gears.

Misalignment of the drivetrain as well as the presence of torsional resonance will also increase the magnitude of the torque oscillations thus increasing the loading on drivetrain components.

6.2.5. Torque Results for Switch-off

The torque characteristics during switch-off of the mill are all common and show an immediate reduction in the torque as the motors are de-energised followed by a reduction in torque as the mill slows down followed again by a period of rocking from side to side until the mill comes to rest. Oscillations on the peaks of the rocking cycles are common and this is believed to be due to backlash of the gears. A typical switch-off cycle is illustrated in Figure 34.

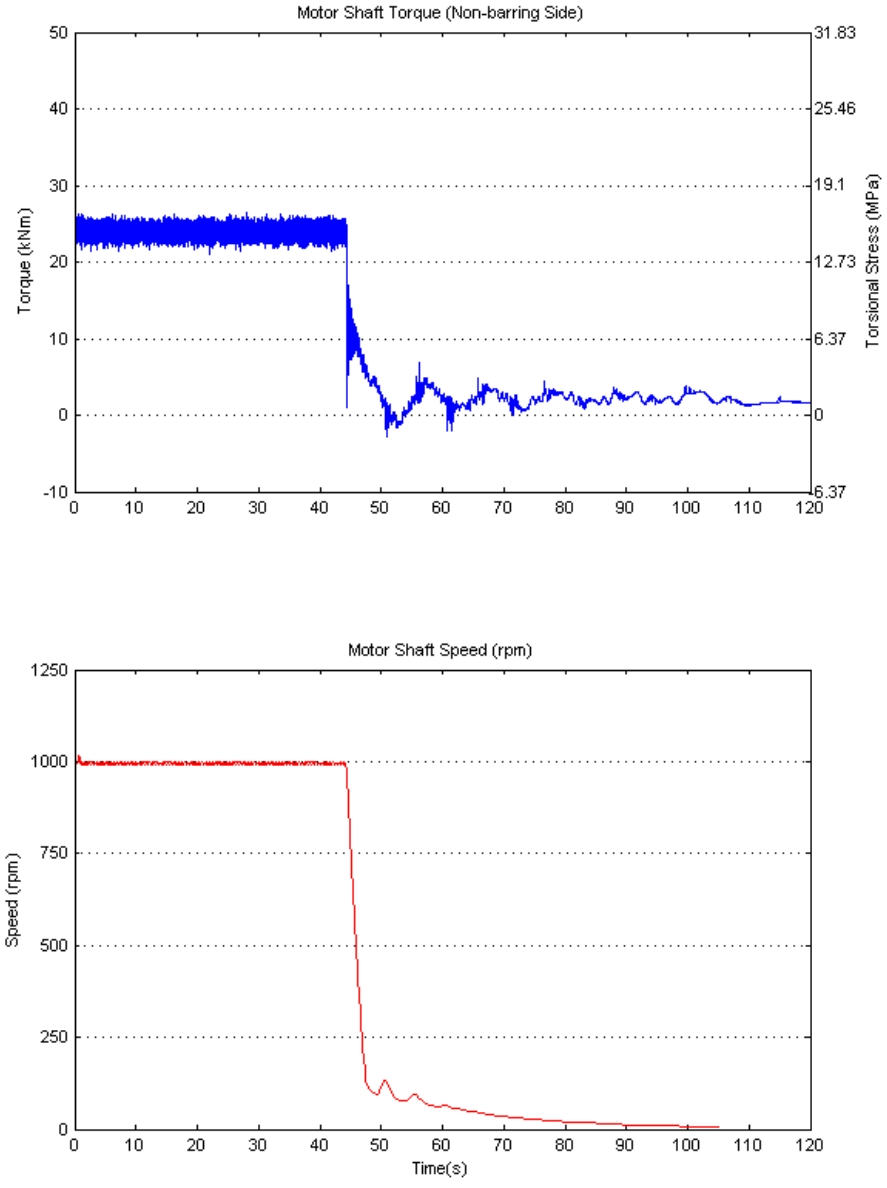

Figure 34 Torque Characteristic for Switch-off

6.2.6. Bending Results

A series of tests were recorded to demonstrate the effect of misalignment on the bending stress values measured on the pinion shaft. Measurements were taken after an extensive realignment of the drivetrain and the bending stress had improved from 88 MPa (measured previously) to 42 MPa on the barring side (a reduction of 52%). Higher alignment tolerances had to be used in order to achieve the lower bending stress. The mill was run for a period of approximately 2 hours so that a steady-state "Delta-T" temperature reading on the mill pinion could be taken (See section 2.2). The measured temperature differential was too high and an adjustment of the NDE pinion bearing was required to correct the temperature differential. 1.2 mm was removed from the NDE bearing. The measured bending stress values increased by 89% to 73.5 MPa thus showing how the adjustment effected the alignment of the drivetrain. The drivetrain was then realigned to account for the adjustment and the bending stress returned to 33.7 MPa. This series of tests highlighted the sensitivity of the system to any misalignment in terms of bending stress in the pinion shaft and has shown that the complete drivetrain must be realigned after any adjustments of the mill pinion for "Delta-T".

The bending stress results measured during barring operations and normal operations were also compared. These results are included in Table 16 and Table 17. The results show that the bending stress values increase by 158% between barring and normal operations on single drive mills and by 300% on dual drive mills.

Table 16 Comparison of Bending Stress Results on Single Drive Mills

No.	Mill	Bending Range during Barring [MPa]	Bending Range during Normal Operation [MPa]
1	Mill A	8	12
2	Mill B	15	17
3	Mill C	1.25	14
4	Mill D	6.3	14
5	Mill E	13	17
6	Mill F	19	25
7	Mill G	5	8
	Average	**9.65**	**15.29**

Table 17 Comparison of Bending Stress Results on Dual Drive Mills

No.	Mill	Bending Range during Barring [MPa]	Bending Range during Normal Operation [MPa]
1	Mill A	14	39
2	Mill B	14	39
3	Mill C	12	39
4	Mill D	10	33
	Average	**12.50**	**37.50**

6.2.7. Frequency Analysis

The expected excitation frequencies as listed in section 6.1.2 were evident in the PSD plots of the test data with the most dominant commonly being the mill pinion gear mesh frequency, the mill shell liner passing frequency and the pinion shaft rotational frequency.

Two examples of the PSD plots from different mills are included in Figure 35 and Figure 36 to illustrate typical results. The excitation frequencies are indicated on the graphs by the coloured dotted lines: Mill Speed (Orange); Pinion Shaft Speed (Blue); Mill Shell Liner Passing Frequency (Green); Motor Shaft Speed (Magenta); Mill Pinion Gear Mesh Frequency (Red); and the Main Reducer Gear Mesh Frequency (Cyan).

Example 1 is a plot for a relatively new mill and corresponds to relatively low values of steady-state torque oscillations – 12% of motor rated torque on the motor shaft and 10% of motor rated torque on the pinion shaft. The frequency analysis results show that only the expected excitation frequencies are present and there is no evidence of any unexplained frequencies that could be as a result of torsional resonance. It can be inferred that due to the new condition of the gears, correct alignment and no torsional resonance, the steady-state torque oscillations remain low and therefore represent no significant increase in the loading of the drivetrain components.

Example 2 is a plot from an older mill and corresponds to some of the highest steady-state torque oscillations recorded – 39% of motor rated torque on the motor shaft and 28% of motor rated torque on the pinion shaft. The frequency analysis results show that the motor shaft speed, a possible resonance at between 10 and 15 Hz as well as 2 significant frequencies on either side of the main reducer gear mesh frequency are the dominant frequencies measured on the motor shaft. The pinion shaft speed and the possible resonance are the 2 dominant frequencies measured on the pinion shaft. It can be inferred that due to the possible torsional resonance, misalignment and worn gearing, the steady-state torque oscillations are appreciable higher and represent a higher loading of the drivetrain components.

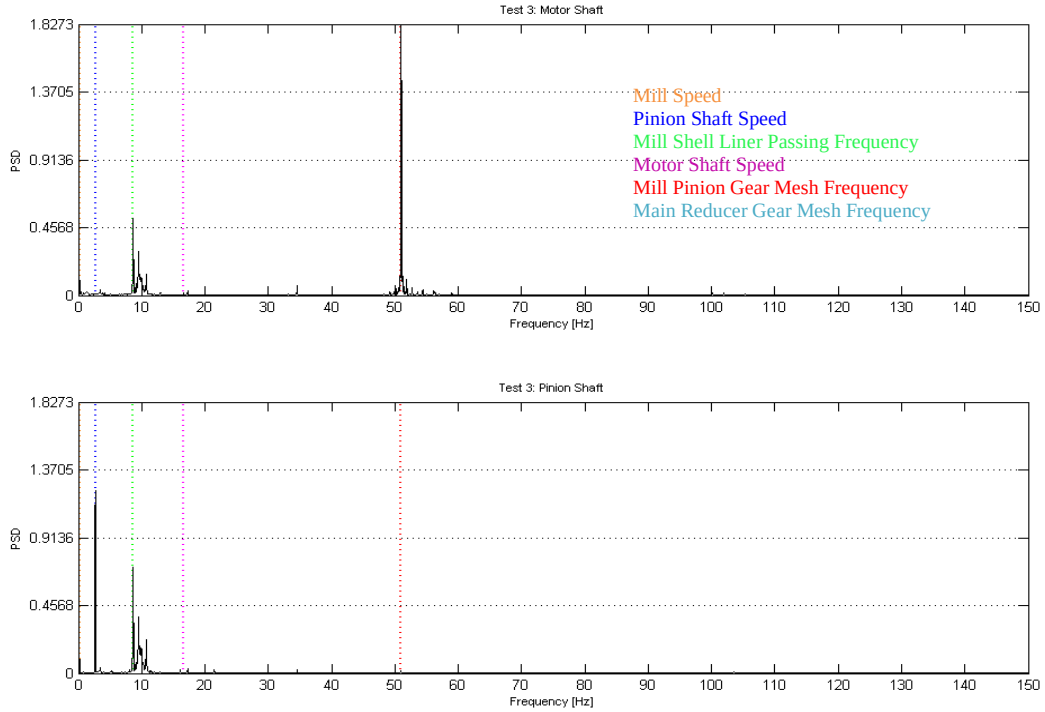

Figure 35 PSD Plot Example 1

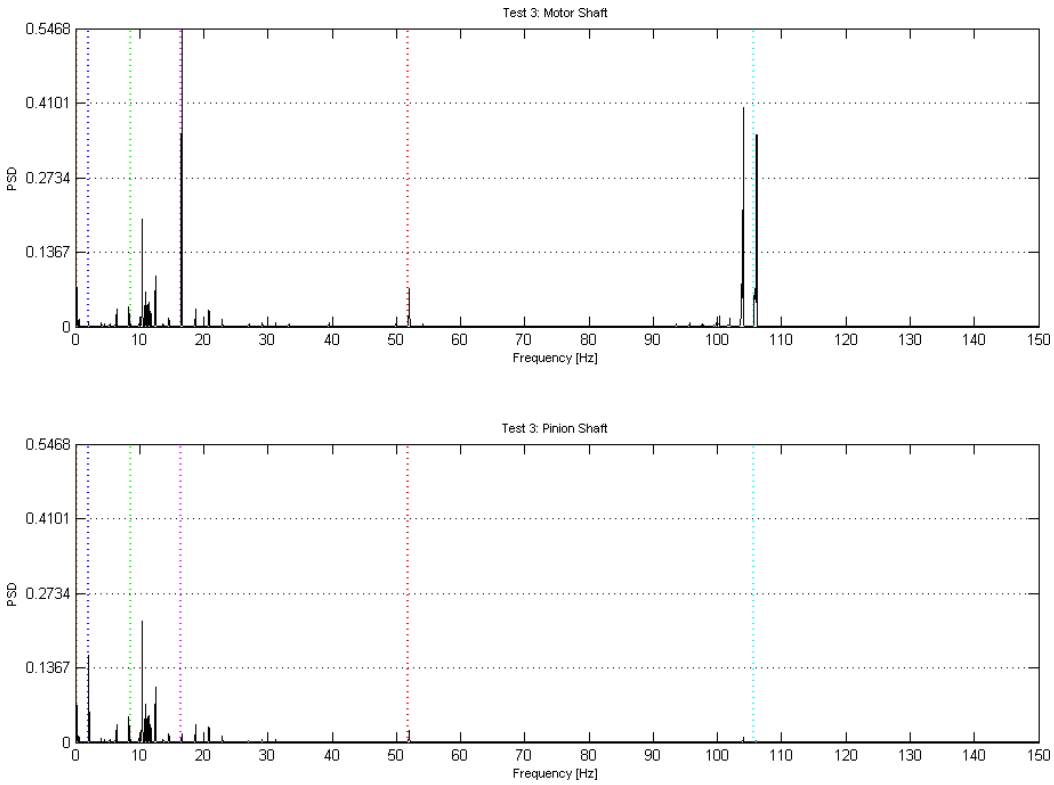

Figure 36 PSD Plot Example 2

6.2.8. Mill Stop/Start Frequency

The mill stop/start frequency data recorded by the site management at the various test sites was analysed and highlighted surprisingly high start/stop frequencies.

During the period of January to November 2006, the peak number of mill stops was 90 and the average for all the mills tested was 22 stops per month. During the same period the least number of stops recorded by any mill was 1.

During the period of January to June 2007, the peak number of mill stops was 71 and the average for all the mills tested was 20 stops per month. During the same period the least number of stops recorded by any mill was 1.

The results show that the drivetrain components were subjected, on average, to up to 4 times more start/stop cycles than the supplier recommended norms.

7. DRIVETRAIN COMPONENT DESIGN REVIEW

The conversion of the measured data into engineering units was described in sections 5.2.3 and 5.2.4 and the summary of the measured torque and bending results are included in section 6. The purpose of this section is to verify that the existing designs of the drivetrain components are adequate for the loads measured and to comment on the appropriateness of the factors of safety used in their design.

7.1. Load Cases

The design calculations for drivetrain components typically use a nominal load value and a suitable safety factor to size the components, however as previously mentioned, the choice of the factor of safety depends on the component itself and on the expected accuracy of the associated analysis.

For the purposes of this review, it was decided to use three load cases from the measured results to evaluate the adequacy of the design of the drivetrain components namely:

- the average nominal torque during steady-state
- the average maximum nominal torque during steady-state which is derived by adding the effect of the torque oscillations to the average steady-state torque.
- the maximum peak torque during start-up

7.2. Shafts

There are several methods available to design shafts and all of them include both the applied torsion and bending moment in the calculations. In the case of the mill pinion shaft, a free body diagram of the pinion shaft, the pinion gear, the coupling weights as well as the bearing reactions is created and the resulting shaft bending moment is calculated. This shaft bending moment and the applied nominal torque together with the endurance strength of the material are then used in the shaft design calculations. The various formulae also usually include a service factor to account for any uncertainties in the applied loads. An iterative process is followed until a suitable shaft diameter is calculated.

In the shaft design calculations that were reviewed, three important shortcomings were identified.

The first was that the range of values used for the service factor varied between 1.75 and 2.0. Based on the torque results presented in Table 6 and Table 11 a service factor of 2.50 (based on average peak values) or as high as 3.0 (based on peak values recorded) would be more suitable. These higher service factors would therefore also provide a design which is capable of withstanding the extra loading coming from the steady-state torque oscillations.

Careful attention should also be paid to the critical sections of the shaft such as changes in section and keyways to ensure that appropriate stress concentration factors have been used. The second shortcoming was identified in a review of the design of the keyways in the shaft, where it was found that high stress

concentrations were present. The stress concentration factor is dependent on the ratio of the fillet radius of the keyway (r) to the diameter of the shaft (D). The keyway of one of the shafts that was reviewed was manufactured according to BS 4235 Part 1:1972 which specifies a fillet radius in the range of 1.2 to 1.6 mm for shafts between 290 and 330 mm in diameter. According to the drawings for the shaft, the fillet radius was 1.6 mm and the shaft diameter was 290 mm, which gives an r/D ratio of approximately 0.004. This ratio corresponds to a stress concentration factor of 4, which is considered to be very high. The design of the keyway would have to be reviewed to incorporate a larger fillet radius. Other examples deigned according to USA key standards made use of larger fillet radii which resulted in stress concentration factors of 2.2.

The third shortcoming occurs because in most shaft design calculations, the drive is assumed to be properly aligned and no provision for any additional bending moment is made. The procedure described above for calculating the bending moment due to gear forces is only valid for the section of the shaft between the pinion bearings. Calculations show that the bending stress due to the gear forces in a typical shaft is approximately 30 MPa. The shaft diameter calculated from this value together with the applied torque would typically then be used for the entire length of shaft. The bending in the section of the shaft between the main reducer and the pinion gear (where most of the failures have occurred), however, is determined by the mass of the shaft and the couplings. This is also the area most susceptible to any misalignment of the shaft. The bending stress measurement results in Table 16 and Table 17 show that some of the measured bending stresses exceed 30 MPa thus indicating that the shaft is under designed. The measured values captured during the alignment exercise further confirm the problem – in one case the measured bending stress was three times higher at approximately 90 MPa. The measured results also highlight the difference in the bending stress between the barring and normal operations thus indicating the presence of dynamic effects which further contribute to higher bending stresses in the shaft.

7.3. Couplings

Most coupling suppliers state that the dimensions of a coupling can only be properly determined if the loading has been accurately quantified. In drives with constant loading, the maximum operating torque corresponds to the coupling torque rating and starting torques are not permitted to exceed the maximum torque value. If increased loading (starting torque, impact torque etc.) is expected, then the coupling should be chosen so that the peak torques are not greater than the rated torque of the coupling.

The standard selection process, for one of the more common suppliers, includes specifying the power, speed and a suitable service factor for the application. In the table provided in the catalogue the values given for mills range between 1.75 and 2.00. It should also be noted that the range of values for all applications listed in the table are between 1.0 and 3.0. The explanation goes on to state that for applications using motors with torque characteristics that are higher than normal; or for applications with intermittent operations, shock loading, inertia effects due to starting and stopping and or system induced repetitive high peak torques, the selection process is altered and instead the system peak torque should be equal to the maximum torque that can exist in the system. A coupling with a torque rating

equal to or greater than this value should then be selected. Note that the service factors are not used in this case as the maximum torque value is known.

In a review of coupling design calculations made by reputable mill suppliers, service factors ranging between 1.75 and 2 were identified, both of which agree with the suggested service factors as provided by the coupling supplier. The results presented in section 6 however, more closely fit the description of high peak torques etc. and would therefore suggest the use of the second approach i.e. to select a coupling with a torque rating equal to the peak torque. This would be equivalent to using the standard approach but increasing the value of the service factor. Such an approach would therefore also account for the steady-state torque oscillations as well. Based on the torque results presented in Table 6 and Table 11 a service factor of 2.50 (based on average peak values) or as high as 3.0 (based on peak values recorded) would be more appropriate.

7.4. Gears

AGMA gear ratings are commonly used to determine the adequacy of mill gear sets by comparing the calculated durability and strength ratings to the recommended minimum service factors for the application.

The AGMA gear rating calculations for both reducer gearboxes and mill pinion/girth gear sets include an allowable pitting resistance power (durability rating) and an allowable bending strength power (strength rating) which are calculated based on the material properties of the gear and expected operating conditions. These calculated powers are compared to the installed (nominal) power of the mill to calculate the durability and bending strength factors as described above. The AGMA calculations show that the contact stress number and the bending strength number are both proportional to the tangential load applied but that neither number can exceed the allowable value which is calculated using material properties. What this means is that when reviewing the durability and bending strength factors an understanding of what the gears are capable of withstanding is obtained but it should be noted that this is not necessarily what the gears are subjected to in practice. If the tangential load is high enough then obviously the contact stress number and the bending strength number will exceed the allowable values and damage will be caused to the gears. The gear ratings are not dependent on the bending stress measured in the shafts but are directly related to the applied torques. The tangential loads used in the AGMA calculations are directly proportional to the measured torque and are calculated by dividing the torque by the pitch circle diameter of the gear.

A review of design calculations highlighted that the majority of mill pinion and girth gears were designed to the minimum recommended AGMA service factors i.e. a service factor for pitting resistance of 1.75 and 2.50 for bending strength. In one case, for a SAG mill, a higher service factor for pitting resistance of 2.0 was specified; however, the rationale for this change could not be established.

A review of design calculations for main reducer gearboxes revealed that service factors between 1.5 and 2.0 were normally used.

These service factors, while appropriate for mills fitted with E-LRS starters, are marginally too low for mills fitted with LRS starters and could therefore explain the gear failures that have been experienced by the various operations. The steady-

state torque oscillations are also important because any given gear tooth will be constantly varying between the totally unloaded and the fully loaded condition as it comes into and out of mesh. Each tooth is therefore subjected to a torque load that varies from zero to the maximum torque applied based on the conservative assumption that there is a point in the cycle where the tooth is forced to take the entire load by itself. Thus, instead of the average operating torque that is normally used, a load equal to the maximum torque, which is equal to the sum of the mean and cyclic torques, should be used.

As shown in Table 14 and Table 15 the average values for the measured steady-state torque oscillations vary between 15 and 25% of the motor rated torque and the maximum recorded value was as high as 45% of the motor rated torque. In cases where the gearing has been designed to be marginal in order to optimize the cost of the gears, this increase in the average nominal torque would result in the contact and bending strength numbers again exceeding the allowable values thus causing damage to the gears.

In cases where the gear damage is isolated to a few gear teeth randomly positioned around the gear, the cause is most likely to be the high peak torques which occur during start-up. Where the damage is evident on all the teeth, then the steady-state torque oscillations are the most likely cause.

7.5. Bearings

The L10h[18] approach is a common means of calculating the lives of the bearings in the main reducer gearboxes. The nominal shaft torques are used together with the gear parameters to calculate the gear forces and subsequently the axial and radial reaction forces at the bearings. The L10h formula is then used to calculate the expected bearing life. Any increase in the shaft torques, therefore, will result in a direct increase in the bearing reaction forces and a reduction of the bearing life.

In some of the design calculations for the reducer gearbox bearings that were reviewed, the expected life was fairly close to the limit specified by the purchaser. Based on the measurement results presented, one can see that the peak torques and the higher than expected levels of torque oscillations would result in a shorter expected life for the bearing and consequently more downtime stoppages for the mill.

To ensure adequate service from the bearings, the designs should be based on the maximum expected bearing forces i.e. maximum applied torques. Based on the torque results presented in Table 6 and Table 11 a service factor of 2.50 times the motor rated torque should be used in the bearing life calculations. The higher service factor would therefore also provide a choice of bearing which is capable of withstanding the extra loading coming from the steady-state torque oscillations.

8. FATIGUE ANALYSIS

In the previous section, it was shown that key values from the measured data were able to provide valuable insights into the design of the various drivetrain components. The purpose of this section is to analyze the overall measurements from a fatigue point of view in an attempt to identify which portions of the operating loads are most contributing to the fatigue damage of the mill drivetrain. It is proposed that these findings can then serve to highlight certain issues which can be shared and result in improving the service life of the machine.

The fatigue analysis is divided into three sections. In the first part, a fundamental approach to determining the fatigue life of the pinion shaft is presented together with the initial findings.

In the second part, this work is expanded upon to conduct the fatigue analysis using the measured results and again the results are discussed.

These findings served as sufficient justification to warrant a formal investigation in the form of a 4th year student's final project which was conducted using the measured data from this project. This work is summarised in the third part and the key findings are discussed.

8.1. Fatigue Resistance of a Pinion Shaft

An analytical assessment of the fatigue strength of the pinion shafts at the keyway was conducted and a relationship between fatigue life, mean torsional stress and cyclic bending stress was derived.

The pinion shaft is manufactured from BS 970, Part 3, 1991, 820M17 alloy steel. The tensile strength varies between 980 MPa and 1420 MPa. For the purpose of this assessment, the following will be assumed:

Ultimate tensile strength, $S_{ut} = 980$ MPa (1)

Endurance limit of rotating beam element, $S'_e = 0.5S_{ut} = 490$ MPa (2)

Following a classic approach, as described in Shigley[19], the endurance limit S_e of the pinion shaft, excluding geometric stress concentration effects which are accounted for later, is calculated using the relation:

$$S_e = k_a k_b k_c k_d S'_e \quad (3)$$

where $k_a = 0.68$ (surface factor, see Shigley, Fig 5-17)

$k_b = 0.75$ (size factor, see Shigley, p190)

$k_c = 0.897$ (90% reliability)

$k_d = 1.0$ (temperature factor)

giving $S_e = 0.4575 S'_e$ (4)

According to Peterson's[20], the stress concentration factor Kt applicable to shaft bending where the keyway bottom radius is r=6 mm and the shaft diameter d=320 mm (r/d = 0.0188) is 2.2. It will be assumed that the notch sensitivity equals 1; hence the fatigue strength reduction factor Kf is given by

$$K_f = K_t = 2.2 \quad (5)$$

The pinion shaft rotates at a speed of 176 rpm, accumulating 1.8×10^6 revolutions per week of continuous operation. With the "knee" of the S-N line occurring between 10^6 and 10^7 cycles, it is clear that stresses alternating once per revolution need to be kept below the endurance limit i.e. the shaft needs to be designed for infinite fatigue life.

The stresses associated with steady operation of the mill can be idealised as a steady alternating bending stress (σ_a) and a constant torsional stress (τ_m). Note that the torque oscillations are not included in this assessment.

The mean von Mises stress is given by:

$$\sigma'_m = \sqrt{3\tau_m^2} \quad (6)$$

where $$\tau_m = \frac{16T}{\pi d^3} \quad (7)$$

T is the torque in the shaft

d is the diameter of the shaft

The alternating von Mises stress is given by

$$\sigma'_a = K_f \sigma_a \quad (8)$$

Note that a stress concentration factor has only been applied to the alternating component of stress, as recommended by Peterson for ductile materials. A failure criterion can now be established by reference to a modified Goodman diagram, as shown in Figure 37.

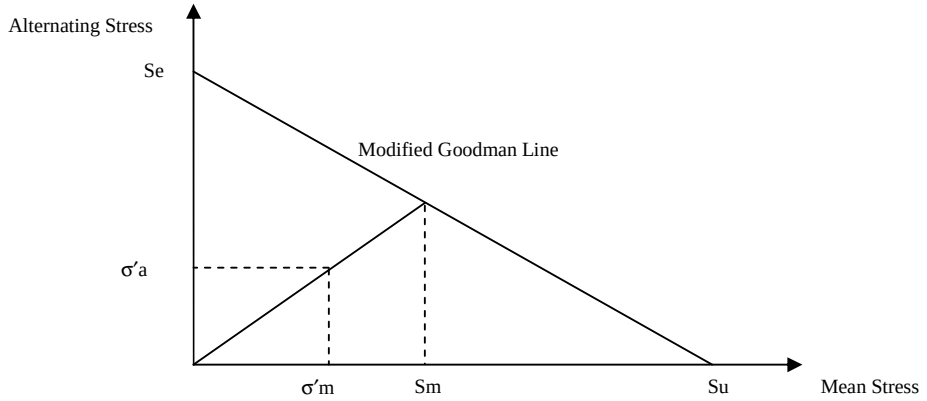

Figure 37 Modified Goodman Diagram

By simple geometry, the equivalent mean stress at failure, Sm, is given by:

$$S_m = \frac{S_e}{\left(\frac{\sigma'_a}{\sigma'_m} + \frac{S_e}{S_u}\right)} \tag{9}$$

And the fatigue reserve factor, or factor of safety against fatigue failure, is given by:

$$FRF = \frac{S_m}{\sigma'_m} \tag{10}$$

Equations (1) to (10) establish a relationship between the steady torque (T) in the pinion shaft, the alternating bending stress (σ_a) and the fatigue reserve factor. The relationship is shown graphically in Figure 38.

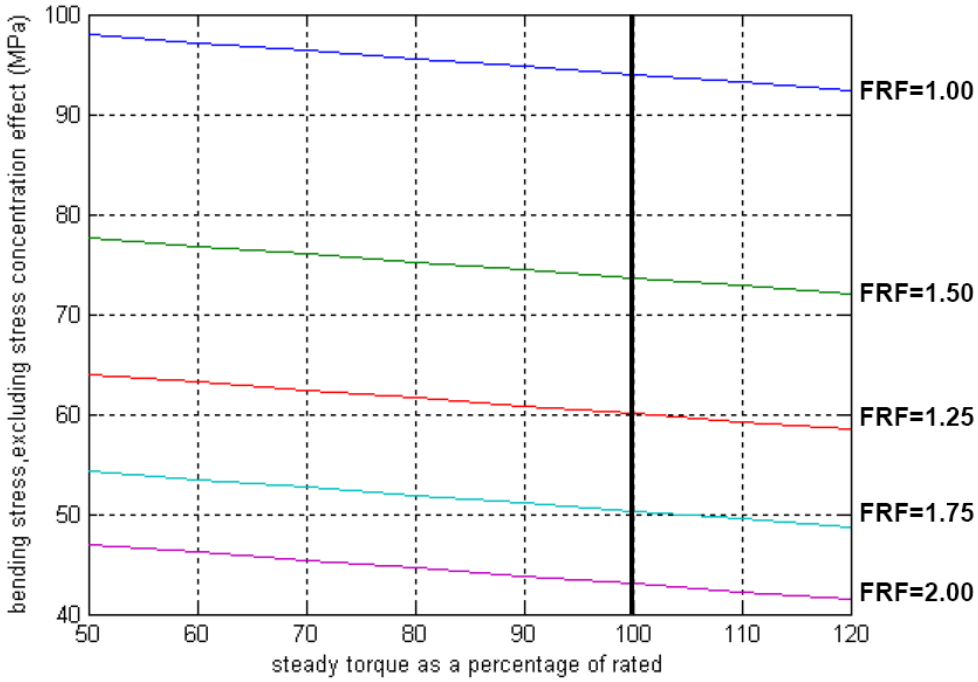

Figure 38 Alternating Bending vs. Steady Torque for Various Fatigue Factors

Based on this analytical assessment, the following points are highlighted:

- The fatigue resistance of the shaft is relatively insensitive to steady torque.
- The bending stress amplitudes need to be limited to below 43 MPa in order to achieve a fatigue reserve factor of 2.00 at rated torque.
- At rated torque, shaft failure due to bending stress is predicted to occur within weeks if the bending stress amplitude exceeds approximately 90 MPa.
- Based on shaft failure experiences, the analytical predictions are non-conservative. Experience suggests that bending stress amplitudes need to be kept below 25 MPa in order to avoid failure. The expected sources of error in

the analysis are poor estimates of material endurance limits and over-simplified treatment of stress concentration at the keyway. These issues could be clarified by:

- Laboratory fatigue testing of samples cut from scrapped pinion shaft ends.
- Finite element analysis of the shafts, focusing on fatigue at the keyways.

8.2. Fatigue Analysis for a Pinion Shaft using Measured Results

The measured test data has shown that the bending and torque values are both significant as far as the pinion shaft is concerned and that the fatigue analysis should be performed on their combined effect. This approach is also verified by the investigation conducted on the stirrer shafts[8] described in section 3.2. The peak values as well as the steady-state values are important in the analysis and thus the entire trace of the complete start/stop cycle was analysed. The bending and torsional stresses were therefore combined to obtain the maximum stress acting in the shaft. The details of this calculation are described below:

According to Hearn[21], the stress system for a shaft with a combined loading of bending and torsion is represented in Figure 39.

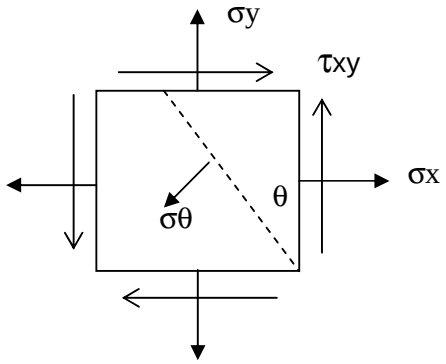

Figure 39 Shaft Stress System

The bending stress values from the strain gauge test represent σx.

σy is equal to zero as there is no force acting perpendicular to the surface of the shaft.

τxy can be calculated using equation 11 where the T represents the torque values obtained from the test.

$$\tau_{xy} = \frac{16T}{\pi d^3} \qquad (11)$$

σx and τxy can then be combined to obtain the maximum stress in the shaft (σθ) as shown in equation 12.

$$\sigma\theta = \frac{1}{2}(\sigma x + \sigma y) + \frac{1}{2}(\sigma x - \sigma y)\cos 2\theta + \tau xy \sin 2\theta \quad (12)$$

The angle of σθ can be calculated as from:

$$\tan 2\theta = \frac{2\tau xy}{(\sigma x - \sigma y)} \quad (13)$$

A graph of θ(t) is plotted to determine the value of θ at the point where the torque peaks occur. The resulting graph show that, on average, an angle of 45 degrees coincides with the torque peaks. The value of 45 degrees is then substituted back into equation 12 to obtain the maximum stress.

Two examples of the resulting combined maximum stress are included below, one with a low bending stress (torque dominated signal) and one with a high bending stress (bending dominated signal).

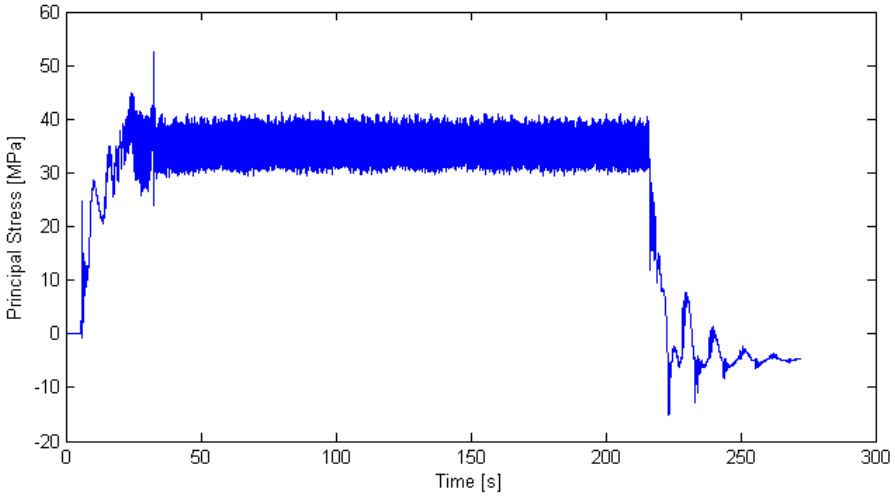

Figure 40 Maximum Stress in a Pinion Shaft – Example 1

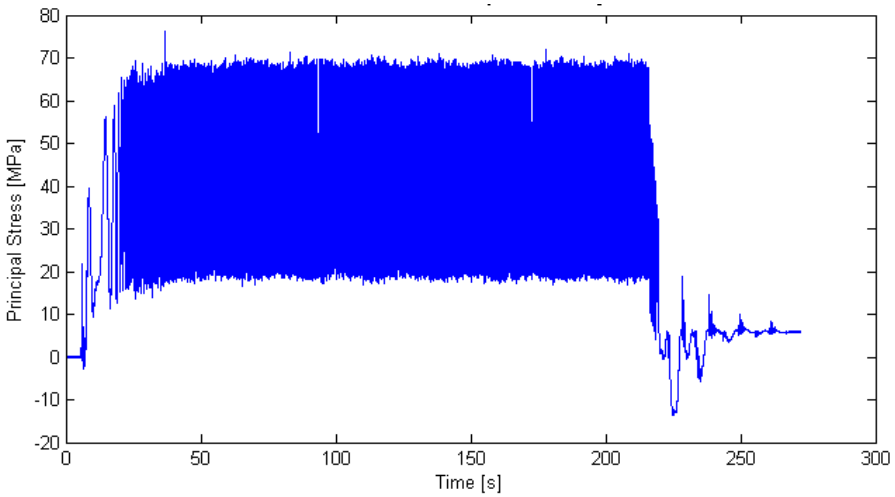

Figure 41 Maximum Stress in a Pinion Shaft – Example 2

This complete trace was then further analysed to calculate the cumulative fatigue damage per start/stop cycle.

A basic S-N curve[19] was created by constructing a line on the logS-logN chart joining $0.8S_{ut}$ at 10^3 cycles and S_e at 10^6 cycles. This can then be used to define the mean fatigue strength S_f corresponding to any life N between 10^3 and 10^6 cycles. This relationship can be represented by equation 14.

$$\log Sf = b\log N + C \tag{14}$$

where:

$$b = -\frac{1}{3}\log\frac{0.8Sut}{Se} \tag{15}$$

and

$$C = \log\frac{(0.8Sut)^2}{Se} \tag{16}$$

S_e is the endurance limit of the shaft and is obtained by multiplying the endurance limit for a rotating-beam specimen by a series of factors as described in the previous section.

The rainflow count analysis is performed on the stress trace of the complete start/stop cycle and serves to represent the trace as a series of stress ranges as well as the number of times which that stress occurs. The cumulative fatigue damage is then calculated using the Palmgren-Miner cycle-ratio summation theory, also called Miner's Rule. A routine in Matlab was used to perform the counting as well as the fatigue damage summation as well as to calculate the estimate service life of the component.

The initial results of this fatigue analysis showed that the service life was less than the expected service life of 20 years in many cases. The analysis also highlighted significantly varying results depending on which input data was used i.e. varying peak torques, varying torque oscillations and different bending stress values.

Another Matlab routine (see Appendix D) was developed to calculate the fatigue damage caused by a typical starting sequence of a mill, the fatigue damage caused by the steady-state operation and the fatigue damage caused during the shut-down sequence. The overall fatigue damage for different operating patterns could then be compared e.g. frequent starts versus long periods of continuous operation, high peak torques at start-up versus high torque oscillations during steady-state operation, high bending versus low bending stress etc. so that further insight could be gained into the drivers of poor service life.

The analysis, although based on properties for the pinion shaft, was thought to be indicative of the expected service life for the overall mill drivetrain and highlighted that the bending, peak torque transients and the frequency of the start/stop cycles were the major contributors to the fatigue damage.

The analysis also, importantly, illustrated the value of such an exercise and thus justified that a formal investigation be carried out to accurately quantify

the fatigue effects of different aspects of the operating cycle. The measured results as presented in section 6 would be used as input data for this investigation.

8.3. Formal Investigation

Alasdair Martin, a final year mechanical engineering student at the University of Cape Town, agreed to perform the investigation as his final project. The work was entitled "The Development of a Life Prediction Model for a Pinion Shaft of a FAG Mill" and was completed in 2009.

The aim of the project was to develop a basis on which to accurately predict the service life of a pinion shaft in a grinding mill drivetrain. Some of the key objectives of the project were:

- To develop a life prediction fatigue model that can accurately determine the service life of a pinion shaft.
- To verify the accuracy of the life prediction model with experimentally obtained results from the sample steel.
- To identify the operational factors which are critical to the premature failure of the mills.
- To suggest measures to be taken to extend pinion shaft service life and optimize inspection schedules.

The investigation focussed on the pinion shaft.

The scope of the project was to develop a retrospective life prediction model for the pinion shaft from the measured data. The model used theoretical formulae for predicting the number of life cycles to failure which were based on empirical constants of typical BS970 EN24 steel. The results predicted by the model where therefore dependent on the validity of the data collected as well as the shaft's compliance to the BS970 EN24 steel properties. The comparison of the fatigue effects of different grinding cycles was also included in the scope of the project.

The life prediction model for the pinion shaft was developed using MATLAB software. The details of the mathematical processes, theoretical models and assumptions are all discussed in the project. Note that the rainflow counting algorithm was used in the model due to its proven accuracy and extensive use in similar studies.

Extensive experimental validation was conducted by the student to verify the accuracy of the Matlab model's predictions. An ESH Universal Servo-Hydraulic Fatigue Testing Machine, a Lieca bi-optical microscope and a hardness testing machine were all used during the experimental fatigue testing. The hardness tester was used to ensure that the steel of the laboratory specimens were all sufficiently uniform. Accurate predictions would be impossible if tests were conducted on varying samples.

The process of fatigue testing requires the repetitive straining of a test specimen in order to produce localized cracking in the material. Once a few of the specimens had been cracked and their crack progression curves had been plotted, it was possible to produce the Paris Curves. By tabulating the

data appropriately, the stress intensities and corresponding crack growth rates were derived. Fatigue testing for the generation of the steel's Paris Curve was undertaken on 4 of the 5 specimens, leaving one specimen solely for prediction purposes.

The accuracy of the MATLAB program's crack prediction was tested in 3 experimental runs. The nature of the testing was increasingly more complex over the three tests so that the program's sensitivity to different factors could be evaluated.

The results from the three validation tests showed that the accuracy of the MATLAB life prediction model was more than sufficient to warrant its use as a tool to predict the fatigue lives of drivetrain components. Some key results of the verification exercise are listed here.

- The model achieved prediction accuracies of less than 1 percent from crack initiation to fracture over 45 000 cycles.
- The model displayed extremely high accuracy for cracks propagating at middle and high stress intensity values.
- Prediction accuracy is convergent and will yield best estimations when predicting the number of cycles to failure.
- Long term predictions are conservative in every case.
- Error can be greatly reduced to at least 0.14% by means of a single crack length inspection midway through a component's life cycle.

Fatigue testing using the MATLAB life prediction model was performed on the load history data according to these three operational cycles i.e. start-up, steady-state operation and shut down. The start-up damage assessed the damage incurred by the start-up operational cycle. While the percentage damage was obviously very small, it represents the amount of damage incurred by a start-up and when analysed comparatively, can tell a great deal about the transient loads. The steady-state damage test assessed the crack growth, as a percentage of the total pinion shaft diameter, during a period of normal operation. The time period over which this is measure was chosen as 50 seconds as this corresponded to a typical start up time. Finally the shut-down damage test was to calculate the crack growth, as a percentage of the total pinion shaft diameter, during a shut-down of the mill. This was assumed to be low, and in most cases negligible; however it was included for thoroughness. Note: As shut down period is generally longer than 50 seconds, the damage will be scaled accordingly for comparative purposes.

Consequently, it was these tests that formed the basis for comparative fatigue analysis of the in-service mill pinion shafts. Two distinct factors from the fatigue results were identified which appear to have a significant bearing on predicted crack propagation; namely the magnitude of transient torsional stresses at start up and the amplitude of bending stress in normal operation. Other operational factors such as shut-down stresses, steady-state torsion and start-up bending appear to have less of an effect on crack growth rates and service life.

The following conclusions were drawn from the fatigue simulations regarding the relative fatigue damage incurred by a mill shaft during different operational cycles.

i. Predicted fatigue life is highly dependent on steady-state alternating bending stress

During the fatigue simulations, the magnitude of the range of bending stress during normal operation dominated over other factors in its effect on predicted life. The huge variation in life expectancies in the different mills tested was almost fully accredited to this value. It can therefore be concluded that the primary way of increasing fatigue life in these components is to reduce the amplitude of bending stress.

ii. Start-up transient peak torque does influence the fatigue life of low stress mills

In mills with lower bending stresses which do not dominate the fatigue loading, transient torsional stresses at start-up do produce significantly higher crack growth rates as compared to normal operation.

iii. Reduction in surface flaws on the pinion shaft extends service life greatly

A consistent service life increase of 75.2% was achieved by reducing the initial crack size from 1mm to 0.1mm. Furthermore, if a good surface finish can be maintained, free of scratches and gouges, at 10μm this increase can be pushed to 200.3%.

9. CONCLUSIONS

Based on the test work, design reviews and fatigue analysis conducted as part of this investigation, the following conclusions can be made:

1. Strain gauge measurements were successfully conducted on the drivetrains of 30 grinding mills. Torque and bending measurements were recorded and analysed and the following key points were highlighted:
    - The torque data consists of several distinct and repeatable characteristics namely, the high peak transients at start-up; torque oscillations during steady-state operation and a switch-off response.
    - The peak starting torques for single drive mills varied depending on the type of starter employed. The E-LRS starter was the best system from a peak loading point of view with an average peak switch-on torque of 92% of motor rated torque and an average peak short-circuit torque of 119% of motor rated torque. The single drive mills with LRS starters had an average peak switch-on torque of 233% of motor rated torque and an average peak short-circuit torque of 197% of motor rated torque. The performance of the single drive mills with grid starter systems was poor with very high peak torques being produced. The average peak switch-on torque was 542% of motor rated torque and the average peak short-circuit torque was 324% of motor rated torque.
    - The dual drive mills fitted with LRS starters had an average peak switch-on torque of 166% of motor rated torque and a peak short-circuit torque of 210% of motor rated torque.
    - Dual drive mills with E-LRS starters also performed better than those with LRS starters from a peak loading point of view. The average peak switch-on torque was 60% of the motor rated torque and the average peak short-circuit torque was 152% of the motor rated torque.
    - The rise times of the peak switch-on torque and the peak short-circuit torque were analysed and confirmed to be shock loads (rise times were all lower than 40 ms).
    - The average values for the measured steady-state oscillating torques varied between 15 and 25% and the maximum recorded value was 45%.
    - The torque results for barring operations show a large difference between single and dual drive mills. The average peak torque values for dual drive mills (238% of motor rated torque) are approximately 2.8 times higher than for single drive mills (84% of motor rated torque). The torque results for barring show that the peak value reached before the material starts to break up was 185% of the motor rated torque for single drive mills and 314% of the motor rated torque for dual drive mills.
    - The bending stress results showed that single drive mills had an average pinion shaft bending stress of 15 MPa and dual drive mills an average of 37 MPa. The bending stress results measured during barring operations and normal operations were also compared. The results show that the

bending stress values increase by 158% between barring and normal operations on single drive mills and by 300% on dual drive mills.

- A series of tests conducted to measure the bending stress in the pinion shaft during an alignment exercise highlighted the sensitivity of the drivetrain system to any misalignment and identified that the complete drivetrain should be realigned after any adjustments of the mill pinion. The exercise showed that the common understanding that when the initial static alignment is conducted accurately, subsequent adjustments at the pinion are generally small enough for the drivetrain couplings to stay within their angular and offset alignment limits is not correct. The exercise also highlighted that considerably higher alignment tolerances, than those specified by the supplier, had to be used in order to achieve the lower bending stress in the pinion shaft.

2. The analysis of the mill stop/start frequency data highlighted that at the majority of the sites tested the number of mill stops was very high. The highest number of stops recorded in a month was 90 and the average was 21.

3. These measured torque and bending loads were used in a review of the engineering design calculations for the drivetrain components. In the review of the design calculations for shafts, couplings, gears and bearings it was found that the service factors used were typically too low when compared to these measured results.

4. The results of the fatigue simulations showed that the magnitude of the range of bending stress occurring in the pinion shafts during normal operation dominated over all other factors in its effect on predicted life. The results of the fatigue simulations also showed that in mills with lower bending stresses which do not dominate the fatigue loading, transient torsional stresses at start-up do produce significantly higher crack growth rates as compared to normal operation. In addition to the bending and high peak torques, the results of the fatigue simulations also showed that the number of start/stop events significantly affected the fatigue life prediction of the drivetrain components.

10. RECOMMENDATIONS

Based on the conclusions of this investigation, the following recommendations can be made. It is intended that these recommendations serve as guidelines for both designers and operators of grinding mills aimed at improving the service life of these machines.

10.1. Pinion Shaft Bending Stress

All operating sites should review the alignment specification for the mill drivetrain and ensure that the alignment levels are appropriate. Pinion alignment will change with time due to several factors such as bearing wear, gear tooth wear, significant changes in loading, and foundation movements. It is imperative that pinion alignment be maintained with time and it should be monitored on a regular basis as part of a regular maintenance program. Operators should strongly consider using bending stress measurements as a means to verify that the alignment is correct and that the bending stress is within allowable limits.

10.2. High Peak Torque Transients

Operators should be aware of the critical role the liquid rheostat starter plays in controlling the torques during start-up and how the high peak torques measured are caused by its faulty operation. The results presented in this project also highlight the detrimental effect these high peak torques have on the service life of the drivetrain components.

Careful maintenance of the starter is required to ensure that it performs properly at all times and strain gauge methods should be used to verify that the electrolyte density is correct for optimum starting performance.

10.3. Mill Stop/Start Frequency

In addition to the bending and high peak torques, the results of the fatigue simulations also showed that the number of stop and start events significantly affected the fatigue life prediction of the drivetrain components.

The analysis of the mill stop/start frequency data highlighted this as a major problem at most sites with the highest number of stops recorded in a month being 90 and the average being 21. Suppliers always recommend that the number of starts should be kept to a minimum in order to reduce the number of times the drivetrain components are exposed to the high start-up loads. The normal number should be in the range of 3 to 5 per month.

Site management must ensure that the number of stop and start events are recorded and scrutinized and every effort should be made to keep the number of starts to a minimum.

10.4. Drivetrain Component Design

It is recommended that a service factor of 2.50 be used in the design calculations of all drive train components on mills fitted with LRS starters. A

reduced service factor of 1.75 is recommended for drivetrain components on mills fitted with E-LRS starters. Designers are urged to review the test results presented in more detail to fine tune the design of the drivetrain components to suit the intended application.

It is strongly recommended that Grid type starters are not used for mill applications due to their unsophisticated design and poor starting performance.

10.5. Steady-State Torque Oscillations

Simple frequency analysis of the steady-state torque oscillations can help operators to determine the major contributors and thus focus their maintenance efforts on reducing the levels of the torque oscillations.

Regardless of the cause of the high oscillations, the net effect is that the drivetrain components experience on average higher fluctuating loads. In cases where the drivetrain components have been designed to be marginal in order to optimize their cost, this increased loading would result in damage being caused.

Fenton**Error! Bookmark not defined.** also showed that harmonic wear due to vibration is related to transient and steady-state vibrations which can lead to shortened service lives and failures of the drivetrain components.

10.6. Real Time Condition Monitoring

Grinding mills, despite their fairly simple design concept, have shown themselves to be complex machines with numerous interacting actions and events taking place which all play a role in affecting the service life of the mill and its drivetrain components. Grinding mills are also expensive, both in terms of repairs and downtime caused by failures.

The test results and findings of this investigation have highlighted the number of parameters that need to be monitored in order to ensure that the mill operates correctly and also that this information cannot easily be obtained without the use of specific instrumentation. The obvious requirement therefore is that a properly specified on-line monitoring system be developed to effectively manage a grinding mill and to ensure that it always operates within its design limits in order to fulfil its full service life.

It is proposed that future work in this field be focussed on developing a system that includes both the instrumentation required to measure various parameters as well as the in-situ processing capability to analyse the data and trigger diagnostic alarms. Reports should be automatically generated and distributed to site management. Opportunities also exist to use a computer receiving the reports to perform long term trending of the data in order to assist continuous improvement initiatives.

REFERENCES

1. Hamilton RH, Wainwright KA and Diering RP (2006) “Lessons learned from recent failures of gear drives on mills in South Africa” SAG Conference 2006

2. ANSI/AGMA 6114-A06, Gear Power Rating for the Cylindrical Shell and Trunnion Supported Equipment (Metric Edition), 2006

3. ANSI/AGMA 2001-C95, Fundamental Rating Factors and Calculation Methods for Involute Spur and Helical Gear Teeth (Metric Edition), 1995

4. Saxer, B and van den Heuvel, B (1989) “Dynamic problems of girth gear drives for ball mills in the cement industry” IEEE Cement Industry Technical Conference

5. Fenton, DA and Taylor, RM (1984) “Torsional vibration analysis and comprehensive field testing on a large rotary kiln” IEEE Cement Industry Technical Conference

6. Becker, E and Cools, K (2002) “Condition monitoring on girth gear units – experience and developments” ZKG International Volume 55, No.8/2002

7. Parida, N (2002) “Failure analysis of coal pulverizer mill shaft” Engineering Failure Analysis Vol. 10 (2003) pp 733 - 744

8. Sonsino, CM and Pfohl, R (1990) “Multiaxial fatigue of welded shaft-flange connections of stirrers under random non-proportional torsion and bending” International Journal of Fatigue Vol. 12 No. 5 pp 425 - 431

9. Vogwell, J (1998) “Analysis of a vehicle wheel shaft failure” Engineering Failure Analysis Vol. 5, No. 4 pp 271 - 277

10. JianPing, J and Guang, M (2007) “Investigation on the failure of the gear shaft connected to extruder” Engineering Failure Analysis

11. Sutherland, HJ (1999) “On the Fatigue Analysis of Wind Turbines” National Technical Information Service, U.S. Department of Commerce

12. Fatemi, A and Yang, L (1997) “Cumulative fatigue damage and life prediction theories: a survey of the state of the art for homogeneous materials” International Journal of Fatigue Vol. 20 No. 1 pp 9 - 34

13. Čačko, J (1992) “Simultaneous computer simulation of operational random processes and continual rainflow counting” International Journal of Fatigue Vol. 14 No. 3 pp 183 - 188

14. Meimaris C, Duncan M and Cox L (2001) “Failure analysis of ball mill gears” SAG Conference 2001

15. Fenton, DA (1996) “Harmonic wear due to vibration on autogenous and semi autogenous mills” SAG Conference 1996

16. Kress, DF and Hanson, DL (1989) “Girth Gears - Design concept through operating criteria” SAG Conference 1989

17. Hoffmann, K (1989) Introduction to Measurements using Strain Gages Hottinger Baldwin Messtechnik GmbH

18. SKF Group (1989) SKF Bearing Catalogue Carl Gerber GmbH

19. Shigley, JE (1986) Mechanical Engineering Design First Metric Edition, McGraw Hill Publishers

20. Pilkey, WD (1997) Peterson's Stress Concentration Factors 2nd Edition, John Wiley & Sons

21. Hearn, EJ (1985) Mechanics of Materials Volume 1, 2nd Edition, Butterworth-Heinemann Ltd

APPENDIX A TEST SUMMARY

Summary of Measurements on Single Drive Mills with LRS Starters

No.	Mill	Nameplate Power [kW]	No. of times tested	Total measurements
1	Mill A	3200	1	2
2	Mill B	2800	1	5
3	Mill C	1800	1	2
4	Mill D	1800	1	3
5	Mill E	1800	1	3
6	Mill F	5200	1	3
7	Mill G	5200	2	4
8	Mill H	6400	1	3
9	Mill I	3250	2	8
10	Mill J	1800	1	4
11	Mill K	2500	1	3
12	Mill L	5200	2	6
13	Mill M	5200	2	7
14	Mill N	5200	1	3
15	Mill O	5200	1	3
16	Mill P	4000	1	2

Summary of Measurements on Single Drive Mills with Grid Starters

No.	Mill	Nameplate Power [kW]	No. of times tested	Total measurements
1	Mill Q	1119	1	5
2	Mill R	1250	1	5
3	Mill S	1100	1	3
4	Mill T	1100	1	3
5	Mill U	1100	1	3

Summary of Measurements on Single Drive Mills with E-LRS Starters

No.	Mill	Nameplate Power [kW]	No. of times tested	Total measurements
1	Mill V	5200	1	6
2	Mill W	5200	1	2

Summary of Measurements on Dual Drive Mills with LRS Starters

No.	Mill	Nameplate Power [kW]	No. of times tested	Total measurements
1	Mill A	5200	4	10
2	Mill B	5200	2	5
3	Mill C	5200	1	1
4	Mill D	3250	1	3
5	Mill E	3250	2	7
6	Mill F	3600	1	5

Summary of Measurements on Dual Drive Mills with E-LRS Starters

No.	Mill	Nameplate Power [kW]	No. of times tested	Total measurements
1	Mill G	5200	4	12

APPENDIX B EQUIPMENT SPECIFICATION SHEETS

Equipment specification sheets for:

- Kyowa Strain Gauges
- Binsfeld TorqueTrak 9000
- SOMAT eDAQ Lite

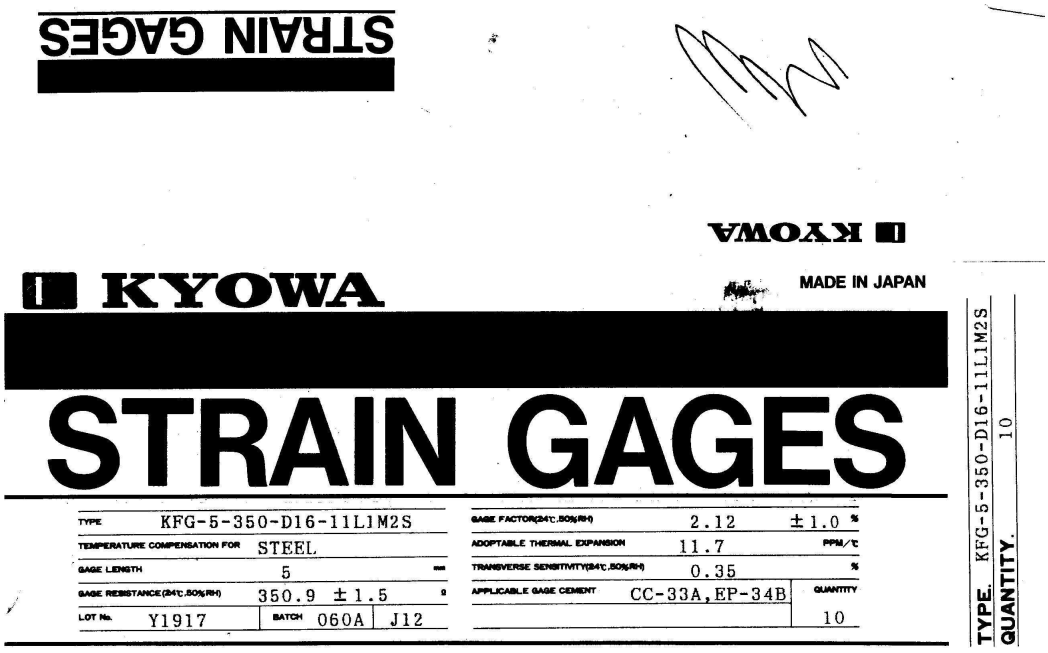

TorqueTrak 9000 Torque Telemetry System

SPECIFICATIONS

BT9000 Transmitter

Sensor Input: Full (four-arm) Wheatstone Bridge strain gage (350Ω standard)
Bridge Input: 5.0 VDC, Regulated
Sensor Range: User selectable per chart below (chart based on gage factor = 2.0):

Transmitter Gain Level	Transmitter Gain	Full Bridge 4 Active Arms (Torque or Bending)	Full Bridge 2 Active Arms (Tension or Compression)	1/4 Bridge 1 Active Arm (Single Gage)
6	8000	±125 microstrain	±192 microstrain	±500 microstrain
5	4000	±250 microstrain	±385 microstrain	±1000 microstrain
4	2000	±500 microstrain	±769 microstrain	±2000 microstrain
3	1000	±1000 microstrain	±1638 microstrain	±4000 microstrain
2	500	±2000 microstrain	±3077 microstrain	±8000 microstrain
1	250	±4000 microstrain	±6154 microstrain	±16,000 microstrain
0	125	±8000 microstrain	±12,307 microstrain	±32,000 microstrain

Sensor & Power Connection: Screw terminal block
Transmitter Power Input: 7.5 to 12VDC, 60mA max with 350Ω bridge (9V battery typical)
Transmission Frequency: 903-922 MHz
Transmitter Battery Life: 12 hours (9V lithium, 350Ω bridge, 25°C)
Transmit Distance: 20 feet or more
G-force Rating: 3000 g's (steady state) (e.g. 6500 rpm on a 5 inch diameter shaft)
Operating Temperature: 0 – 70°C (32 – 158°F)
Size and Weight: 1.05" x 1.95" x 0.70" 2 oz

RD9000 Receiver

Receiver Output Signal: ±10 VDC, field adjustable down to ±5 VDC
Receiver Output Connection: 5-way binding posts (banana jacks)
Receiver Power Input: 12VDC nominal (10 - 18VDC acceptable), 250mA max (110VAC or 220VAC adapter provided)
Operating Temperature: 0 – 70°C (32 – 158°F)
Size and Weight: 5.5" x 7.5" x 1.5" 3 lbs

TT9000 System

Resolution: 14 bits (±full scale = 16,384 points)
Gain Error: ±0.1% (±0.5% before scale calibration)
Gain Drift: ±0.02%FS/°C over operating temperature range
Zero Error: ±0.1%FS (±1% typical before activating AutoZero)
Zero Drift: ±0.02%FS/°C over operating temperature range
Frequency Response: 0 - 250 Hz (-3dB max @ 250Hz)
Delay: 5.4 msec, typical
Slew Rate: 6V/msec, typical
Sample Rate: 1276 samples/sec

Specifications subject to change without notice.

BINSFELD ENGINEERING INC.

4571 W. MacFarlane Rd. ▪ Maple City, MI 49664 ▪ USA
Phone: (+1) 231.334.4383 ▪ Fax: (+1) 231.334.4903 ▪ Toll Free: 800.524.3327 ▪ www.binsfeld.com

8690013

nCode
Managing Durability

Specification Sheet
eDAQ–lite
Data Acquisition System

SoMat Products Division

Removal and replacement of only four screws (on top) are all that is required to add or remove a layer!

Modular. Versatile.
Overview

The rugged eDAQ–lite is a stand-alone compact data acquisition system designed for field testing and unattended monitoring in harsh environments. Its footprint is half the size of the eDAQ and takes advantage of the eDAQ's proven technology. A single system can handle up to 8 boards of any type, and layers are easily added, removed, or replaced. All channels are simultaneously sampled, and it is easy to configure this modular system to meet your testing needs. Some of the types of transducers the eDAQ–lite can support are vehicle bus, strain, pressures, displacements, acceleration, temperatures, digital inputs, pulse counters, quadrature encoders, and internal GPS.

Rugged. Reliable.
Base Specifications

- Size: 6.875in L x 5.625in W x 1.75in H (18cm L x 14cm W x 4.5cm H)
- Supports up to eight boards of any type
- Transducers Supported:
  - Vehicle bus
  - Strain
  - Pressure
  - Displacement
  - Acceleration
  - Temperature
  - Digital input
  - Pulse counter
  - Quadrature encoder
  - Internal GPS
- Memory, Power, Temperature, Connectivity, and Software Specifications on reverse side.

The eDAQ–lite is so compact, it can fit in the palms of your hands!

For details or sales offices visit www.somat.com/sales_rep_locator/

nCode
Managing Durability

SoMat Products Division

Power and Temperature

- Power up: 10 V, Base Run: 9 V, Operating: 9–18 V
- Same 15 pin Dsub power connector as eDAQ
- Internal NiCad battery with ability to keep system running for 4–5 seconds to properly shut system down on power loss
- Remote power switch for remote on and off
- Operating temperature at ambient temperatures -10^{O} to 65^{O} C average (typical system running at 35 watts internal power dissipation)

Power Consumption

Sample configurations of eDAQ–lite field computer systems are provided at the bottom of the page. Working with this grid and your sales representative, you can get an idea of the average power consumption for your configuration.

Memory/Connectivity

- 100BaseTEthernet
- Network with other eDAQ-lites or eDAQs
- Default memory: 64MB DRAM, 256MB Internal CF
  Can upgrade to 256MB DRAM or either 1GB or 2GB Internal CF

Software: Test Control Environment (TCE)

- Included with system and maintenance/updates are free
- Ability to transfer data over wireless Ethernet or modem
- Ability to create setup files, define, and calibrate channels
- Ability to document ISO Test Procedures within software
- Triggering for bursts and many data modes available
- **Need More Functionality?** Inquire about **InField,** our robust field data analysis package!

Board Expansion Options

The eDAQ–lite is an amazingly versatile data acquisition system. The available expansion options are below.

The Digital I/O Board (ELDIO–B) with GPS Option (ELDIO–GPS) is an 8 channel board that can be used for digital or pulse counter inputs and offers 4 additional digital inputs.

Each board is about the size of a standard DVD case.

The Bridge Board (ELBRG)* measures independent signals from analog and strain inputs. It is available in 350 ohm and 120 ohm options.

The Simultaneous High Level Board (ELHLS) offers 4 simultaneously sampled, independent, differential inputs. It is compatible with the Strain Gage, ICP Conditioning, and Thermocouple Smart Modules.

Configuration Type	Power at 13.6V (watts)	Power Current (amps)
eDAQ-lite and 2 ELBRG* boards with 8–350mA Full Bridge inputs at 10 V	10.74	0.79
eDAQ-lite with 4 ELBRG* with 16–350mA Full Bridge inputs at 10 V	18.09	1.33
eDAQ-lite with 4 ELBRG* with 16–350mA Quarter Bridge inputs at 5 V	11.56	0.85

For details or sales offices visit www.somat.com/sales_rep_locator/

APPENDIX C DATA PROCESSING MATLAB ROUTINES

Routine 1: Calculate the full scale voltage from the shunt calibration recording

```
%Calculates calibration voltage by calculating the mean of the
selected full scale voltage and subtracts the mean of the selected
"zero" voltage
%Use mouse to select regions in the order zero1, zero2, full1, full2
where position2>position1

clear, clc;

%Enter filename
%Load data
fname='Cal_P';
eval(['load ',fname,'.asc']);
eval(['data=',fname,';']);
eval(['clear ',fname,';']);

%Figure size
scrsz = get(0,'ScreenSize');
pos1=[(scrsz(3)-0.95*scrsz(3))/2 (scrsz(4)-0.7071*0.95*scrsz(3))/2
0.95*scrsz(3) 0.7071*0.95*scrsz(3)];     %landscape
%pos1=[(scrsz(3)-0.7071*0.95*scrsz(4))/2 (scrsz(4)-0.95*scrsz(4))/2
0.7071*0.95*scrsz(4) 0.95*scrsz(4)];    %portrait

[p,q]=size(data);
xy=[];
for i=1:q
    figure('Position',pos1);
    plot(data(:,i));
    [x,y]=ginput(4);
    CalVP(i)=mean(data(round(x(3)):round(x(4)),i))-
mean(data(round(x(1)):round(x(2)),i));
    close
end

 save CalVP CalVP
```

Routine 2: Calculate the “zero offset” value

```
%Select zero offset region with mouse

clear, clc;
tests = input('Number of tests = ');

%Enter filename
fname='TRP_Test0';

%Figure size
scrsz = get(0,'ScreenSize');
pos1=[(scrsz(3)-0.85*scrsz(3))/2 (scrsz(4)-0.7071*0.85*scrsz(3))/2
0.85*scrsz(3) 0.7071*0.85*scrsz(3)];     %landscape
%pos1=[(scrsz(3)-0.7071*0.85*scrsz(4))/2 (scrsz(4)-0.85*scrsz(4))/2
0.7071*0.85*scrsz(4) 0.85*scrsz(4)];    %portrait

duration=40;    %plots first x seconds
fsamp=1000;     %sample frequency

%Load data and select zero offset
for k=1:tests
    eval(['load ',fname,num2str(k),'.mat']);
    eval(['data',num2str(k),'=',fname,num2str(k),';']);
    eval(['clear ',fname,num2str(k),';']);
    eval(['[p,q]=size(data',num2str(k),');']);
    xy=[];
    for i=1:q
        figure('Position',pos1);
        eval(['plot(data',num2str(k),'(1:duration*fsamp,i));']);
        [x,y]=ginput(2);

eval(['zoffsetP_t',num2str(k),'(i)=mean(data',num2str(k),'(round(x(1)
):round(x(2)),i));']);
        close
    end
    eval(['save zoffsetP_t',num2str(k),' zoffsetP_t',num2str(k)]);
end
```

Routine 3: Conversion of measured signals into engineering units

```
%Data processing for Mill Tests
clear, clc;

%Load Test Data
tests = input('Number of tests = ');

%Enter filename
fname='TRP_Test0';

%Load data and select zero offset
for k=1:tests
    eval(['load ',fname,num2str(k),'.mat']);
    eval(['load zoffsetP_t',num2str(k),'.mat']);
end

load CalVP.mat

%Data Description
% Ch1           Time axis
% Ch2           Torque - Motor Shaft
% Ch3           Torque - Pinion Shaft
% Ch4           Bending - Pinion Shaft
% Ch5           Speed - Measured on pinion shaft

%Input data
Rs      = 350000;           %shunt resistance in ohm
R       = 350;              %gauge resistance in ohm
kk      = 2.11;             %gauge factor
dmm     = 0.225;            %shaft diameter in m
dp      = 0.355;            %pinion shaft diameter in m
E       = 207E+9;           %elastic modulus in Pa
pois    = 0.3;              %Poisson's ratio
fsamp1  = 1000;             %Sample frequency

%Preliminary calcs
G       = 0.5*E/(1+pois);   %shear modulus in Pa
Jmm     = (1/16)*pi*dmm^3;  %Motor Shaft-polar moment of area in m^3
Jp      = (1/16)*pi*dp^3;   %Pinion Shaft-polar moment of area in m^3
Ip      = (1/32)*pi*dp^3;   %Pinion #-second moment of area in m^3
BFb     = 2*(1+pois);       %bridge factor for bending

% Create time axis for each test

for k=1:tests
    eval(['taxis',num2str(k),'=
0:(1/fsamp1):((length(',fname,num2str(k),')-1)/fsamp1);']);
end

% Speed calculation

for n=1:tests
    eval(['data',num2str(n),'=',fname,num2str(n),'(:,4)>101;']);
%Enter a midway value
    eval(['spike',num2str(n),'=[data',num2str(n),';0]-
[0;data',num2str(n),'];']);

eval(['times',num2str(n),'=(find(spike',num2str(n),'==1))/fsamp1;']);
```

```
    eval(['speed',num2str(n),'=(60/8)./(times',num2str(n),'(2:end)-
times',num2str(n),'(1:(end-1)));']); %60/no. of reflectors

eval(['speedf',num2str(n),'=myfilter(speed',num2str(n),','L'',60,fsa
mp1);']);
    eval(['spdtms',num2str(n),'= times',num2str(n),'(2:end);']);
    eval(['spdP',num2str(n),'=[spdtms',num2str(n),'
speedf',num2str(n),'];']);
    eval(['save spdP',num2str(n),' spdP',num2str(n),]);
end

%Apply scale and offset
calE    = (1/kk)*(Rs/(R+Rs)-1);     %shunt-induced apparent strain
EperV   = calE ./ CalVP;            %m/m per volt
TperEmm = 0.5*G*Jmm/1000;           %torque in kNm per indicated m/m
TperEp  = 0.5*G*Jp/1000;            %torque in kNm per indicated m/m
BperE   = (1/BFb)*E*Ip/1000; %bending moment in kNm per indicated m/m
GV      = EperV .* [TperEmm TperEp BperE];   %gain vector for
tests(bending & torque in kNm)
GV2     = (GV/1000) ./ [Jmm Jp Ip];         %gain vector for tests
(direct & shear stress in MPa)
%
fname2='TRP_Test0';

for k=1:tests
    for i=1:3

eval([fname2,num2str(k),'_kNm(:,i)=(',fname,num2str(k),'(:,i)-
','zoffsetP_t',num2str(k),'(i))*GV(i);']);  %kNm

eval([fname2,num2str(k),'_MPa(:,i)=(',fname,num2str(k),'(:,i)-
','zoffsetP_t',num2str(k),'(i))*GV2(i);']); %MPa
    end
    eval([fname2,num2str(k),'_kNm','=[taxis',num2str(k),'''
',fname2,num2str(k),'_kNm(:,1)*-1 ',fname2,num2str(k),'_kNm(:,2)*-1
',fname2,num2str(k),'_kNm(:,3)];']);
    eval([fname2,num2str(k),'_MPa','=[taxis',num2str(k),'''
',fname2,num2str(k),'_MPa(:,1)*-1 ',fname2,num2str(k),'_MPa(:,2)*-1
',fname2,num2str(k),'_MPa(:,3)];']);
    eval(['save ',fname2,num2str(k),'_kNm
',fname2,num2str(k),'_kNm']);
    eval(['save ',fname2,num2str(k),'_MPa
',fname2,num2str(k),'_MPa']);
end
```

Routine 4: Calculation of the average range of the bending stress

```
%Steady State Max Bending Stress Range [MPa] and [kNm]

clear, clc;
tests = input('Number of tests = ');
bch = 4;    %Bending channel number
sch = 2;    %Speed channel number
spdpos = input('Was the speed measured on the motor shaft (0) or the
pinion shaft (1) = ');
fsamp = 1000; %Sample frequency
gratio =(47/26)*(65/16);          %gearbox ratio

%Enter filename
%Load data
fname='TRP_Test0';

for k=1:tests
    eval(['load ',fname,num2str(k),'_MPa.mat']); eval(['load
',fname,num2str(k),'_kNm.mat']);
    eval(['datam',num2str(k),'=',fname,num2str(k),'_MPa',';']);
eval(['datak',num2str(k),'=',fname,num2str(k),'_kNm',';']);
    eval(['clear ',fname,num2str(k),'_MPa',';']); eval(['clear
',fname,num2str(k),'_kNm',';']);
    eval(['load spdP',num2str(k),'.mat']);
end

disp('Use mouse to select the area over which the average bending
stress range will be calculated.');
disp('Select by clicking before and after the area. ');
disp('');

%Figure size
scrsz = get(0,'ScreenSize');
pos1=[(scrsz(3)-0.85*scrsz(3))/2 (scrsz(4)-0.7071*0.85*scrsz(3))/2
0.85*scrsz(3) 0.7071*0.85*scrsz(3)];     %landscape
%pos1=[(scrsz(3)-0.7071*0.85*scrsz(4))/2 (scrsz(4)-0.85*scrsz(4))/2
0.7071*0.85*scrsz(4) 0.85*scrsz(4)];    %portrait

for i=1:tests
    figure('Position',pos1);
    eval(['plot(spdP',num2str(i),'(:,sch))',';']);eval(['title(''Test
',num2str(i),''');']);eval('xlabel(''Time
[s]'');');eval('ylabel(''Pinion Shaft Speed [rpm]'');');
    [xs,ys]=ginput(2);
    close

eval(['speed',num2str(i),'=mean(spdP',num2str(i),'(round(xs(1)):round
(xs(2)),2));']);
end

for i=1:tests
    figure('Position',pos1);

eval(['plot(datam',num2str(i),'(:,1),datam',num2str(i),'(:,bch))',';'
]);eval(['title(''Test ',num2str(i),''');']);eval('xlabel(''Time
[s]'');');eval('ylabel(''Bending Stress [MPa]'');');
    [xb,yb]=ginput(2);
```

```
    close

eval(['bdata',num2str(i),'=datam',num2str(i),'(round(xb(1))*fsamp:rou
nd(xb(2))*fsamp,bch);']);

eval(['bkdata',num2str(i),'=datak',num2str(i),'(round(xb(1))*fsamp:ro
und(xb(2))*fsamp,bch);']);
    %if spdpos==0

%eval(['speed',num2str(i),'=(mean(myfilter(datam',num2str(i),'(round(
xb(1))*fsamp:round(xb(2))*fsamp,sch),',''''L'',5,fsamp)))/gratio;']);
    %else

%eval(['speed',num2str(i),'=mean(myfilter(datam',num2str(i),'(round(x
b(1))*fsamp:round(xb(2))*fsamp,sch),',''''L'',5,fsamp));']);
    %end
    eval(['points=round((1/(speed',num2str(i),'/60))*fsamp);']);
    eval(['loops=round(length(bdata',num2str(i),')/points)-2;']);
    for n=1:loops

eval(['localmaxm(n)=max(bdata',num2str(i),'(n*points:(n+1)*points));'
]);

eval(['localminm(n)=min(bdata',num2str(i),'(n*points:(n+1)*points));'
]);

eval(['localmaxk(n)=max(bkdata',num2str(i),'(n*points:(n+1)*points));
']);

eval(['localmink(n)=min(bkdata',num2str(i),'(n*points:(n+1)*points));
']);
    end
    eval(['BMdata_t',num2str(i),'=[mean(localmaxm)-mean(localminm)
mean(localmaxk)-mean(localmink)]']);

eval(['xlswrite(''BMdata_P'',BMdata_t',num2str(i),',1,',''''B',num2str
(2*i),''');']);
end
```

Routine 5: Speed conversion

```
% Converts pulse trace into speed

%Load Test Data
clear, clc;
tests = input('Number of tests = ');

%Enter filename

fname='TRP_Test0';

%Load data and select zero offset
for k=1:tests
    eval(['load ',fname,num2str(k),'.mat']);
    eval(['load zoffsetP_t',num2str(k),'.mat']);
end

%Input data

fsamp1  = 1000;             %Sample frequency

for k=1:tests
    eval(['taxis',num2str(k),'=
0:(1/fsamp1):((length(',fname,num2str(k),')-1)/fsamp1);']);   %time
axis for tests
end

%Speed
for n=1:tests
    eval(['data',num2str(n),'=',fname,num2str(n),'(:,4)>101;']);
%Enter a midway value
    eval(['spike',num2str(n),'=[data',num2str(n),';0]-
[0;data',num2str(n),'];']);

eval(['times',num2str(n),'=(find(spike',num2str(n),'==1))/fsamp1;']);
    eval(['speed',num2str(n),'=(60/8)./(times',num2str(n),'(2:end)-
times',num2str(n),'(1:(end-1)));']); %60/no. of reflectors

eval(['speedf',num2str(n),'=myfilter(speed',num2str(n),','''L'',100,fs
amp1);']);
    eval(['spdtms',num2str(n),'= times',num2str(n),'(2:end);']);
    eval(['spd',num2str(n),'=[spdtms',num2str(n),'
speedf',num2str(n),'];']);
    eval(['save spd',num2str(n),' spd',num2str(n),]);
end
```

Routine 6: Plotting the processed data

```
%creates plots of test data

%Test 1
clear, clc;
load TRP_Test01_kNm.mat;
load TRP_Test01_MPa.mat;
load spdP1.mat;

fsamp=1000;

plot1_kNm=TRP_Test01_kNm;
plot1_MPa=TRP_Test01_MPa;    %rename variable
plot1_Speed=spdP1;

x1=0;
xs=50;
x2=600;             %time limits and intervals in seconds

ylm1=-15;
ylm2=135;            %y limit for motor
ysm=15;             %y intervals - motor

ylg1=-100;
ylg2=600;           %y limit for pinion
ysg=100;             %y intervals - pinion

ylp1=-60;
ylp2=60;           %y limit for pinion
ysp=15;             %y intervals - pinion

Conver1=2.2365;     %conversion factors to convert from kNm to MPa -
motor shaft torque (polar moment of inertia)
Conver2=8.7845;     %conversion factors to convert from kNm to MPa -
pinion shaft torque
Conver3=4.3922;     %conversion factors to convert from kNm to MPa -
pinion shaft Bending

yl1=((ylm2-ylm1)/Conver1/10);    %rescale for MPa
yl2=((ylg2-ylg1)/Conver2/7);
yl3=((ylp2-ylp1)/Conver3/8);

%Channel Nos
mtc=2;              %motor torque channel
ptcg=3;             %pinion torque channel
pbc=4;              %pinion bending channel

scrsz = get(0,'ScreenSize');
pos1=[(scrsz(3)-0.7071*0.85*scrsz(4))/2 (scrsz(4)-0.85*scrsz(4))/2
0.7071*0.85*scrsz(4) 0.85*scrsz(4)];
figure('Position',pos1);

subplot(4,1,1)
[ax1,h11,h12]=plotyy(plot1_kNm(:,1),plot1_kNm(:,mtc),plot1_kNm(:,1),p
lot1_MPa(:,mtc),'plot');
title('Test 1: Motor Shaft Torque (Primary Mill)','Fontsize',8)
axes(ax1(1))
```

```
set(gca,'XTick',x1:xs:x2);
set(gca,'TickLength',[0.005 0.025]);
set(gca,'Fontsize',8);
set(gca,'ygrid','on');
ylabel('Torque (kNm)','Fontsize',8)
set(gca,'xlim',[x1 x2]);
set(gca,'ylim',[ylm1 ylm2]);
set(gca,'YTick',ylm1:ysm:ylm2);
set(gca,'YColor',[0 0 0]);
axes(ax1(2))
ylabel('Torsional Stress (MPa)','Fontsize',8)
xlabel('Time (s)','Fontsize',8)
set(gca,'xlim',[x1 x2]);
set(gca,'ylim',[ylm1/Conver1 ylm2/Conver1]);
set(gca,'Fontsize',8);
set(gca,'XTick',x1:xs:x2);
set(gca,'TickLength',[0.0 0.025]);
set(gca,'YTick',ylm1/Conver1:yl1:ylm2/Conver1);
set(gca,'YColor',[0 0 0]);
set(gca,'YTickLabel',{num2str(-1*yl1,3);num2str(0,3); num2str(yl1,3);
num2str(2*yl1,3); num2str(3*yl1,3); num2str(4*yl1,3);
num2str(5*yl1,3); num2str(6*yl1,3); num2str(7*yl1,3);
num2str(8*yl1,3); num2str(9*yl1,3)})
delete (h12);

subplot(4,1,2)
[ax2,h21,h22]=plotyy(plot1_kNm(:,1),plot1_kNm(:,ptcg),plot1_kNm(:,1),
plot1_MPa(:,ptcg),'plot');
title('Test 1: Pinion Shaft Torque (Primary Mill)','Fontsize',8)
set(h21,'Color','r')
axes(ax2(1))
set(gca,'XTick',x1:xs:x2);
set(gca,'TickLength',[0.005 0.025]);
set(gca,'Fontsize',8);
set(gca,'ygrid','on');
ylabel('Torque (kNm)','Fontsize',8)
set(gca,'xlim',[x1 x2]);
set(gca,'ylim',[ylg1 ylg2]);
set(gca,'YTick',ylg1:ysg:ylg2);
set(gca,'YColor',[0 0 0]);
axes(ax2(2))
ylabel('Torsional Stress (MPa)','Fontsize',8)
xlabel('Time (s)','Fontsize',8)
set(gca,'xlim',[x1 x2]);
set(gca,'ylim',[ylg1/Conver2 ylg2/Conver2]);
set(gca,'Fontsize',8);
set(gca,'XTick',x1:xs:x2);
set(gca,'TickLength',[0.0 0.025]);
set(gca,'YTick',ylg1/Conver2:yl2:ylg2/Conver2);
set(gca,'YColor',[0 0 0]);
set(gca,'YTickLabel',{num2str(-1*yl2,3);num2str(0,3); num2str(yl2,3);
num2str(2*yl2,3); num2str(3*yl2,3); num2str(4*yl2,3);
num2str(5*yl2,3); num2str(6*yl2,3)})
delete (h22);

subplot(4,1,3)
[ax3,h31,h32]=plotyy(plot1_kNm(:,1),plot1_kNm(:,pbc),plot1_kNm(:,1),p
lot1_MPa(:,pbc));
title('Test 1: Pinion Shaft Bending (Primary Mill)','Fontsize',8)
set(h31,'Color',[0 0.502 0])
axes(ax3(1))
```

```
set(gca,'ygrid','on');
set(gca,'XTick',x1:xs:x2);
set(gca,'TickLength',[0.005 0.025]);
set(gca,'Fontsize',8);
ylabel('Bending Moment (kNm)','Fontsize',8)
set(gca,'xlim',[x1 x2]);
set(gca,'ylim',[ylp1 ylp2]);
set(gca,'YTick',ylp1:ysp:ylp2);
set(gca,'YColor',[0 0 0]);
axes(ax3(2))
ylabel('Bending Stress (MPa)','Fontsize',8)
xlabel('Time (s)','Fontsize',8)
set(gca,'xlim',[x1 x2]);
set(gca,'ylim',[ylp1/Conver3 ylp2/Conver3]);
set(gca,'Fontsize',8);
set(gca,'XTick',x1:xs:x2);
set(gca,'TickLength',[0.0 0.025]);
set(gca,'YTick',ylp1/Conver3:yl3:ylp2/Conver3);
set(gca,'YTickLabel',{num2str(-4*yl3,3);num2str(-3*yl3,3);num2str(-
2*yl3,3); num2str(-1*yl3,3); num2str(0,3); num2str(yl3,3);
num2str(2*yl3,3); num2str(3*yl3,3); num2str(4*yl3,3)})
set(gca,'YColor',[0 0 0]);
delete (h32);

subplot(4,1,4)
[ax4]=plot(plot1_Speed(:,1),plot1_Speed(:,2),'m');
title('Test 1: Pinion Shaft Speed (rpm)','Fontsize',8)
set(gca,'Fontsize',8);
set(gca,'ygrid','on');
ylabel('Speed (rpm)')
xlabel('Time(s)')
set(gca,'xlim',[x1 x2]);
set(gca,'XTick',x1:xs:x2);
set(gca,'ylim',[0 140]);
set(gca,'YTick',0:20:140);
set(gca,'TickLength',[0.005 0.025]);
```

Routine 7: Data extraction

```
% Extraction of key torque results for all tests

clear, clc;
tests = input('Number of tests = ');

%Enter filename
%Load data
for k=1:tests
    fname='TRP_Test0';
    eval(['load ',fname,num2str(k),'_kNm.mat']);
    eval(['data',num2str(k),'=',fname,num2str(k),'_kNm',';']);
    eval(['clear ',fname,num2str(k),'_kNm',';']);
end

n=994;              %rated motor speed in rpm
P=5200;             %motor power in kW
GR=(47/26)*(65/16); %reducer gearbox ratio
MRT=P/(2*pi*n/60);  %motor rated torque
PRT=MRT*GR;         %pinion rated torque
fsamp=1000;

%Channel Nos
mtcbs1=2;            %motor torque channel - barring side
ptcbs2=3;            %pinion torque channel
%pbcbs=4;             %pinion Bending channel


%Figure size
scrsz = get(0,'ScreenSize');
pos1=[(scrsz(3)-0.85*scrsz(3))/2 (scrsz(4)-0.7071*0.85*scrsz(3))/2
0.85*scrsz(3) 0.7071*0.85*scrsz(3)];     %landscape
%pos1=[(scrsz(3)-0.7071*0.85*scrsz(4))/2 (scrsz(4)-0.85*scrsz(4))/2
0.7071*0.85*scrsz(4) 0.85*scrsz(4)];    %portrait

disp('Use mouse to select spikes and then select the average
operating portion of the test signal.');
disp('Select by clicking before and after the area. ');
disp('');
spikes = input('Number of torque transients (e.g. switch-on + short-
circuit = 2) = ');

per=0.25;

for i=1:tests
    figure('Position',pos1);

eval(['plot(data',num2str(i),'(1:round(per*length(data',num2str(i),')
),1),data',num2str(i),'(1:round(per*length(data',num2str(i),')),mtcbs
1));']);eval(['title(''Test ',num2str(i),''');']);eval('xlabel(''Time
[s]'');');eval('ylabel(''Torque [kNm]'');');
    [xp,yp]=ginput(2*spikes);
    [xm,ym]=ginput(2);
    close

eval(['tavem1bs=mean(data',num2str(i),'(round(xm(1))*fsamp:round(xm(2
))*fsamp,mtcbs1));']);   %mean operating torque - bs
```

```
eval(['tavem2bs=mean(data',num2str(i),'(round(xm(1))*fsamp:round(xm(2
))*fsamp,ptcbs2));']);

%eval(['tavepbs=mean(data',num2str(i),'(round(xm(1))*fsamp:round(xm(2
))*fsamp,ptcbs));']);
%
eval(['tavem1nbs=mean(data',num2str(i),'(round(xm(1))*fsamp:round(xm(
2))*fsamp,mtcnbs1));']);   %mean operating torque - nbs
%
eval(['tavem2nbs=mean(data',num2str(i),'(round(xm(1))*fsamp:round(xm(
2))*fsamp,ptcnbs2));']);

%eval(['tavepnbs=mean(data',num2str(i),'(round(xm(1))*fsamp:round(xm(
2))*fsamp,ptcnbs));']);
    if spikes==1

eval(['tsom1bs=max(data',num2str(i),'(round(xp(1))*fsamp:round(xp(2))
*fsamp,mtcbs1));']);    %switch-on torque - bs

eval(['tsom2bs=max(data',num2str(i),'(round(xp(1))*fsamp:round(xp(2))
*fsamp,ptcbs2));']);

%eval(['tsopbs=max(data',num2str(i),'(round(xp(1))*fsamp:round(xp(2))
*fsamp,ptcbs));']);
%
eval(['tsom1nbs=max(data',num2str(i),'(round(xp(1))*fsamp:round(xp(2)
)*fsamp,mtcnbs1));']);    %switch-on torque - nbs
%
eval(['tsom2nbs=max(data',num2str(i),'(round(xp(1))*fsamp:round(xp(2)
)*fsamp,ptcnbs2));']);

%eval(['tsopnbs=max(data',num2str(i),'(round(xp(1))*fsamp:round(xp(2)
)*fsamp,ptcnbs));']);
        %eval('output=[tsom1bs tavem1bs MRT (tsom1bs/MRT)*100
(tavem1bs/MRT)*100 (tsom1bs/MRT)*100*2 ; tsom2nbs tavem2nbs MRT
(tsom2nbs/MRT)*100 (tavem2nbs/MRT)*100 (tsom2nbs/MRT)*100*2 ; tsopbs
tavepbs PRT (tsopbs/PRT)*100 (tavepbs/PRT)*100 (tsopbs/PRT)*100*2;
tsom1bs tavem1bs MRT (tsom1bs/MRT)*100 (tavem1bs/MRT)*100
(tsom1bs/MRT)*100*2 ; tsom2nbs tavem2nbs MRT (tsom2nbs/MRT)*100
(tavem2nbs/MRT)*100 (tsom2nbs/MRT)*100*2 ; tsopbs tavepbs PRT
(tsopbs/PRT)*100 (tavepbs/PRT)*100 (tsopbs/PRT)*100*2];');
        eval('output=[tsom1bs tavem1bs MRT (tsom1bs/MRT)*100
(tavem1bs/MRT)*100 (tsom1bs/MRT)*100*2 ; tsom1bs tavem1bs MRT
(tsom1bs/MRT)*100 (tavem1bs/MRT)*100 (tsom1bs/MRT)*100*2];');
    elseif spikes==2

eval(['tsom1bs=max(data',num2str(i),'(round(xp(1))*fsamp:round(xp(2))
*fsamp,mtcbs1));']);

eval(['tsom2bs=max(data',num2str(i),'(round(xp(1))*fsamp:round(xp(2))
*fsamp,ptcbs2));']);

%eval(['tsopbs=max(data',num2str(i),'(round(xp(1))*fsamp:round(xp(2))
*fsamp,ptcbs));']);

eval(['tsc1m1bs=max(data',num2str(i),'(round(xp(3))*fsamp:round(xp(4)
)*fsamp,mtcbs1));']);    %short-circuiting torque 1

eval(['tsc1m2bs=max(data',num2str(i),'(round(xp(3))*fsamp:round(xp(4)
)*fsamp,ptcbs2));']);
```

```
%eval(['tsc1pbs=max(data',num2str(i),'(round(xp(3))*fsamp:round(xp(4)
)*fsamp,ptcbs));']);
%
eval(['tsom1nbs=max(data',num2str(i),'(round(xp(1))*fsamp:round(xp(2)
)*fsamp,mtcnbs1));']);
%
eval(['tsom2nbs=max(data',num2str(i),'(round(xp(1))*fsamp:round(xp(2)
)*fsamp,ptcnbs2));']);

%eval(['tsopnbs=max(data',num2str(i),'(round(xp(1))*fsamp:round(xp(2)
)*fsamp,ptcnbs));']);
%
eval(['tsc1m1nbs=max(data',num2str(i),'(round(xp(3))*fsamp:round(xp(4
))*fsamp,mtcnbs1));']);    %short-circuiting torque 1
%
eval(['tsc1m2nbs=max(data',num2str(i),'(round(xp(3))*fsamp:round(xp(4
))*fsamp,ptcnbs2));']);

%eval(['tsc1pnbs=max(data',num2str(i),'(round(xp(3))*fsamp:round(xp(4
))*fsamp,ptcnbs));']);
        %eval('output=[tsom1bs tsc1m1bs tavem1bs MRT
(tsom1bs/MRT)*100 (tsc1m1bs/MRT)*100 (tavem1bs/MRT)*100
(tsom1bs/MRT)*100*2 (tavem1bs/MRT)*100+2*(((tsc1m1bs-
tavem1bs)/MRT)*100); tsom2bs tsc1m2bs tavem2bs MRT (tsom2bs/MRT)*100
(tsc1m2bs/MRT)*100 (tavem2bs/MRT)*100 (tsom2bs/MRT)*100*2
(tavem2bs/MRT)*100+2*(((tsc1m2bs-tavem2bs)/MRT)*100); tsopbs tsc1pbs
tavepbs PRT (tsopbs/PRT)*100 (tsc1pbs/PRT)*100 (tavepbs/PRT)*100
(tsopbs/PRT)*100*2 (tavepbs/PRT)*100+2*(((tsc1pbs-tavepbs)/PRT)*100);
tsom1nbs tsc1m1nbs tavem1nbs MRT (tsom1nbs/MRT)*100
(tsc1m1nbs/MRT)*100 (tavem1nbs/MRT)*100 (tsom1nbs/MRT)*100*2
(tavem1nbs/MRT)*100+2*(((tsc1m1nbs-tavem1nbs)/MRT)*100); tsom2nbs
tsc1m2nbs tavem2nbs MRT (tsom2nbs/MRT)*100 (tsc1m2nbs/MRT)*100
(tavem2nbs/MRT)*100 (tsom2nbs/MRT)*100*2
(tavem2nbs/MRT)*100+2*(((tsc1m2nbs-tavem2nbs)/MRT)*100); tsopnbs
tsc1pnbs tavepnbs PRT (tsopnbs/PRT)*100 (tsc1pnbs/PRT)*100
(tavepnbs/PRT)*100 (tsopnbs/PRT)*100*2
(tavepnbs/PRT)*100+2*(((tsc1pnbs-tavepnbs)/PRT)*100)];');
        eval('output=[tsom1bs tsc1m1bs tavem1bs MRT (tsom1bs/MRT)*100
(tsc1m1bs/MRT)*100 (tavem1bs/MRT)*100 (tsom1bs/MRT)*100*2
(tavem1bs/MRT)*100+2*(((tsc1m1bs-tavem1bs)/MRT)*100); tsom2bs
tsc1m2bs tavem2bs PRT (tsom2bs/PRT)*100 (tsc1m2bs/PRT)*100
(tavem2bs/PRT)*100 (tsom2bs/PRT)*100*2
(tavem2bs/PRT)*100+2*(((tsc1m2bs-tavem2bs)/PRT)*100)];');
    elseif spikes==3

eval(['tsom1bs=max(data',num2str(i),'(round(xp(1))*fsamp:round(xp(2))
*fsamp,mtcbs1));']);

eval(['tsom2bs=max(data',num2str(i),'(round(xp(1))*fsamp:round(xp(2))
*fsamp,ptcbs2));']);

%eval(['tsopbs=max(data',num2str(i),'(round(xp(1))*fsamp:round(xp(2))
*fsamp,ptcbs));']);

eval(['tsc1m1bs=max(data',num2str(i),'(round(xp(3))*fsamp:round(xp(4)
)*fsamp,mtcbs1));']);

eval(['tsc1m2bs=max(data',num2str(i),'(round(xp(3))*fsamp:round(xp(4)
)*fsamp,ptcbs2));']);
```

```
%eval(['tsc1pbs=max(data',num2str(i),'(round(xp(3))*fsamp:round(xp(4)
)*fsamp,ptcbs));']);

eval(['tsc2m1bs=max(data',num2str(i),'(round(xp(5))*fsamp:round(xp(6)
)*fsamp,mtcbs1));']);    %short-circuiting torque 2

eval(['tsc2m2bs=max(data',num2str(i),'(round(xp(5))*fsamp:round(xp(6)
)*fsamp,ptcbs2));']);

%eval(['tsc2pbs=max(data',num2str(i),'(round(xp(5))*fsamp:round(xp(6)
)*fsamp,ptcbs));']);
%
eval(['tsom1nbs=max(data',num2str(i),'(round(xp(1))*fsamp:round(xp(2)
)*fsamp,mtcnbs1));']);
%
eval(['tsom2nbs=max(data',num2str(i),'(round(xp(1))*fsamp:round(xp(2)
)*fsamp,ptcnbs2));']);

%eval(['tsopnbs=max(data',num2str(i),'(round(xp(1))*fsamp:round(xp(2)
)*fsamp,ptcnbs));']);

eval(['tsc1m1nbs=max(data',num2str(i),'(round(xp(3))*fsamp:round(xp(4
))*fsamp,mtcnbs1));']);

eval(['tsc1m2nbs=max(data',num2str(i),'(round(xp(3))*fsamp:round(xp(4
))*fsamp,ptcnbs2));']);

%eval(['tsc1pnbs=max(data',num2str(i),'(round(xp(3))*fsamp:round(xp(4
))*fsamp,ptcnbs));']);
%
eval(['tsc2m1nbs=max(data',num2str(i),'(round(xp(5))*fsamp:round(xp(6
))*fsamp,mtcnbs1));']);    %short-circuiting torque 2
%
eval(['tsc2m2nbs=max(data',num2str(i),'(round(xp(5))*fsamp:round(xp(6
))*fsamp,ptcnbs2));']);

%eval(['tsc2pnbs=max(data',num2str(i),'(round(xp(5))*fsamp:round(xp(6
))*fsamp,ptcnbs));']);
        %eval('output=[tsom1bs tsc1m1bs tsc2m1bs tavem1bs MRT
(tsom1bs/MRT)*100 (tsc1m1bs/MRT)*100 (tsc2m1bs/MRT)*100
(tavem1bs/MRT)*100 (tsom1bs/MRT)*100*2
(tavem1bs/MRT)*100+2*(((tsc1m1bs-tavem1bs)/MRT)*100)
(tavem1bs/MRT)*100+2*(((tsc2m1bs-tavem1bs)/MRT)*100); tsom2bs
tsc1m2bs tsc2m2bs tavem2bs MRT (tsom2bs/MRT)*100 (tsc1m2bs/MRT)*100
(tsc2m2bs/MRT)*100 (tavem2bs/MRT)*100 (tsom2bs/MRT)*100*2
(tavem2bs/MRT)*100+2*(((tsc1m2bs-tavem2bs)/MRT)*100)
(tavem2bs/MRT)*100+2*(((tsc2m2bs-tavem2bs)/MRT)*100); tsopbs tsc1pbs
tsc2pbs tavepbs PRT (tsopbs/PRT)*100 (tsc1pbs/PRT)*100
(tsc2pbs/PRT)*100 (tavepbs/PRT)*100 (tsopbs/PRT)*100*2
(tavepbs/PRT)*100+2*(((tsc1pbs-tavepbs)/PRT)*100)
(tavepbs/PRT)*100+2*(((tsc2pbs-tavepbs)/PRT)*100); tsom1nbs tsc1m1nbs
tsc2m1nbs tavem1nbs MRT (tsom1nbs/MRT)*100 (tsc1m1nbs/MRT)*100
(tsc2m1nbs/MRT)*100 (tavem1nbs/MRT)*100 (tsom1nbs/MRT)*100*2
(tavem1nbs/MRT)*100+2*(((tsc1m1nbs-tavem1nbs)/MRT)*100)
(tavem1nbs/MRT)*100+2*(((tsc2m1nbs-tavem1nbs)/MRT)*100); tsom2nbs
tsc1m2nbs tsc2m2nbs tavem2nbs MRT (tsom2nbs/MRT)*100
(tsc1m2nbs/MRT)*100 (tsc2m2nbs/MRT)*100 (tavem2nbs/MRT)*100
(tsom2nbs/MRT)*100*2 (tavem2nbs/MRT)*100+2*(((tsc1m2nbs-
tavem2nbs)/MRT)*100) (tavem2nbs/MRT)*100+2*(((tsc2m2nbs-
tavem2nbs)/MRT)*100); tsopnbs tsc1pnbs tsc2pnbs tavepnbs PRT
```

```
(tsopnbs/PRT)*100 (tsc1pnbs/PRT)*100 (tsc2pnbs/PRT)*100
(tavepnbs/PRT)*100 (tsopnbs/PRT)*100*2
(tavepnbs/PRT)*100+2*(((tsc1pnbs-tavepnbs)/PRT)*100)
(tavepnbs/PRT)*100+2*(((tsc2pnbs-tavepnbs)/PRT)*100)];');
        eval('output=[tsom1bs tsc1m1bs tsc2m1bs tavem1bs MRT
(tsom1bs/MRT)*100 (tsc1m1bs/MRT)*100 (tsc2m1bs/MRT)*100
(tavem1bs/MRT)*100 (tsom1bs/MRT)*100*2
(tavem1bs/MRT)*100+2*(((tsc1m1bs-tavem1bs)/MRT)*100)
(tavem1bs/MRT)*100+2*(((tsc2m1bs-tavem1bs)/MRT)*100); tsom2bs
tsc1m2bs tsc2m2bs tavem2bs PRT (tsom2bs/PRT)*100 (tsc1m2bs/PRT)*100
(tsc2m2bs/PRT)*100 (tavem2bs/MRT)*100 (tsom2bs/PRT)*100*2
(tavem2bs/PRT)*100+2*(((tsc1m2bs-tavem2bs)/PRT)*100)
(tavem2bs/PRT)*100+2*(((tsc2m2bs-tavem2bs)/MRT)*100)];');
    end
    eval(['Tdata_t',num2str(i),'=output'])

eval(['xlswrite(''Tdata_P'',Tdata_t',num2str(i),',1,',''''B',num2str(7
*i),''');']);
end
```

APPENDIX D FATIGUE DAMAGE MATLAB ROUTINE

```
%Generate relative fatigue damage values for Pinion Shaft of Primary
and Secondary Mills for indicative comparisons of mill data
%October 2005
clear;
load Primary.mat;
load Secondary.mat;
fsamp=200;                  %Sampling frequency [Hz]

%Ch1 = Time in seconds
%Ch2 = Torsional Stress [MPa]
%Ch3 = Bending stress [MPa]

%SECTION 1 - "Shigley" SN Curve

%Material Values and calculation of constants for rainflow program
Sut = 850;                  %Ultimate tensile strength [MPa]
d   = 0.32;                 %Pinion shaft diameter [m]
ka  = 0.8;                  %Surface condition fatigue modification
factor
kb  = 0.688;                %Size fatigue modification factor
kc  = 0.814;                %Reliability goal fatigue modification
factor
kd  = 1.0;                  %Temperature fatigue modification factor
ke  = 1.0;                  %Fatigue modification factor for stress
concentration
kf  = 1.0;                  %Miscellaneous effects fatigue
modification factor
Set = 0.5*Sut;              %Endurance limit for rotating-beam
specimen [MPa]
Kt  = 2;                    %Theoretical stress concentration factor
Se=ka*kb*kc*kd*ke*kf*Set;   %Endurance limit of the shaft [MPa]

%Shigley SN Curve log(Sf)=b*log(Ni)+C
%b=(-1/3)*log10((0.8*Sut)/Se);
%C=log10(((0.8*Sut)^2)/Se);
%Ni=10^-(C/b)*(Sf)^(1/b)    %Sf [MPa]

%Substitute material values to calculate b1 and sigf for rainflow
program
b=log((0.8*Sut)/Se)/log(1/1000);
sf=0.8*Sut/(1000^b);

%Comparative starts per unit time
%use 4 scenarios
%5 starts per day
%1 start per day
%1 start per week
%1 start per month
td  = 24*60*60;             %Time for 1 day [s]
tw  = td*7;                 %Time in a week [s]
tm  = tw*4;                 %Time in a month [s]

%Designated portions of the test signals
start_p   = [1:60*fsamp];                   %mill start portion of
the signal
```

```
run_p     = [60*fsamp+1:181*fsamp];         %steady state portion of
the signal
stop_p    = [181*fsamp+1:length(Primary)];  %mill stop portion of the
signal

start_s   = [1:36*fsamp];                   %mill start portion of
the signal
run_s     = [36*fsamp+1:70*fsamp];          %steady state portion of
the signal
stop_s    = [70*fsamp+1:length(Secondary)]; %mill stop portion of the
signal

%have to add start and stop portions to form one signal else rainflow
misses the one complete cycle
SS_p=[Primary(start_p,2);Primary(stop_p,2)];
SS_s=[Secondary(start_s,2);Secondary(stop_s,2)];

%Rainflow counting of various portions of the test signals - Torque
Only!
[dam,percent,Ranges,Means,y1,damage]=rainflow(Kt*SS_p,sf,b,b);
dam_ssp=dam;
[dam,percent,Ranges,Means,y1,damage]=rainflow(Kt*Primary(run_p,2),sf,
b,b);
dam_rp=dam;
[dam,percent,Ranges,Means,y1,damage]=rainflow(Kt*SS_s,sf,b,b);
dam_sss=dam;
[dam,percent,Ranges,Means,y1,damage]=rainflow(Kt*Secondary(run_s,2),s
f,b,b);
dam_rs=dam;

%Calculate damage figures for comparative starts
%Primary
ffp=round((td-5*(length(SS_p)/fsamp))/(length(run_p)/fsamp));
f1p=round((td-(length(SS_p)/fsamp))/(length(run_p)/fsamp));
damtp_5s=5*dam_ssp+ffp*dam_rp;
%damage value for 5 starts per day
damtp_1=dam_ssp+f1p*dam_rp;
%damage value for 1 start per day
f2p=round((tw-(length(SS_p)/fsamp))/(length(run_p)/fsamp));
damtp_2=dam_ssp+f2p*dam_rp;
%damage value for 1 start per week
f3p=round((tm-(length(SS_p)/fsamp))/(length(run_p)/fsamp));
damtp_3=dam_ssp+f3p*dam_rp;
%damage value for 1 start per month

% Length=[(5*length(SS_p)+ffp*length(run_p))*7*4;
% (length(SS_p)+f1p*length(run_p))*7*4;
% (length(SS_p)+f2p*length(run_p))*4;
% (length(SS_p)+f3p*length(run_p));]

%Secondary
ffs=round((td-5*(length(SS_s)/fsamp))/(length(run_s)/fsamp));
f1s=round((td-(length(SS_s)/fsamp))/(length(run_s)/fsamp));
damts_5s=5*dam_sss+ffs*dam_rs;
%damage value for 5 starts per day
damts_1=dam_sss+f1s*dam_rs;
%damage value for 1 start per day
f2s=round((tw-(length(SS_s)/fsamp))/(length(run_s)/fsamp));
damts_2=dam_sss+f2s*dam_rs;
%damage value for 1 start per week
```

```
f3s=round((tm-(length(SS_s)/fsamp))/(length(run_s)/fsamp));
damts_3=dam_sss+f3s*dam_rs;
%damage value for 1 start per month

%Convert all damage values into common units i.e. damage per month
dp100st = damtp_5s*7*4;  %damage per month for 5 starts per day
dp20st  = damtp_1*7*4;   %damage per month for 1 start per day
dp4st   = damtp_2*4;    %damage per month for 1 start per week
dp1st   = damtp_3;      %damage per month for 1 start per month

ds100st = damts_5s*7*4;  %damage per month for 5 starts per day
ds20st  = damts_1*7*4;   %damage per month for 1 start per day
ds4st   = damts_2*4;    %damage per month for 1 start per week
ds1st   = damts_3;      %damage per month for 1 start per month

%Repeat the process but on the combined stress - torque and bending

%Calculate theta
theta_p=max((atan((2*Primary(:,2))./Primary(:,3)))/2);
theta_s=max((atan((2*Secondary(:,2))./Secondary(:,3)))/2);
%Combine torsional stress and bending stress
ms_p=0.5.*Primary(:,3)+0.5.*Primary(:,3).*cos(2*theta_p)+Primary(:,2)
.*sin(2*theta_p);
ms_s=0.5.*Secondary(:,3)+0.5.*Secondary(:,3).*cos(2*theta_s)+Secondar
y(:,2).*sin(2*theta_s);

%have to add start and stop portions to form one signal else rainflow
misses the one complete cycle
SSB_p=[ms_p(start_p);ms_p(stop_p)];
SSB_s=[ms_s(start_s);ms_s(stop_s)];

%Rainflow counting of various portions of the test signals - Torque
and Bending
[dam,percent,Ranges,Means,y1,damage]=rainflow(Kt*SSB_p,sf,b,b);
dam_ssbp=dam;
[dam,percent,Ranges,Means,y1,damage]=rainflow(Kt*ms_p(run_p),sf,b,b);
dam_rbp=dam;
[dam,percent,Ranges,Means,y1,damage]=rainflow(Kt*SSB_s,sf,b,b);
dam_ssbs=dam;
[dam,percent,Ranges,Means,y1,damage]=rainflow(Kt*ms_s(run_s),sf,b,b);
dam_rbs=dam;

%Calculate damage figures for comparative starts
%Primary
damtbp_5s=5*dam_ssbp+ffp*dam_rbp;
%damage value for 5 starts per day
damtbp_1=dam_ssbp+f1p*dam_rbp;
%damage value for 1 start per day
damtbp_2=dam_ssbp+f2p*dam_rbp;
%damage value for 1 start per week
damtbp_3=dam_ssbp+f3p*dam_rbp;
%damage value for 1 start per month
%Secondary
damtbs_5s=5*dam_ssbs+ffs*dam_rbs;
%damage value for 5 starts per day
damtbs_1=dam_ssbs+f1s*dam_rbs;
%damage value for 1 start per day
damtbs_2=dam_ssbs+f2s*dam_rbs;
%damage value for 1 start per week
```

```
damtbs_3=dam_ssbs+f3s*dam_rbs;
%damage value for 1 start per month

%Convert all damage values into common units i.e. damage per month
dbp100st = damtbp_5s*7*4;  %damage per month for 5 starts per day
dbp20st  = damtbp_1*7*4;   %damage per month for 1 start per day
dbp4st   = damtbp_2*4;    %damage per month for 1 start per week
dbp1st   = damtbp_3;      %damage per month for 1 start per month

dbs100st = damtbs_5s*7*4;  %damage per month for 5 starts per day
dbs20st  = damtbs_1*7*4;   %damage per month for 1 start per day
dbs4st   = damtbs_2*4;    %damage per month for 1 start per week
dbs1st   = damtbs_3;      %damage per month for 1 start per month

%Display Damage Values for SECTION 1 - "Shigley" SN Curve
Dam_comp1_p=[dp100st dp20st dp4st dp1st;
    dbp100st dbp20st dbp4st dbp1st;]

Dam_comp1_s=[ds100st ds20st ds4st ds1st;
    dbs100st dbs20st dbs4st dbs1st;]

xlswrite('Fatigue',Dam_comp1_p,1,'A1');
xlswrite('Fatigue',Dam_comp1_s,1,'A4');

%SECTION 2 - with fatigue limit
b1=b;
m1=-1/b1;
m2=2*m1-1;
b2=-1/m2;

%Rainflow counting of various portions of the test signals - Torque
Only!
[dam,percent,Ranges,Means,y1,damage]=rainflow(Kt*SS_p,sf,b1,b2,1,1);
dam_ssp2=dam;
[dam,percent,Ranges,Means,y1,damage]=rainflow(Kt*Primary(run_p,2),sf,
b1,b2,1,1);
dam_rp2=dam;
[dam,percent,Ranges,Means,y1,damage]=rainflow(Kt*SS_s,sf,b1,b2,1,1);
dam_sss2=dam;
[dam,percent,Ranges,Means,y1,damage]=rainflow(Kt*Secondary(run_s,2),s
f,b1,b2,1,1);
dam_rs2=dam;

%Rainflow counting of various portions of the test signals - Torque
and Bending
[dam,percent,Ranges,Means,y1,damage]=rainflow(Kt*SSB_p,sf,b1,b2,1,1);
dam_ssbp2=dam;
[dam,percent,Ranges,Means,y1,damage]=rainflow(Kt*ms_p(run_p),sf,b1,b2
,1,1);
dam_rbp2=dam;
[dam,percent,Ranges,Means,y1,damage]=rainflow(Kt*SSB_s,sf,b1,b2,1,1);
dam_ssbs2=dam;
[dam,percent,Ranges,Means,y1,damage]=rainflow(Kt*ms_s(run_s),sf,b1,b2
,1,1);
dam_rbs2=dam;

%Primary
damt2p_5s=5*dam_ssp2+ffp*dam_rp2;          %damage value for 5
starts per day
```

```
damt2p_1=dam_ssp2+f1p*dam_rp2;              %damage value for 1 start
per day
damt2p_2=dam_ssp2+f2p*dam_rp2;              %damage value for 1 start
per week
damt2p_3=dam_ssp2+f3p*dam_rp2;              %damage value for 1 start
per month

damt2bp_5s=5*dam_ssbp2+ffp*dam_rbp2;        %same but for the torque
and bending case
damt2bp_1=dam_ssbp2+f1p*dam_rbp2;
damt2bp_2=dam_ssbp2+f2p*dam_rbp2;
damt2bp_3=dam_ssbp2+f3p*dam_rbp2;

%Secondary
damt2s_5s=5*dam_sss2+ffs*dam_rs2;           %damage value for 5
starts per day
damt2s_1=dam_sss2+f1s*dam_rs2;              %damage value for 1 start
per day
damt2s_2=dam_sss2+f2s*dam_rs2;              %damage value for 1 start
per week
damt2s_3=dam_sss2+f3s*dam_rs2;              %damage value for 1 start
per month

damt2bs_5s=5*dam_ssbs2+ffs*dam_rbs2;        %same but for the torque
and bending case
damt2bs_1=dam_ssbs2+f1s*dam_rbs2;
damt2bs_2=dam_ssbs2+f2s*dam_rbs2;
damt2bs_3=dam_ssbs2+f3s*dam_rbs2;

%Convert all damage values into common units i.e. damage per month
d2p100st = damt2p_5s*7*4;  %damage per month for 5 starts per day
d2p20st  = damt2p_1*7*4;   %damage per month for 1 start per day
d2p4st   = damt2p_2*4;    %damage per month for 1 start per week
d2p1st   = damt2p_3;      %damage per month for 1 start per month

d2bp100st = damt2bp_5s*7*4;  %damage per month for 5 starts per day
d2bp20st  = damt2bp_1*7*4;   %damage per month for 1 start per day
d2bp4st   = damt2bp_2*4;    %damage per month for 1 start per week
d2bp1st   = damt2bp_3;      %damage per month for 1 start per month

d2s100st = damt2s_5s*7*4;  %damage per month for 5 starts per day
d2s20st  = damt2s_1*7*4;   %damage per month for 1 start per day
d2s4st   = damt2s_2*4;    %damage per month for 1 start per week
d2s1st   = damt2s_3;      %damage per month for 1 start per month

d2bs100st = damt2bs_5s*7*4;  %damage per month for 5 starts per day
d2bs20st  = damt2bs_1*7*4;   %damage per month for 1 start per day
d2bs4st   = damt2bs_2*4;    %damage per month for 1 start per week
d2bs1st   = damt2bs_3;      %damage per month for 1 start per month

%Display Damage Values for SECTION 2 - with fatigue limit
Dam_comp2_p=[d2p100st d2p20st d2p4st d2p1st;
    d2bp100st d2bp20st d2bp4st d2bp1st;]

Dam_comp2_s=[d2s100st d2s20st d2s4st d2s1st;
    d2bs100st d2bs20st d2bs4st d2bs1st;]

xlswrite('Fatigue',Dam_comp2_p,2,'A1');
xlswrite('Fatigue',Dam_comp2_s,2,'A4');
```

```
%SECTION 3 - separate SN curves for bending and torque

mn  = 3;        %slope for normal stress SN curve (steel)
ms  = 5;        %slope for shear stress SN curve (steel)
bn  = -1/mn;
bs  = -1/ms;

FAT_ns  = 160;      %normal stress - fatigue strength at 2e6 cycles
(IWE fatigue class)
FAT_ss  = 100;      %shear stress - fatigue strength at 2e6 cycles
(IWE fatigue class)

sfn     = FAT_ns/(2e6^bn);
sfs     = FAT_ss/(2e6^bs);

Se_ns   = sfn*(5e6)^bn;
Se_ss   = sfs*(1e8)^bs;

% Se_ns   = 117.89;   %normal stress - fatigue limit at 5e6 cycles
% Se_ss   = 45.73;    %shear stress - fatigue limit at 1e8 cycles
% bn      = log((FAT_ns)/Se_ns)/log(2e6/5e6);
% bs      = log((FAT_ss)/Se_ss)/log(2e6/1e8);

%Rainflow counting of various portions of the test signals - Torque
Only!
[dam,percent,Ranges,Means,y1,damage]=rainflow(Kt*SS_p,sfs,bs,bs,1,1);
dam_ssp3=dam;
[dam,percent,Ranges,Means,y1,damage]=rainflow(Kt*Primary(run_p,2),sfs
,bs,bs,1,1);
dam_rp3=dam;
[dam,percent,Ranges,Means,y1,damage]=rainflow(Kt*SS_s,sfs,bs,bs,1,1);
dam_sss3=dam;
[dam,percent,Ranges,Means,y1,damage]=rainflow(Kt*Secondary(run_s,2),s
fs,bs,bs,1,1);
dam_rs3=dam;

%Bending
SS_pb=[Primary(start_p,3);Primary(stop_p,3)];
SS_sb=[Secondary(start_s,3);Secondary(stop_s,3)];

%Rainflow counting of various portions of the test signals - Bending
Only!
[dam,percent,Ranges,Means,y1,damage]=rainflow_5m(Kt*SS_pb,sfn,bn,bn,1
,1);
dam_ssbp3=dam;
[dam,percent,Ranges,Means,y1,damage]=rainflow_5m(Kt*Primary(run_p,3),
sfn,bn,bn,1,1);
dam_rbp3=dam;
[dam,percent,Ranges,Means,y1,damage]=rainflow_5m(Kt*SS_sb,sfn,bn,bn,1
,1);
dam_ssbs3=dam;
[dam,percent,Ranges,Means,y1,damage]=rainflow_5m(Kt*Secondary(run_s,3
),sfn,bn,bn,1,1);
dam_rbs3=dam;

%Add the two damage values
dam_ssp3t=dam_ssp3+dam_ssbp3;
dam_rp3t=dam_rp3+dam_rbp3;
```

```
dam_sss3t=dam_sss3+dam_ssbs3;
dam_rs3t=dam_rs3+dam_rbs3;

%Primary
%Torque
damt3p_5s=5*dam_ssp3+ffp*dam_rp3;           %damage value for 5
starts per day
damt3p_1=dam_ssp3+f1p*dam_rp3;              %damage value for 1 start
per day
damt3p_2=dam_ssp3+f2p*dam_rp3;              %damage value for 1 start
per week
damt3p_3=dam_ssp3+f3p*dam_rp3;              %damage value for 1 start
per month

%Bending
damt3bp_5s=5*dam_ssbp3+ffp*dam_rbp3;        %same but for the bending
case
damt3bp_1=dam_ssbp3+f1p*dam_rbp3;
damt3bp_2=dam_ssbp3+f2p*dam_rbp3;
damt3bp_3=dam_ssbp3+f3p*dam_rbp3;

%Combined
damt3pt_5s=5*dam_ssp3t+ffp*dam_rp3t;         %same but for the
combined case
damt3pt_1=dam_ssp3t+f1p*dam_rp3t;
damt3pt_2=dam_ssp3t+f2p*dam_rp3t;
damt3pt_3=dam_ssp3t+f3p*dam_rp3t;

%Secondary
%Torque
damt3s_5s=5*dam_sss3+ffs*dam_rs3;           %damage value for 5
starts per day
damt3s_1=dam_sss3+f1s*dam_rs3;              %damage value for 1 start
per day
damt3s_2=dam_sss3+f2s*dam_rs3;              %damage value for 1 start
per week
damt3s_3=dam_sss3+f3s*dam_rs3;              %damage value for 1 start
per month

%Bending
damt3bs_5s=5*dam_ssbs3+ffs*dam_rbs3;        %same but for the bending
case
damt3bs_1=dam_ssbs3+f1s*dam_rbs3;
damt3bs_2=dam_ssbs3+f2s*dam_rbs3;
damt3bs_3=dam_ssbs3+f3s*dam_rbs3;

%Combined
damt3st_5s=5*dam_sss3t+ffs*dam_rs3t;         %same but for the
combined case
damt3st_1=dam_sss3t+f1s*dam_rs3t;
damt3st_2=dam_sss3t+f2s*dam_rs3t;
damt3st_3=dam_sss3t+f3s*dam_rs3t;

%Convert all damage values into common units i.e. damage per month
d3p100st = damt3p_5s*7*4;  %damage per month for 5 starts per day
d3p20st  = damt3p_1*7*4;   %damage per month for 1 start per day
d3p4st   = damt3p_2*4;    %damage per month for 1 start per week
d3p1st   = damt3p_3;      %damage per month for 1 start per month

d3bp100st = damt3bp_5s*7*4;  %damage per month for 5 starts per day
```

```
d3bp20st  = damt3bp_1*7*4;   %damage per month for 1 start per day
d3bp4st   = damt3bp_2*4;    %damage per month for 1 start per week
d3bp1st   = damt3bp_3;      %damage per month for 1 start per month

d3pt100st = damt3pt_5s*7*4;  %damage per month for 5 starts per day
d3pt20st  = damt3pt_1*7*4;   %damage per month for 1 start per day
d3pt4st   = damt3pt_2*4;    %damage per month for 1 start per week
d3pt1st   = damt3pt_3;      %damage per month for 1 start per month

d3s100st = damt3s_5s*7*4;  %damage per month for 5 starts per day
d3s20st  = damt3s_1*7*4;   %damage per month for 1 start per day
d3s4st   = damt3s_2*4;    %damage per month for 1 start per week
d3s1st   = damt3s_3;      %damage per month for 1 start per month

d3bs100st = damt3bs_5s*7*4;  %damage per month for 5 starts per day
d3bs20st  = damt3bs_1*7*4;   %damage per month for 1 start per day
d3bs4st   = damt3bs_2*4;    %damage per month for 1 start per week
d3bs1st   = damt3bs_3;      %damage per month for 1 start per month

d3st100st = damt3st_5s*7*4;  %damage per month for 5 starts per day
d3st20st  = damt3st_1*7*4;   %damage per month for 1 start per day
d3st4st   = damt3st_2*4;    %damage per month for 1 start per week
d3st1st   = damt3st_3;      %damage per month for 1 start per month

%Display Damage Values for SECTION 3 - with fatigue limit
Dam_comp3_p=[d3p100st d3p20st d3p4st d3p1st;
    d3bp100st d3bp20st d3bp4st d3bp1st;
d3pt100st d3pt20st d3pt4st d3pt1st;]

Dam_comp3_s=[d3s100st d3s20st d3s4st d3s1st;
    d3bs100st d3bs20st d3bs4st d3bs1st;
d3st100st d3st20st d3st4st d3st1st;]

xlswrite('Fatigue',Dam_comp3_p,3,'A1');
xlswrite('Fatigue',Dam_comp3_s,3,'A5');
```